Low temperature scanning tunneling microscopy on mesoscopic systems

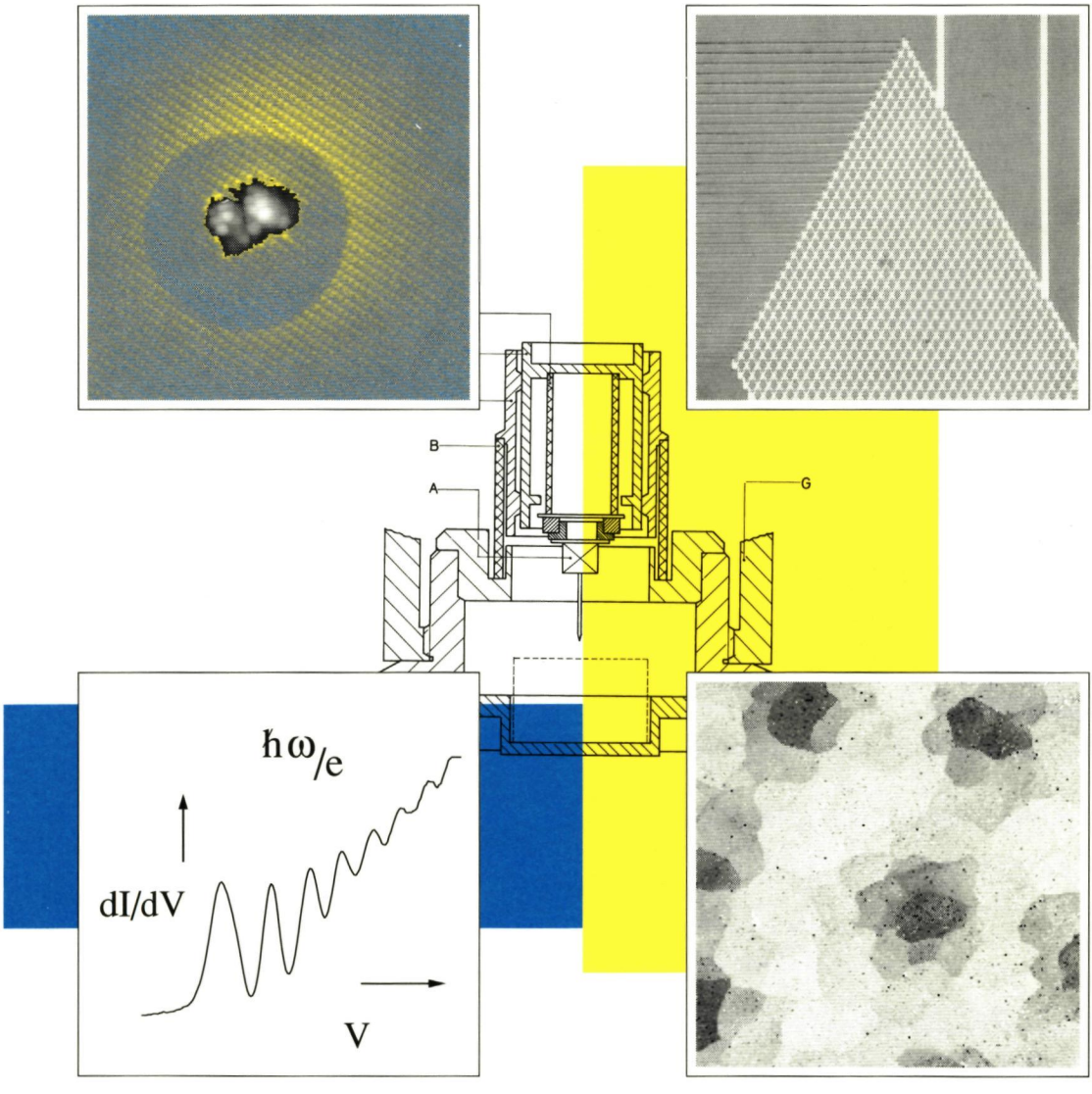

Jeroen Wildöer

Low temperature scanning tunneling microscopy on mesoscopic systems

The work described in this thesis has partially been performed at the Katholieke Universiteit Nijmegen (KUN) and partially at the Technische Universiteit Delft (TU Delft)

Low temperature scanning tunneling microscopy on mesoscopic systems

een wetenschappelijke proeve op het gebied van

de Natuurwetenschappen

Proefschrift

ter verkrijging van de graad van doctor aan

de Katholieke Universiteit Nijmegen,

volgens besluit van het College van Decanen

in het openbaar te verdedigen op

dinsdag 18 juni 1996

des namiddags om 3 30 uur precies

door

Jeroen Walter Gerard Wildöer

geboren op 10 maart 1967

te Andijk

Promotor.

Prof. Dr. H van Kempen

Copromotor·

Dr C J P M. Harmans

Manuscript Committee:

Dr. P.J.M. van Bentum

Dr. L.J. Geerligs

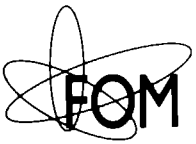

This work is part of the research program of the Stichting voor Fundamenteel Onderzoek der Materie (FOM), which in turn is financially supported by the Nederlandse Organisatie voor Wetenschappelijk Onderzoek (NWO)

Wildoer, Jeroen Walter Gerard

Low temperature scanning tunneling microscopy
on mesoscopic systems.
Proefschrift Katholieke Universiteit Nijmegen. - Met lit opg -
Met samenvatting in het Nederlands.
ISBN 90-9009573-x
Trefw : scanning tunneling microscopy, tunneling spectroscopy,
superconductors, semiconductor surfaces, Josephson junctions.

Preface

This thesis covers the main results of a project which started at the end of 1991 with the objective to investigate mesoscopic systems by using scanning tunneling microscopy in combination with artificially fabricated nanostructures One of the initial ideas was to use the STM-tip as a displaceable contact in transport mesurements on nanostructures This kind of experiments requires an STM with coarse positioning facilities in three dimensions, and operation at very low temperatures, preferably in the milliKelvin regime Another idea was for example to use the STM to directly image the edge channels in a two dimensional electron gas by spatially resolved tunneling spectroscopy

Most of these ideas were not feasible by standard means, and a significant fraction of the work was dedicated to finding solutions for various experimental restrictions Fortunately however a large part of the time could still be devoted to contriving, doing, and interpreting experiments

The work described in this thesis has been performed in two groups The first two years of the project were spent in Nijmegen, in the group of Herman van Kempen The group has a long tradition in scanning tunneling microscopy Already in 1982, shortly after the invention of STM by Binnig and Rohrer, first steps were taken in this field of research Nowadays between seven and ten Ph D students and several Post-Docs work on various STM related topics, like break-junctions, low-temperature and ulta-high vacuum STM, spin polarized tunneling, and ballistic electron-emission spectroscopy

In Nijmegen I benefited from the large amount of experience in the group and the numerous discussions about theoretical and technological STM issues Very usefull were the two-weekly STM meetings Together with Andre van Roij I developed the low temperature ^{4}He-STM described in chapter 2 of this thesis, which is now also used by other Ph D students So, I hope my stay was of mutual benefit I enjoyed the warm atmosphere of the group and the remnants of its 30 years history Old inserts decorate the walls of the experimental rooms and with every one of them goes a funny story Photographs of colloquia in the 1970s corfirm that beards were more if fashion amongst Ph D students then, than they are nowadays

After two years I moved to Delft, where I joined the group of Hans Mooij, called Quantum Transport In this group of about 40 people, the field of research is mesoscopic phenomena in artificially fabricated submicron structures

In the period in Delft two lines of activities evolved Experimements were performed on charge density waves, superconductor normal structures, and resonant tunneling diode pillars Meanwhile efforts were undertaken to enable STM-experiments

at temperatures well below 1 K on artificially fabricated nanostructures, resulting in a new STM, dedicated for these experiments. Also, together with Gerton de Goey, the energy resolution of the STM spectroscopy measurements was improved.

In the Delft group I benefitted from the extensive knowledge of the field of mesoscopic physics. Discussions in the so-called mesoclub about recent mesoscopic topics, and the lectures given by a large number of famous foreign guests were very inspiring.

The unusual framework of project left open a lot of freedom concerning the choice of the subjects and the strategy to follow. The support of Herman van Kempen during these four years was essential. Our conversations were not restricted to only the physics subjects, but also covered the more technological STM-related issues. Kees Harmans' critical attitude prevented many time consuming mistakes, and also he was a very conscientious supervisor. I very much enjoyed the cooperation with Andre van Roij during the two years in Nijmegen. His technical skills, perseverance, and creativity have contributed importantly to the results described in this thesis

With the wide variety of subjects I was involved in, I very much appreciated the cooperation and discussions with Ph.D.-student collegues, post-Docs, and technicians. Jan Gerritsen and Jan Hermsen shared a great deal of their STM-knowledge with me, and I was very lucky with Jerome Dubois as a low-temperature STM collegue. With Edwin Boon, Dick Heslinga, Sergei Shafranjuk, and Luuk Mur I had many discussions about superconductivity in general, and the proximity effect in particular Maurice van der Wielen and Ronnie Janssen gave useful feedback on the various traps in tunneling spectroscopy on semiconductor surfaces. Together with Alexander van Oudenaarden the first experiment on an artificially fabricated structure at temperatures below 1 K was performed. Unfortunately no time was left for more advanced projects. Further, I appreciated discussions with Leo Kouwenhoven, Hans Mooij, Bart van Wees, Menno Prins, Bart Geerligs, and Jan van Bentum The last two also spent a lot of their scarce time in reading the manuscript of this thesis I am indebted to Edwin Boon and Sven Wallage for their help with computers.

In de experimentele fysica lukken dingen vaker niet dan wel. De afgelopen vier jaar hebben me geleerd dat deze regel zeker op STM-werk van toepassing is De donderdagavonden die met Robert en Jerome al experimenterend werden ingezet, maar na weer een hoeveelheid malheur in "St. Anneke" werden beeindigd, zal ik me altijd blijven herrinneren Volgens het principe gedeelde smart is halve smart, en met een flinke dosis humor, werd de geest weer helder gemaakt

Tenslotte wil de mensen bedanken die iets verder van de natuurkunde afstaan. ouders, familie en vrienden. Vooral het laatste jaar was vrije tijd een schaars goed, en was ik vaak niet beschikbaar. Met de voltooiing van dit proefschrift hoop ik deze ontwikkeling ten goede te keren.

Contents

Preface i

1 Low temperature scanning tunneling microscopy on mesoscopic systems 1

1 1 Mesoscopic systems 1
1 2 Variable tunnel contact experiments 3
1 3 Spatially resolved tunneling spectroscopy 5
1 4 Positionable normal contact experiments 9
1 5 Atomic scale manipulation and spectroscopy 10
1 6 Limitations 11
1 7 Thesis outline 12
References 13

2 Two low-temperature scanning tunneling microscopes for use on artificially fabricated nanostructures 17

2 1 Introduction 18
2 2 Mechanical stability 19
2 3 STM at low temperatures 22
2 4 The ^{4}He-STM 24
2 5 The ^{3}He-STM 30
2 6 Surface conditions and preparation 35
2 7 STM control electronics 36
2 8 Measurement modes 36
2 9 Energy resolution in tunneling spectroscopy 38
2 10 Acknowledgements 40
2 11 Appendix A 40
References 44

3 Scanning tunneling microscopy on the InAs(110) surface: Landau levels, tip induced accumulation, and Fermi-level pinning by a single step edge **49**
3.1 Introduction 50
3 2 Observation of Landau levels 52
3 2 1 B = 0 52
3 2.2 B ≠ 0 54
3 3 Tip influences 58
3 4 Step edge Fermi-level pinning 60
3 5 Thin oxides 64
3 6 Conclusions 66
3 7 Acknowledgements 67
References 67

4 Semiconductor band-switching by charging a small grain with a single electron **69**
References 79

5 Proximity induced mosaic vortices observed by scanning tunneling microscopy **81**
References 91

6 The scanning tunneling microscope-tip as a positionable contact: probing a Josephson-junction array at subKelvin temperatures **93**
6.1 Introduction 94
6.2 Josephson-junction arrays 95
6 3 Sample design and experimental setup 97
6 4 Results 99
6.5 Conclusions 101
References 101

Samenvatting **103**

Summary **105**

Curriculum vitae **107**

Chapter 1

Low temperature scanning tunneling microscopy on mesoscopic systems

1.1 Mesoscopic systems

The present understanding of the electronic properties of the solid state has only become possible after the inception of quantum mechanics at the beginning of this century Quantum theory is essential to understand the elementary processes in solids, however to describe electron transport through a macroscopic conductor rather phemenogical classical laws are often sufficient The validity of these transport laws is a consequence of the large number of particles that is present in a typical conductor, which will cause it to show only ensemble averaged properties When dimensions are reduced towards the atomic scale the classical description no longer holds and quantum mechanics is required. In this regime it is possible again to observe single particle processes, instead of ensemble averages Also it becomes important at these length scales that quantities like charge or magnetic flux are not continuous but quantized. Furthermore, when dimensions are of the order of the Fermi-wavelength quantum size effects can dominaate the transport properties The physics of small solid state entities is often considered as a cross-over between macroscopic and microscopic physics, and therefore systems in this regime are usually referred to as mesoscopic

The physics of small solid state systems has become experimentally accessible during the last decade due to two major technological developments. The first one is that the continuing scale reduction in lithographic techniques has made it feasible to define solid state structures with sizes well below one micrometer The advanced technology required to reach these lengthscales has emerged largely from the semiconductor industies in their continuing effort to increase the

number of unit circuits integrated on a single chip In semiconductor industry still optical (UV) methods are used to define patterns, however to access length scales far below one micron, electron beam techniques are required In state of the art Electron Beam Pattern Generators (EBPGs) or Scanning Electron Microscopes (SEM) electron beams are available with spot sizes below 10 nm With lithographic techniques mesoscopic systems can be patterned on chip, including bondpads to connect the structure to external current sources or voltmeters The second major technological development is the inception of various scanning probe techniques, initiated by the invention of the Scanning Tunneling Microscope (STM) by Binnig and Rohrer in 1982 [1] An STM is capable of imaging a surface with atomic resolution by probing it with a needle-shaped conducting tip Between STM-tip and sample a small tunnel current is established Other scanning probe techniques now available are the Atomic Force Microscope [2] (AFM) and the Scanning Near field Optical Microscope [3] (SNOM) Scanning probe techniques allow to image and manipulate surfaces, but also to investigate various physical properties at the surface with very high spatial resolution, i e on a very local scale

Electron transport measurements through lithographically fabricated mesoscopic structures have shown a large variety of new phenomena during the last decade Well known examples are quantized conductance [4, 5], single electron tunneling [8] and correlated electron transport [9, 10] Nanolithography allows the fabrication of structures with well controlled sizes and shapes In transport measurements a number of leads is attached to a structure, and by monitoring the transport properties under various conditions, like different gate voltages, temperatures, or magnetic fields, it is possible to extract the relevant physical processes Very versatile systems in this respect are semiconductor heterostructures By lithographically patterning a metallic gate on top of a heterostructure a two dimensional electron gas located directly under the surface can be depleted selectively In this way quantum points contacts [4, 5] and quantum dots [6, 7] can be defined in a two dimensional electron gas, and their sizes and shapes can be varied, simply by adjusting the voltages applied to the gate electrodes Nanolithography also provides simple methods to fabricate very small tunnel junctions, using shadow evaporation techniques Other mesoscopic structures fabricated by nanolithography are superconductor-semiconductor-superconductor junctions [11], Aharanov Bohm [12] rings and Josephson junction arrays [13, 14, 15] Since the relevant energies of most of these systems are small, low temperatures are required to investigate the mesoscopic phenomena

The use of the scanning tunneling microscope to resolve the electronic properties of mesoscopic systems may at first sight seem peculiar, since STMs are known in the first place for their ability to image the topography of surfaces with high spatial resolution The important property of an STM in a mesoscopic experiment is the versatility of the STM-tip positioning Whereas in ordinary transport measurements the number of leads, their position and their degree of coupling are fixed, the use of an STM offers a variable tunnel contact Another advantage of using an STM in investigating mesoscopic systems is that it provides access to much smaller length scales than can be fabricated by lithography Therefore mesoscopic phenomena can be observed already at higher temperatures

In this thesis several experiments are described in which an STM is used to investigate mesoscopic phenomena in the solid state As the characteristic energy scales of most mesoscopic systems are small, the experiments have been performed at low temperatures Before discussing the results of our work in the following chapters, I use this chapter to introduce the various ways in which an STM can be applied in a mesoscopic experiment I do so by presenting a brief overview of some of the important results obtained in the last decade The experiments in this overview are grouped in four categories, depending on the specific way in which the STM was used in the experiment The categories are Variable tunnel contact experiments (Section 1 2), Spatially resolved tunneling spectroscopy (1 3), Positionable normal contact experiments (1 4), and Atomic scale manipulation and spectroscopy (1 5) For the present discussion it suffices to realize that an STM allows to position a conducting tip above a conducting surface, that its position can be varied, and that the distance between tip and sample should be so small that a detectable tunnel current can cross the vacuum barrier

1.2 Variable tunnel contact experiments

In the first category of experiments the STM-tip is used to establish a variable tunnel contact As an example we discuss charge quantization experiments performed with an STM In this kind of experiments [16, 17] the tip acts as one of the leads to a small metallic grain, which is situated on a thin insulating layer on top of a conducting substrate (this is the other lead) Figure 1 1a shows the experimental situation If the capacitance of the grain to its environment is sufficiently small charging energies dominate the electron transport Charge quantization in a single metallic island was for the first time shown Fulton and Dolan [8] in 1987,

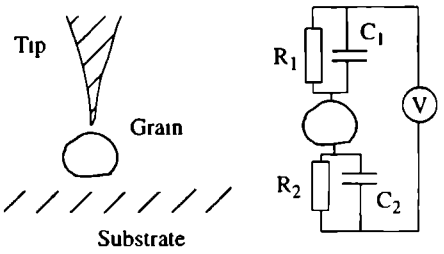

Figure 1 1 *(a) The STM geometry for tunneling through a small metallic grain The surface of the substrate has to be insulating and usually consists of an oxide (b) Both tunnel junctions can be represented by a capacitor and a resistor in parallel*

using a lithographically fabricated structure One year later van Bentum *et al* [16] demonstrated the same effect in an STM geometry

Charge quantization effects become important when the energy required to charge a metallic island with a single electron is larger than the thermal energy k_BT In this case a so-called Coulomb blockade can occur, which at low bias voltages suppresses the current through a double junction geometry When the bias voltage is raised charged states at higher energies in the island become available for electron transport With every new state the tunnel current will increase sharply, which results in the so-called Coulomb staircase an $I - V$ curve with sharp rises in the current at equal voltage intervals (Figure 1 2) The width of the intervals is determined by the capacitances of the tunneljunctions An ad-

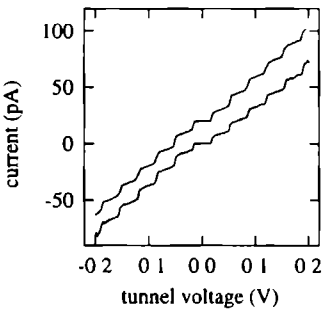

Figure 1 2 *Experimental and calculated Coulomb staircase The measured tunnel characteristic is obtained above a Pd_{561} cluster (lower curve) The fit parameters used in the calculated curve are R_1=2 3 GΩ, R_2=7 MΩ, C_1=4 7 aF, C_2=3 aF, Q_0=0 and T=4 2 Kelvin Image courtesy of J G A Dubois*

vantage of using STM to form these geometries instead of using lithographically fabricated structures is that the tunnel resistance and the capacitance of one of the junctions can be varied by changing the position of the tip In recent years especially the dynamics of offset charges has been investigated with STM [18, 19]

To fabricate the samples used in these kind of experiments only a standard evaporator is required The metallic island in the geometry of Figure 1 1 consists of one of the isolated grains that appear on the surface when a very thin layer is evaporated The sizes of these grains are much smaller than the metallic islands that can be defined by lithographic techniques, and therefore charging effects are present at higher temperatures already With an STM single electron tunneling has been observed at room temperature [20] The very small sizes of some grains even allows the observation of quantum size effects in metallic particles This has been demonstrated by Dubois *et al* , using ligand stabilized Pt clusters, with a well defined size and shape [21, 22] Quantum size effects in very small metallic grains have also been observed by Ralph *et al* [23] using lithographic point contacts The actual system they obtain is very similar to the STM geometry (Figure 1 3) However its advantage is that it is much more stable In charge quantization experiments the presence of the tip will influence both the electrochemical and the electrostatic potential of the metal islands at the sample surface Therefore in these systems the STM-tip is not just a non-invasive probe, but actually affects the surface electronic properties

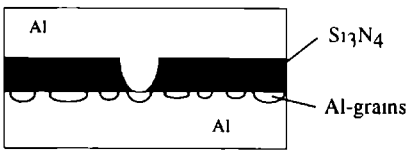

Figure 1 3 *System investigated by Ralph et al [23] By evaporating and subsequently oxidizing Al on both sides of a lithographycally patterned hole in a Si_3N_4 membrane, electron transport through a single isolated grain can be realized The actual system resembles the STM geometry of Figure 1 1a*

1.3 Spatially resolved tunneling spectroscopy

A second category of experiments uses the unique possibility STMs offer to perform spatially resolved tunneling spectroscopy Tunneling spectroscopy [24] is

a powerful technique to investigate the density of states in a solid and was pioneered by Giaever in the 1960s [25, 26] using planar junctions In tunneling spectroscopy two electrodes are separated by a tunnel barrier The Fermi energies of the two electrodes can be shifted with respect to each other by applying a bias voltage The number of states available for tunneling between the two electrodes is determined by the magnitude of the bias voltage, and the densities of states in the energy interval between the two Fermi energies So, by sweeping the bias voltage, the number of states available for tunneling will be varied Assuming every state contributes equally to the total tunnel current, and that the Fermi-Dirac distribution can be approximated by a step function, the tunnel current is given by

$$I = \frac{4\pi e}{\hbar} \int_0^{eV} \rho_1(E - eV + \epsilon)\rho_2(E + \epsilon)\,|M|^2\, d\epsilon \qquad (1\,1)$$

where $\rho_1(E)$ and $\rho_2(E)$ are the densities of states (DOS) of the two electrodes, and M is the tunneling matrix element [27] Over small voltage intervals M can be taken constant

So, in principle, by sweeping the bias voltage, and recording the dI/dV, one can obtain the dependence of the density of states as a function of energy Equation 1 1 represents the basic concept of tunneling spectroscopy, however it is oversimplified for a large number of cases [28] For example, if the density of states is just due to the independent particle bandstructure of a solid the tunneling matrix element contains a factor inversionally proportional to the density of states (this is because the particle velocity, which is included in $|M|$, equals $\hbar^{-1}\partial E/\partial k$ [29]) In other words, in these cases the density of states is cancelled in equation 1 1 Spectroscopy measurements with two normal electrodes therefore contain in first order no information on the density of states In the case of superconductor-normal junctions however the quasi-particle density of states is governed by the electron-electron interaction in the superconductor, and for this case equation 1 1 can be applied [27] directly Also in systems where the states are localized, or in the vicinity of discontinuities in the density of states, tunneling spectroscopy is able to reveal the energies of the most prominent features

In the STM-geometry, one of the electrodes consists of the STM-tip, and the other is the surface under investigation DOS of tip and sample in (1 1) are interchangeable, however if the tip density of states resembles a free electron gas and only the sample DOS is structured, the derivative of the current with respect to the applied voltage dI/dV can be taken proportional to $\rho_S(E_F - eV)$ The advantage of using an STM for tunneling spectroscopy is that it allows to

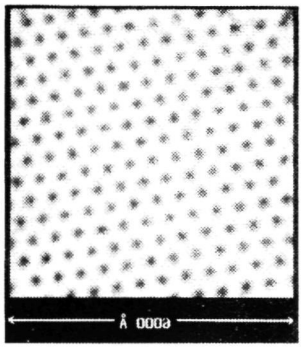

Figure 1.4: *Abrikosov flux lattice produced by a 1-T magnetic field in $NbSe_2$ at 1.8 K. The lattice is imaged by recording the dI/dV at 1.3 mV as a function of position. (Reproduced from [30], with permission.)*

investigate the density of states spatially resolved. An important condition in tunneling spectroscopy is that the tunnel electrode does not influence the surface electronic properties of the investigated sample. This condition is for example not fulfilled in the previously discussed charge quantization experiments where the presence of the tip does influence both the electrochemical and the electrostatic potential of the metal islands at the sample surface.

The opportunity to investigate the density of states spatially resolved is very useful in studying mesoscopic systems. An example here is the STM-observation of excitations inside the core of a vortex by Hess *et al.* [30]. Vortices consist of small normal area's in a superconductor, each one corresponding to a single magnetic flux quantum penetrating the condensate. By measuring the local density of states a vortex lattice can be imaged, since in the superconducting regions no single quasi-particle states are available within the superconducting gap, while within the vortices regions the DOS should reflect a normal behavior. By scanning tunneling spectroscopy Hess was able to map the Abrikosov flux lattice on $NbSe_2$, a superconductor known for its excellent surface quality. The image is shown in Figure 1.4. Within the vortex the superconducting gap indeed disappeared, but instead of the expected normal density of states, a pronounced peak in the dI/dV at small bias was observed at the center of the vortex, as is shown in Figure 1.5. The height of the peak appeared to be very sensitive to the tip position relative to the vortex center.

The vortex can be considered as a quantum well for quasiparticles, with a depth equal to the superconducting gap and a radius equal to superconducting

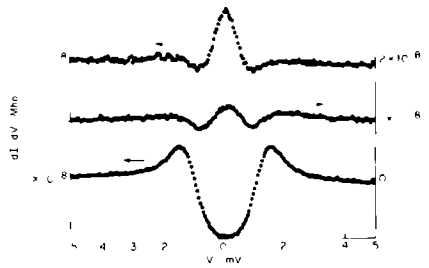

Figure 1 5 *dI/dV vs V for $NbSe_2$ at 1 85 K and a 0 02-T field, taken at three positions on a vortex (top curve), about 75 Å from a vortex, and 2000 Å from a vortex (bottom curve) (Reproduced from [30], with permission)*

coherence length The obvious explanation for the zero bias peak, that it reflects a single bound state, can not be valid, since the size of the vortex would give an energy splitting between the bound states much smaller than $k_B T$ By solving the Bogoliubov-de Gennes equations Shore *et al* [31] showed that the zero bias peak still should be attributed to bound states, however not to a single one, but to all the states that have an amplitude *at the STM-tip position* The bound states in the solution are characterized by an energy E and an angular momentum μ (note that there is cylindrical symmetry about the axis of the vortex) The lowest-energy bound states (small μ) will have wavefunctions which are peaked close to the center of the vortex, whereas higher-energy bound states (large μ) have a low amplitude at the vortex center (Figure 1 6) Therefore dI/dV curves taken at this spot show a larger density of states at zero bias than at bias voltages just below the superconducting gap The zero bias peak thus reflects the position dependent quasiparticle amplitude Several predictions made by Shore *et al* concerning the spatial dependence of anomalies in the dI/dV inside the vortex core were later experimentally confirmed in another experiment by Hess *et al* [32] The elegant fully quantum mechanical treatment of the problem presented by Shore *et al* is of course only valid in very pure crystals Renner *et al* [33] showed that the zero bias peak in $NbSe_2$ vortices does not appear when a small amount of disorder is present in the crystal

Although scanning tunneling spectroscopy is potentially a very powerful technique to investigate the inhomogeneous properties of superconductors, the results obtained thus far are modest A major constraint in applying the technique is formed by the severe demands that are put forward to the quality of the surface For this reason almost all experiments that have been reported have been

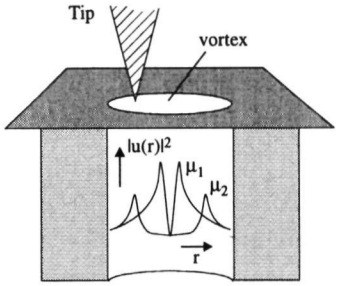

Figure 1.6: *Schematic representation of wavefunction amplitudes of different states inside a vortex.* $\mu_2 > \mu_1$.

performed on $NbSe_2$. Recently, however, also vortices of the high temperature superconductor $YBa_2Cu_3O_{7-\delta}$ have been investigated [34]. These vortices are much smaller than the ones in $NbSe_2$ and in the spectra signatures of single bound states may have been observed. In order to obtain clean high-T_c surfaces several groups cleave their samples in situ at liquid helium temperature, in this way preventing undesirable oxygen diffusion [35].

1.4 Positionable normal contact experiments

A less sophisticated application of the scanning tunneling microscope in investigating mesoscopic systems is to use the tip as a displaceable contact. As was discussed previously, nanolithography allows the fabrication of very small solid state structures. However, in some cases contacting these structures can be a problem by itself. Leads may have to cross vital parts of the pattern, or structures may be so small that the danger of short-circuits exists. By using an STM in these situations, difficult regions can be contacted directly by the STM-tip. This method has been used for example by Weiner *et al.* [36] to contact very small resonant tunneling heterostructures. Figure 1.7 shows the tip contacting a InGaAs/InAlAs pillar. The pillars were etched out of a large double barrier resonant tunneling heterostructure. Contacting the top of a pillar by lithographic techniques is delicate, since short-circuits to the quantum well are detrimental for the experiment. With the STM Weiner *et al.* first imaged the pillars and then positioned the tip on top of one of them. The STM allows to compare I-V's obtained on a large number of adjacent pillars.

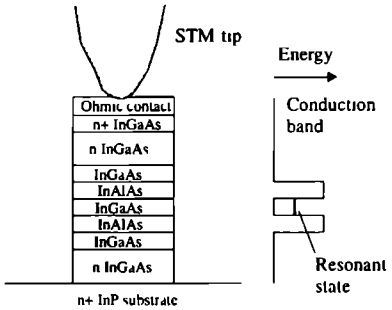

Figure 1 7 *Tip contacting an InGaAs/InAlAs resonant tunneling pillar The bound state is the resonant level*

1.5 Atomic scale manipulation and spectroscopy

As a last example we discuss a series of experiments performed by Eigler *et al* [37, 38, 39, 40] which have opened the perspective of atomic scale devices In their experiments the STM is used both to fabricate a structure as well as to determine its electronic properties via tunneling spectroscopy (as discussed in Section 1 3) Fabrication takes place on the atomic scale With the STM-tip individual adatoms on a flat surface can be pulled to desired locations and in this way it is possible to construct arbitrary geometries atom by atom

The adatom sliding process is possible due to the finite force that is always exerted by the STM-tip on an atom By adjusting the tip-atom distance and the tip voltage this force can be tuned [37] This allows to either drag atoms to differ-

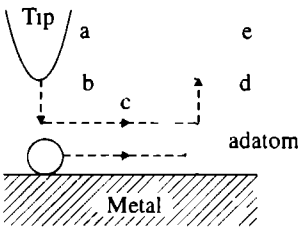

Figure 1 8 *The process for sliding an atom across a surface used by Eiglei et al [37] First, the tip is located directly over an atom (a) Then the tip is lowered to postion (b) At this tip-atom distance the attractive force is sufficient to drag the atom (c) to a different spot (d) Finally, the tip is withdrawn to (e) At this distance the atoms can be imaged without changing their position*

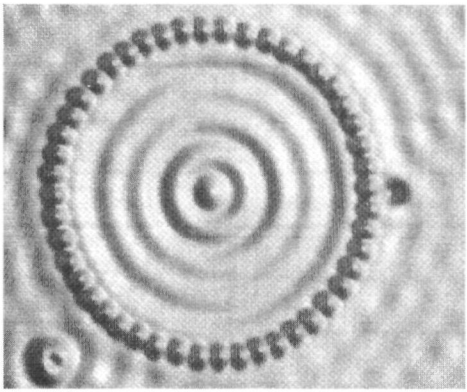

Figure 1.9: *A corral of Fe atoms, fabricated atom by atom on top of a Cu surface. Inside and outside the corral the interference pattern can be clearly observed. (Reproduced from [39], with permission.)*

ent spots, or to image them without changing their position. The process Eigler *et al.* use to move the atoms is shown in Figure 1.8. The very low contamination rates and the stability required for their experiments is achieved by performing the experiments at a temperature of 4 K, in a UHV compatible instrument.

Artificial structures fabricated by the adatom sliding technique can be used to confine conduction electrons at a nanometer lengthscale. At the close-packed surfaces of noble metals electrons form a two-dimensional nearly free electron gas. Adatoms on top of this surface scatter the two-dimensional electron gas and in the vicinity of these atoms standing wave patterns in the local density of states at the metal surface have been observed. By fabricating corrals or stadiums of adatoms electrons are not only scattered, but can also be confined inside these closed structures. With spatially resolved tunneling spectroscopy (see Section 2.3) Eigler *et al.* have succeeded in imaging (Figure 1.9) the local amplitudes of the bound states wavefunctions expected from these confinements [39, 40, 41].

1.6 Limitations

At the end of this brief overview it is important to note that there are several limitations to scanning tunneling microscopy. An important one is that the technique can only be used on conducting surfaces. Once the tip encounters an insulating area the STM-feedback system will push the tip into the sample,

which will usually end the experiment This complicates for instance the use of STM in combination with the transport structures discussed previously (in these structures large parts of the surface are insulating) To overcome this limitation atomic force microscopy can be a good alternative Atomic force microscopes can be operated on insulating surfaces When the tip of the AFM-cantilever is coated with a metal layer similar spectroscopic abilities as with an STM should be within reach

A second limitation is the sensitivity of STM for contaminants at the surface Contaminated surfaces give unpredictable effects in the local density of states, and complicate the interpretation of the results The reason that very small disturbances already can dominate the observed spectra, is the absence of spatial averaging in STM measurements Apart from the advantages of the very high spatial resolution of scanning tunnelin microscopy, it also imposes severe demands on the quality of the surfaces

1.7 Thesis outline

In Chapter 2 of this thesis several technological aspects of low temperature scanning tunneling microscopy will be addressed In the first part the two microscopes that have been developed during this research are discussed as well as the considerations that have led to the two designs Both STMs are designed for operation at low temperatures, one for ^{4}He-temperatures (the ^{4}He-STM) the other for temperatures below 1K (the ^{3}He-STM) In the second part of the chapter we focus on the STM-electronics

Chapter 3 reports about our low temperature STM studies of the InAs (110) surface The objective of this work was to investigate the possibilities for investigating a surface two dimensional electron gas (2DEG) with an STM Such 2DEGs have been reported to be present at InAs surfaces, and therefore this material was chosen for our experiments In magnetic field we have been able to observe the Landau levels with the STM These measurements are the first observations of Landau levels with a scanning probe technique

In Chapter 4 we show the dramatic effects in the band-bending at a semiconductor surface, when a small grain on top of it is charged with a single electron In the experiment the STM-tip is both used to charge the grain and to probe the electron density The experiment shows that the quantized charge on the grain results in switching of the band-bending at the semiconductor surface when the grain is charged

In Chapter 5 we report the observation of vortices in a normal film on top of a superconductor The vortices have a mosaic-like shape and are due to the proximity of the superconductor The measurements are an extension to the planar junction spectroscopy experiments on the proximity effect in the 1960s With STM we have been able to perform tunnel spectroscopy with a high spatial resolution and to relate these measurements to the topography of the sample It appears that the mosaic-like shape of the vortices reflects the granular structure of the normal metal film

Chapter 6 describes an experiment in which we have used the ^{3}He-STM to investigate the spatial properties of vortices in a Josephson junction array In this experiment it was necessary to coarse position the tip at ^{3}He-temperatures Further the experiment allows to investigate the influence of the STM on the temperature of the system

References

[1] G Binnig, H Rohrer, Ch Gerber, and E Weibel, Appl Phys Lett **40**, 178 (1992)

[2] G Binnig, C F Quate, and C Gerber, Phys Rev Lett **56**, 930 (1986)

[3] *Near field optics*, edited by D W Pohl and D Courjon, (Kluwer, Dordrecht, 1993)

[4] B J van Wees, H van Houten, C W J Beenakker, J G Williamson, L P Kouwenhoven, D van Marel, and C T Foxon, Phys Rev Lett **60**, 848 (1988)

[5] D A Wharam, T J Thornton, R Newbury, M Pepper, J E F Frost, D G Hasko, D C Peacock, D A Ritchie, and G A C Jones, J Phys C **21**, L209 (1988)

[6] M A Reed, J N Randall, R J Aggerwal, R J Matyi, T M Moore, and A E Wetsel, Phys Rev Lett **60**, 535 (1988)

[7] C G Smith, M Pepper, H Ahmed, J E Frost, D G Hasko, D C Peacock, D A Ritchie, and G A C Jones, J Phys C **21**, L893 (1988)

[8] T A Fulton and G J Dolan, Phys Rev Lett **59**, 109 (1987)

[9] L S Kuzmin and D B Haviland, Phys Rev Lett **67**, 2890 (1990)

[10] Physics Today, 21 (June 1994), F P Millikan, C P Umbach, and R A Webb, Solid State Commun **97**, 309 (1996)

[11] H Takayanagi and T Kawakami, Phys Rev Lett **54**, 2449 (1985)

[12] R A Webb, S Washburn, C P Umbach, and R B Laibowitz, Phys Rev Lett **54**, 2696 (1985)

[13] L J Geerligs, M Peters, L E M de Groot, A Verbruggen, and J E Mooij, Phys Rev Lett **63**, 326 (1989)

[14] H S J van der Zant, F C Fritschy, W J Elion, L J Geerligs, and J E Mooij, Phys Rev Lett **69**, 2971 (1992)

[15] W J Elion, J J Wachters, L L Sohn, and J E Mooij, Phys Rev Lett **71**, 2311 (1993)

[16] P J M van Bentum, R T M Smokers, and H van Kempen, Phys Rev Lett **60**, 2543 (1988)

[17] R Wilkins, E Ben-Jacob, and R C Jaklevic, Phys Rev Lett **63**, 801 (1989)

[18] J G A Dubois, E N G Verheijen, J W Gerritsen, and H van Kempen, Phys Rev B **48**, 11260 (1993)

[19] C T Black, M T Tuominen, and M Tinkham, Phys Rev B **50**, 7888 (1994)

[20] C Schonenberger, H van Houten, and H C Donkersloot, Europhysics Lett **20**, 249 (1992)

[21] J G A Dubois, J W Gerritsen, E J G Boon G Schmid, and H van Kempen, in *Coulomb and interference effects in small electronic structures*, eds D C Glattli, M Sanquer, and J Trân Thanh Vân (Editions Frontières), 305 (1994)

[22] J G A Dubois, J W Gerritsen, S E Shafranjuk, E J G Boon, G Schmid, and H van Kempen, Europhysics Lett **33**, 279 (1996)

[23] D C Ralph, C T Black, and M Tinkham, Phys Rev Lett **74**, 3241 (1995)

[24] E L Wolf, *Principles of electron tunneling spectroscopy* (Clarendon press, New York, 1985)

[25] I Giaever, Phys Rev Lett **5**, 147 (1960)

[26] I Giaever, Rev Mod Phys **46**, 245 (1974)

[27] J Bardeen, Phys Rev Lett **6**, 57 (1961)

[28] A more extended discussion about the role of the density of states in tunneling characteristics can be found in R T M Smokers, Ph D thesis (1992), University of Nijmegen, the Netherlands

[29] W A Harrison, Phys Rev **123**, 85 (1961)

[30] H F Hess, R B Robinson, R C Dynes, J M Valles, Jr and J V Waszcak, Phys Rev Lett **62**, 214 (1989)

[31] J D Shore, M Huang, A T Dorsey, and J P Sethna, Phys Rev Lett **62**, 3089 (1989)

[32] H F Hess, R B Robinson, J V Waszcak, Phys Rev Lett **64**, 2711 (1990)

[33] Ch Renner, A D Kent, Ph Niedermann, Ø Fischer, and F Lévy, Phys Rev Lett **67**, 1650 (1991)

[34] I Maggio-Aprile, Ch Renner, A Erb, E Walker, and Ø Fischer, Phys Rev Lett **75**, 2754 (1995)

[35] H L Edwards, J T Markert, and A L de Lozanne, Phys Rev Lett **69**, 2967 (1992)

[36] J S Weiner, H F Hess, R B Robinson, T R Hayes, D L Sivco, A Y Cho, and M Ranade, Appl Phys Lett **58**, 2402 (1991)

[37] D M Eigler and E K Schweitzer, Nature **344**, 524 (1990)

[38] M F Crommie, C P Lutz, and D M Eigler, Nature **363**, 524 (1993)

[39] M F Crommie, C P Lutz, and D M Eigler, Science **262**, 218 (1993)

[40] E J Heller, M F Crommie, C P Lutz, and D M Eigler, Nature **369**, 464 (1994)

[41] S Crampin, M H Boon, and J E Inglesfield, Phys Rev Lett **73**, 1015 (1994)

Chapter 2

Two low-temperature scanning tunneling microscopes for use on artificially fabricated nanostructures

Abstract: We have developed two scanning tunneling microscopes (STMs), one for ^{4}He-temperatures, the other for temperatures below 1 K, dedicated for use in mesoscopic experiments. The designs have emerged from a number of requirements, such as mechanical stability, operation at low temperatures and the ability to coarse position the STM-tip relative to the sample in three dimensions. In order to optimize the mechanical stability several design criteria are deduced from a simple, but powerful model. The complications of scanning tunneling microscopy at low temperatures are discussed The main differences in the two designs are a consequence of the different methods used for cooling tip, sample and the other parts. Both STMs have coarse approach mechanisms in three dimensions at low temperatures and therefore they enable experiments in which mesoscopic phenomena are investigated by using the unique combination of scanning tunneling microscopy and artificially fabricated nanostructures Also in this chapter some general aspects of scanning tunneling microscopy are addressed, like surface preparation and the electronic setup

Parts of this chapter have been published in *A Low-temperature scanning tunneling microscope for use on artificially fabricated nanostructures*, by J.W G Wildöer, A J.A van Roij, H van Kempen, and C J P M Harmans, Review of Scientific Instruments **65**, 2849 (1994)

2.1 Introduction

When scanning tunneling microscopy was invented in the early 1980s by Binnig and Rohrer [1, 2] its potential was recognized immediately Although the motivation for the invention did come from solid state physics, scanning tunneling microscopy and other scanning probe techniques are now used throughout science STMs for various conditions are commercially available nowadays, however still technological limitations form often a major obstacle in their application This can be due to special constraints in the experiment, like operation at very high or very low temperatures, or scanning at high speeds or with extreme stability But also the preparation of the sample can impose difficulties In 1991 when this research was started low temperature STMs where scarcely available and seldom with good reputations Therefore, and because of our own specific requirements, it was decided to develop the STM(s) ourselves

In scanning tunneling microscopy a conducting tip is positioned above a conducting surface close enough to establish a tunnel current through the vacuum barrier In order to control the width of this barrier, the tip is mounted on an actuator consisting of a piezo-electric element [3] If now the tip is moved parallel to the surface the tunnel current can be kept constant by continuously adjusting the actuator (Figure 2 1) The control of the tunnel current is performed by a feedback system By monitoring the signal applied to the actuator a topographic picture of the surface can be obtained

The piezo-elements for adjusting the vacuum barrier and for moving the tip in

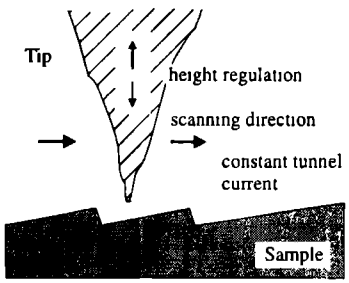

Figure 2 1 *Schematic of a scanning tunneling microscope The tip height is regulated by an actuator The recorded image corresponds with the profile of constant tunnel current*

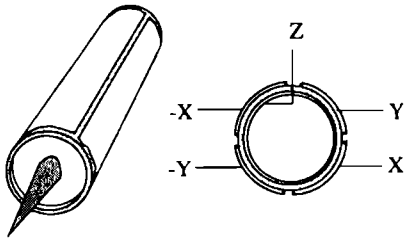

Figure 2 2 *Scan tube Voltages applied to the outer electrodes give a deflection of the pieze tube in the x or y direction With the inner electrode the tube can be contracted or elongated*

the lateral directions are almost always integrated in one piezo-electric tube the scan tube [4], shown in Figure 2 2 The configuration of the electrodes makes it possible to bend the tube perpendicular to its axis (x,y direction) and to elongate it along its axis (z direction) The range of a scan tube is however limited to a few μm in all three directions Therefore, to bring the tip within this range of the sample, a coarse approach mechanism is required The coarse positioner should be accurate (within a μm) and not influence the stability of the STM For this problem quite a number of solutions has been developed since the invention of scanning tunneling microscopy [5, 6, 7, 8] For low-temperature STMs the reliability of the coarse positioner(s) is a serious point of concern

2.2 Mechanical stability

The mechanical stability of an STM is of crucial importance To achieve a stable tunnel barrier, variations in the tip-sample distance caused by vibrations, thermal drift or other sources have to be less then 0 01 nm Building vibrations have typical amplitudes of 10 to 100 nm, at frequencies ranging from 1 to 100 Hz [9, 10], and so attenuation of these vibrations is required This reduction of the effective vibration amplitudes is achieved in two ways

The first measure is to decouple the STM mechanically from its environment (preferably a very quiet one) This is usually done by placing the STM or the STM setup on dampers, or suspending it with springs These kinds of vibration isolation form low-pass filters for the external disturbances [10]

Secondly, the STM itself acts as a high-pass filter for vibrations Vibrations may stir the STM as a whole, but the relevant displacements are those from tip

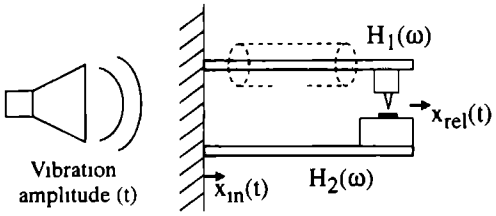

Figure 2 3 *Two stiff, one-sided-clamped beams, representing the STM model Vibrations enter via their mechanical connection to the environment The dotted cylinder represents the scantube, which limits the smallest possible beam length*

and sample relative to each other Because of the stiffness of the STM construction, vibrations of low frequency that enter the STM will move tip and sample in the same way, giving only small relative displacements, while with vibrations of higher frequencies these relative displacements will be larger To investigate this high-pass behavior we can model an STM by two stiff beams, one suspending the tip, and the other the sample holder At one end, both beams are clamped Tip and sample holder are at the free ends of the beams (Figure 2 3) Both beams have their own (high) resonance frequency and will each show a low-pass behavior, but since it is the relative displacement from tip to sample that matters, the total response is the difference between the two and forms a high-pass filter It is important to note that this argument only holds when the vibrational perturbations come in at *one* point in the STM The resonance frequency of the STM is then the lowest resonance frequency of the two levers Figure 2 4 shows the model and the response function of both the vibration isolation and the STM itself The combination of the two response functions gives the total response to external vibrations The attenuation factor is to first approximation given by the squared ratio of the two resonance frequencies $(\nu_2/\nu_1)^2$ (the attenuation is lower if damping terms are included, for example in the springs with which the STM is suspended) [11]

So, concerning the effect of vibrations, mechanical stability is achieved by installing the experimental set-up at a quiet area of the laboratory, using a suspension with a low resonance frequency and ensuring that the STM has a high resonance frequency High resonance frequencies are obtained by constructing the STM to be rigid, lightweight, and as compact as possible In Appendix A calculations are performed on a beam as in Figure 2 3 From these calculations a qualitative understanding can be obtained of how the various parameters influence the resonance frequency of the STM The most important conclusion is that

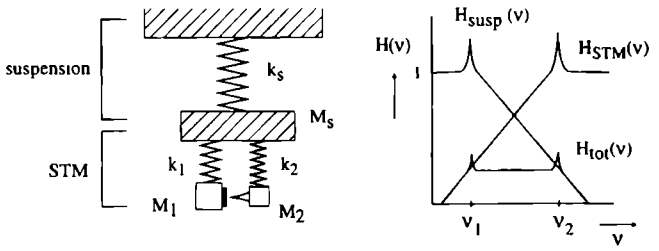

Figure 2 4 *Schematic representation of the model which describes the reponse to vibrations of the STM The spring constants k_s, k_1, k_2, and the Masses M_s, M_1, M_2 determine the resonance frequencies ν_1 and ν_2 The result is a band-pass filter which gives a large attenuation of the external vibrations (the scales in the plot are logarithmic)*

the resonance frequency of a beam is roughly inversely proportional to its length squared The mass M with which the levers are loaded lowers the resonance frequency with $\sqrt{M}$, while the material of which the levers are constructed gives a factor $\sqrt{E/\rho}$, where E is the elasticity and ρ the specific mass More details about these dependences can be found in Appendix A The smallest possible size of an STM is determined by the length of its scantube Therefore the design is usually a compromise between a large scan range (long scan tube) and a high stability (compact design) The used materials in an STM are usually stainless steel or titanium, however always some parts of the STM consist of piezoelectric material, which is less stiff than those two materials Some relevant materials properties are summarized [12] in Table 2 1 In optimizing the design, one has to consider which parts of the STM have a supporting function and which parts act as a load The masses of the loads have to be kept as small as possible

From our STM model of Figure 2 3 we can deduce yet another design consideration With a given length of the mechanical connection, through the STM, between tip to sample (for example because of the length of the scantube), the resonance frequency can still be optimized by choosing the point where the vibrations enter the STM very carefully In the model it is the lowest resonance frequency of the two beams that determines the response function of the STM Carefully selecting the entrance point for the external vibrations can increase the lowest resonance frequency of the two and therefore the total resonance frequency Figure 2 5 shows an arbitrary (A) an optimized (B) case

Material	Elastic modulus E (10^{10} Pa)	Density ρ (10^3kg m^{-3})	$\sqrt{E/\rho}$ (10^3Hz m)	Thermal conductivity (W m^{-1} K^{-1}) at 4 K
Stainless steel	21	7.8	5.2	0.2 - 0.3
Titanium	12	4.5	5.2	1 - 2
Copper	12	8.9	3.8	10^2 - 10^3
Berilium	30	1.8	12.9	2.5
Piezo	12.8	7.8	4.1	1.5 (300 K)

Table 2.1: *Some relevant material parameters. The highest value for $\sqrt{E/\rho}$ is achieved by using berilium, however this material is toxic. The thermal conductivity values of the metals are obtained from [13] (polycrystaline, non-anealed metals). For copper the thermal conductivity is stongly dependent on the purity of the material. The value given for stainless steel is for AINSI 316 (as is used in both STMs. The piezo-electric is PZT5A, the thermal conductivity is a room temperature value [14] (No value for 4 K was available).*

2.3 STM at low temperatures

Scanning tunneling microscopy at low temperatures relies on the same principles as are discussed already, however some technical problems complicate the design. An obvious constraint is that thermal expansion coefficients of the different parts of the STM should be comparable. Since the scanhead always includes one or more parts of piezo-electric ceramics, this implies that the choice of the other materials is restricted to those with a thermal expansion coefficient (at room temperature) of the order of 2×10^{-6} K^{-1} [15]. For example stainless steel and titanium meet this requirement. These materials however are bad heat conductors at low temperatures (see Table 2.1), and therefore cooling the STM, tip and

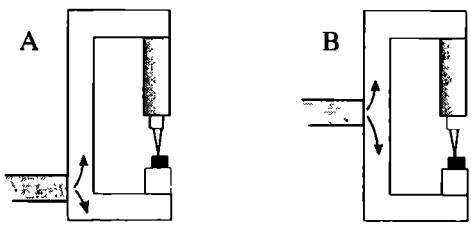

Figure 2.5: *The entrance point for mechanical vibrations in an arbitrary (A) and an optimized case (B).*

sample requires additional measures At ^{4}He temperatures the STM is either immersed directly in the helium bath [16] or is enclosed by a vacuum can filled with helium gas [17] (for heat exchange with the helium bath) before it is cooled down At temperatures below 1 K exchange gas can not be used anymore Temperatures below 1 K can be achieved in a dilution refrigerator or by pumping down a can with ^{3}He liquid In these setups cooling can take place either by attaching heat sinks to the STM, or by placing the whole STM in the mixing chamber of the dilution refrigerator or the ^{3}He-can of the ^{3}He-insert The use of heat sinks has the disadvantage that the attachment of a number of leads to the STM will reduce its mechanical stability and will complicate the functioning of coarse approach mechanisms In addition the temperature will be less well defined The solution of placing the STM in a ^{3}He-^{4}He mixing chamber or a ^{3}He-can guarantees a well defined temperature but dramatically complicates operation ^{3}He is an expensive gas and precautions have to be taken not to spoil it Also, the solution requires the use of special purpose cryogenic systems since the commercially available ones in general do not offer entrance to the mixing chamber or the ^{3}He-can

For coarse positioning tip and sample at low temperature it is preferable not to use methods which require mechanical feedthroughs from room temperature Specially for temperatures below 1 K a mechanical feedthrough introduces many complications [18] and can give rise to substantial heat input at low temperature Therefore usually coarse approach mechanisms are used which operate with piezoelectric elements The forces or displacements generated with the piezoelectric elements are used to move parts of the STM with respect to each other Most of these approach mechanisms depend very critically on the friction forces between the sliding surfaces Large changes in the friction forces due to cooling down or wear of the sliding surfaces will result in unreliable operation

One of our objectives has been to investigate mesoscopic systems, using STM in combination with artificially fabricated nanostructures A critical aspect in these experiments is to position the tip above the nanostructure Thermal deformation of the STM in cooling from room temperature will be substantial, and as generally only one structure will be available on a substrate, coarse approach mechanisms in the plane of the sample are necessary In combination with these coarse approach mechanisms smart systematic searching procedures are required since the probability of finding the very small nanostructure by chance is extremely small

In the course of this project we have developed two STMs, one for ^{4}He tem-

peratures and one for temperatures below 1 K Of the first type four units have been build, which all have slight differences, depending on the kind of experiments for which they are used Of the second type one example has been build First we will discuss the ^{4}He STM [19]

2.4 The ^{4}He-STM

Figure 2 6 shows the ^{4}He-STM The scantube [20] is mounted inside a plunger which can be moved up and down by an inertial slip-stick mechanism [21, 22] The motion is activated by the outer piezo tube (B) For positioning in the x-y plane we use a sample holder which can translate the sample separately in x and y direction The compact sample holder also uses an inertial slip-stick mechanism and is easily mounted to the rest of the STM We will describe the sample holder in detail later on If no positioning in the x-y plane is required the sample holder is replaced by one without an x-y translation facility The STM is attached to an insert or any other holder as shown in the figure Vibrational perturbations reach the STM through this mechanical connection In order to prevent the mass of our x-y sample holder from decreasing the resonance frequency of the STM, we have chosen the connection area close to the position of the sample holder

The inertial slip-stick mechanism employs the very large accelerations that can be generated by piezoelectric elements A mass will slide if the inertial force acting on it is larger than the static friction The stainless steel plunger (D) is clamped by two leafsprings which are spark eroded in a stainless steel tube (C) as shown in Figure 2 7 [23] This holder is glued on the outer piezo tube with Stycast low-temperature epoxy [24] An appropriate waveform applied to the piezotube enables the plunger to slide To prevent degrading by wear we covered the very smooth surface of the plunger with a hard ceramic layer [25] The plunger has a mass of 4 2 g and the static friction force between holder and plunger is adjusted between one and two Newton by deforming the two leafsprings Since the plunger is only coated with a thin ceramic layer, but essentially is made of the same material as its holder, large changes in the friction force during cooling down are avoided The outer piezo tube, a PZT 5A tube with length 12 7 mm and thickness 0 8 mm, also thermally compensates the scan tube

To bring the tip within tunneling range, the plunger is moved downwards with single steps In between the steps the scantube is elongated and contracted with the STM feedback system operating, sensing if a next step can be made As soon as a tunnel current is detected, the approach is stopped and the scan tube

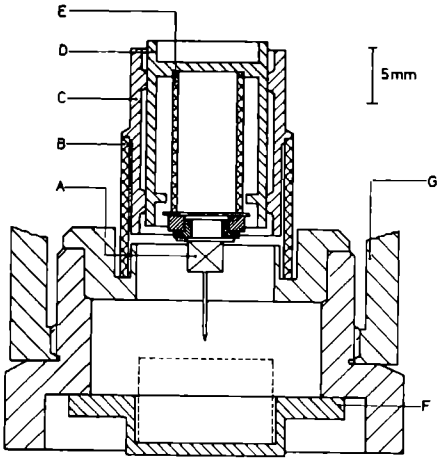

Figure 2.6: ^{4}*He-STM: (A) tip holder, (B) outer piezo tube, (C) holder for plunger, shown more in detail in Figure 2.7, (D) plunger, (E) scantube, (F) sample holder, the dashed line indicates the total size of the x-y course positioner, (G) suspension of the STM.*

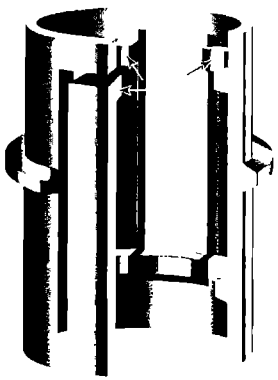

Figure 2.7: *Holder for plunger. The friction force can be adjusted by deforming the two leafsprings. The plunger tightly fits in the holder, giving large contact area's at the sliding points (indicated by the arrows). This will reduce wear of the sliding surfaces.*

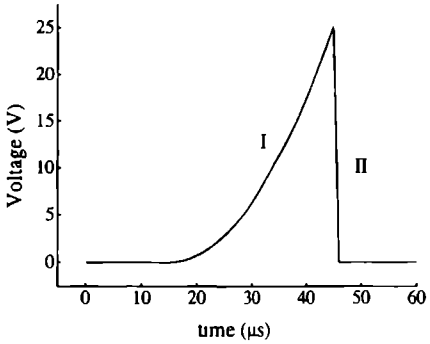

Figure 2 8 *Waveform applied to the outer piezo tube during tip approach At room temperature we use an amplitude of 25 V At 4 2 K a four times larger amplitude is required*

will regulate the tip-sample distance By approaching in this way the occurence of tip-crash will be avoided The waveform we apply to the outer piezo for the approach is depicted in Figure 2 8 The first part of the waveform will accelerate the holder downwards in such a way that the inertial force on the plunger is lower than the static friction force So both holder and plunger will gain velocity in the downward direction during this interval This part of the waveform is parabolic, giving a large constant acceleration Immediately after this the piezo tube is elongated very rapidly by the second part of the waveform, forcing the plunger to slide downwards with respect to the holder The waveform is generated by a Wavetek arbitrary waveform generator [26] and amplified by a homebuild high-voltage amplifier with a bandwidth of 50 kHz To move upward we just change the polarity of the waveform At room temperature voltages between 20 and 30 V are required to move the plunger

Precise lateral positioning of the sample with respect to the tip can be essential for some of the experiments The sample holder we developed for this purpose is shown in Figure 2 9 It also uses the inertial slip-stick mechanism, but here the accelerations are generated in the horizontal plane [8, 27] Piezo plates are used, which are polarized to give a shear deformation To simplify searching we have separated translations in x and y direction, in this way eliminating the rotational degree of freedom The sample holder consists of two shear piezo's (C) and two sliders, one set for each direction Because the sliders can only move in the direction of the supporting rails, rotation of the sample in the x-y plane is prevented To improve the stability the two sliders are clamped to the

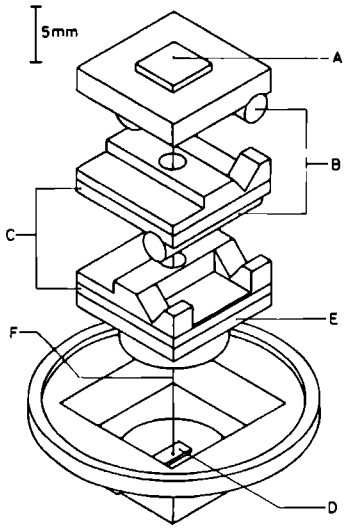

Figure 2 9 *Sample holder (A) sample, (B) zirconium oxide rods, (C) shear piezo plates, (D) leafspring used for clamping the sliders, (E) stainless steel support, (F) wire connecting the upper sample holder plate to the leafspring*

other parts of the sample holder by a wire connected to a leafspring (D) This measure also prevents the sliders from moving unintentionally The waveform we use for moving the sliders is the same as the one that drives the plunger However, because masses and friction forces are different, the amplitudes and the frequencies have to be adapted To prevent degrading by wear of the sliding surfaces we aimed for large contact areas at the three points of support of the slider Therefore the sliding surfaces are polished with a large radius in at least one direction That means that for instance the grooves opposite of (B) are slightly curved in the direction of the axis of (B) Also we covered the sliders with the same ceramic we used for the plunger The supporting rods are made of zirconium oxide, also a hard, wear-resistant ceramic

During cool down residual gases may condense on the STM, tip and sample Since the moveable parts of the STM are sensitive to contamination, the STM, when used at low temperatures, is enclosed by a vacuum can, which is filled with pure helium gas The helium gas provides the heat exchange during cooling down At low temperatures, because of reduced piezo sensitivity, higher voltages are needed to operate the course positioners of the STM At 4 2 K we use voltages that are four times higher than at room temperature With these two measures

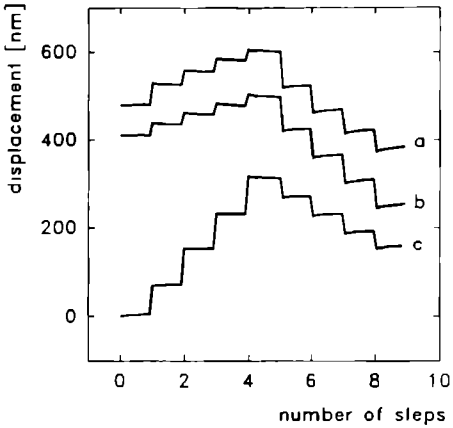

Figure 2 10 *Sequences of single steps, measured in both directions for all three coarse positioners The measurements are taken at 4 2 K For the x and y coarse positioner we used an amplitude of 130 V, for the z coarse positioner 110 V*

taken the STM shows very reliable performance

Single steps of the coarse positioners can be measured with the tip within tunneling range A step in the vertical direction will then be depicted by the STM feedback system as a change in height By tunneling on a smooth tilted surface steps in the x and y direction can be measured in the same way In Figure 2 10 sequences of single steps are shown for all three course positioners measured in this way on graphite Although the covered distance with each step appears to be dependent on the direction of the step in each curve [28], all three coarse positioners show reliable performance

To isolate the STM from building vibrations the whole cryostat is suspended by bungee cords Extensive vibration isolation of the STM itself by using spring or levers in the insert is often awkward, for example in the case when high magnetic fields should be available However the STM has to be isolated in some way from the vibrations caused by the boiling liquid nitrogen in the cryostat In our setup this isolation was achieved by separating the cryostat and the insert by two sets of O-rings as shown in Figure 2 11 By this construction the metal-metal contact between cryostat and STM is interrupted so that the high-frequency vibrations are damped Another measure to reduce external vibrations is the use of plastic bellows for the helium recovery

Since in some experiments only a few (sometimes only one), very small structures will be available on a sample precise relative positioning of the tip can be

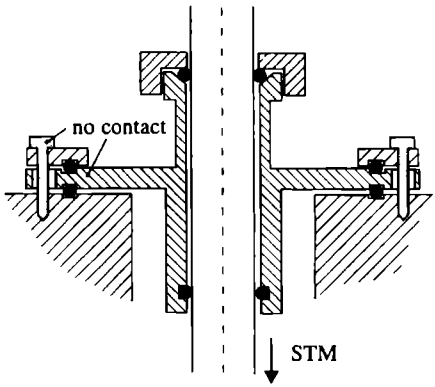

Figure 2 11 *The STM-insert is mechanically isolated from the high frequency vibrations of the cryostat by two sets of O-rings*

essential Initial positioning at room temperature will not suffice, because the thermal deformation of both scan tube and sample holder will be substantial Once at low temperatures, the exact position of the tip relative to the structure is unknown Fortunately scanning tunneling microscopy offers the possibility to determine the position of the tip by doing topography For this purpose dedicated markers have to be present on the sample, offering sufficient information to search for the mesoscopic structure in a systematic way Such topographic information can be fabricated on the sample by using standard submicron lithography techniques

We can estimate the change in position of the tip relative to the sample after cooling to be well below 100 μm in each direction Therefore the topographic information only needs to be present in the direct vicinity of the structure of interest The approach is to position the tip at room temperature somewhere in the middle of the so-called searching pattern, then retract the tip a few hundred microns, and then start cooling After filling the cryostat with liquid helium, the tip is brought within tunneling range again and with the information offered by the search pattern the sample is moved in such a way that finally the tip can be located at the desired position

An example of a search pattern is depicted in Figure 2 12 The pattern consists of 25-nm-high lines of gold on a gold surface The lines have widths of 100, 200, and 300 nm and have a period in one direction of 2 μm The searching strategy is to first follow the vertical lines with the y coarse approach until the horizontal line is reached The width of the lines provides information whether large displacements can be made or that small ones are required After this we

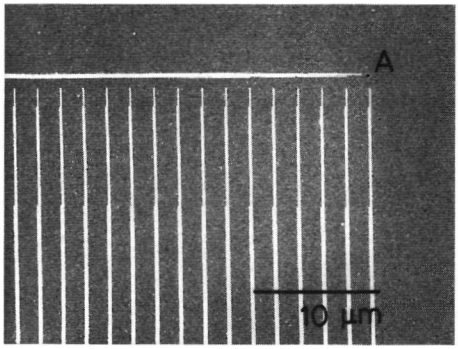

Figure 2.12: *Search pattern. By using the x-y translation facility and the described coarse approch strategy, we can position the tip at any arbitrary spot (here A) of a surface.*

follow the horizontal line using the coarse x approach. Finally, we will reach position A (Figure 2.13), where we want to locate the tip. The advantage of this approach is that, since x and y movements are independent, only single line scans, either in x or y direction, are required to determine the next action. Furthermore, the searching procedure does not rely on an exactly reprodicable step size.

2.5 The ^{3}He-STM

The ^{3}He-STM was developed for use in an existing ^{3}He setup with a closed ^{3}He-can. In the inner vacuum chamber of the ^{3}He insert a rigid copper cold finger provides the thermal contact with the ^{3}He-can. In this system the STM can only be cooled down effectively by attaching heat sinks to it. The obvious material for heat sinks is copper, because of its good thermal conductivity at low temperatures. Heat sinks can for example consist of strips, copper parts or copper wires of a sufficient diameter.

The heat sinks attached to the moving parts of the STM are critical. These heat sinks have to be flexible, but also should give sufficient heat transport. Both requirements are met to some extent by using bundles of thin copper wires. In the ^{3}He-STM a sample holder like the one shown in Figure 2.9 can not be used, since the mechanical forces exerted by the copper wires exceed the inertial forces that can be generated to move the sample (the inertial forces are small because the masses of the sample holder are small). So, to be able to coarse position the

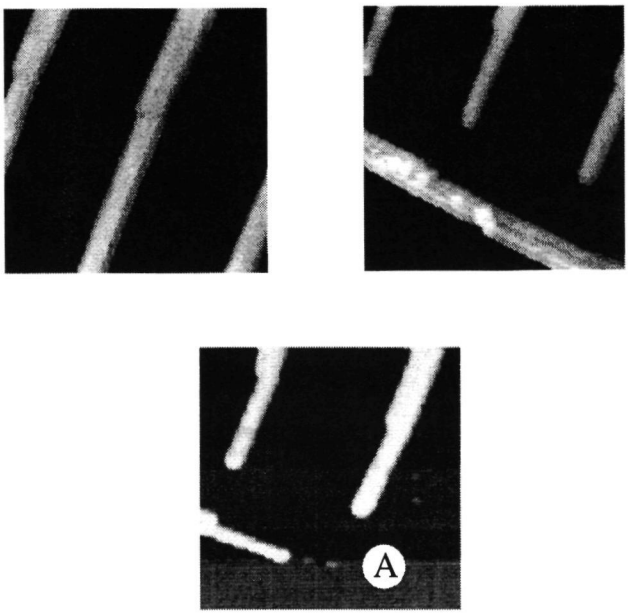

Figure 2.13: *Images made during the searching process. The scan range is about 3μm. The first image is taken directly after tip approach and shows only vertical lines. After reaching the horizontal line the second image is made. The third image shows position A is reached.*

sample also at ^{3}He temperatures a different approach is required.

One way to decrease the sensitivity of the slip-stick mechanism for external forces is to increase the mass of the sliding body, since this will give larger inertia forces. Therefore in the ^{3}He-STM x-y course positioning is achieved by moving the scan head, instead of the small sample sliders as in the ^{4}He-STM. A desirable consequence of this choice is that the sample can be fixed on a static copper holder, which assures very good thermal contact of the sample with the cold finger.

The STM can not be made completely out of copper. Copper is not very stiff (see Table 2.1), and reduces the resonance frequency of the STM. But also it is quite soft, which makes it unsuitable for sliding surfaces. A third problem is the large thermal expansion coefficient of copper. In our ^{3}He-STM we used copper where it was possible, and other materials when necessary. The ^{3}He-STM is shown in Figure 2.14. The scanhead can be moved in the x-y plane by the

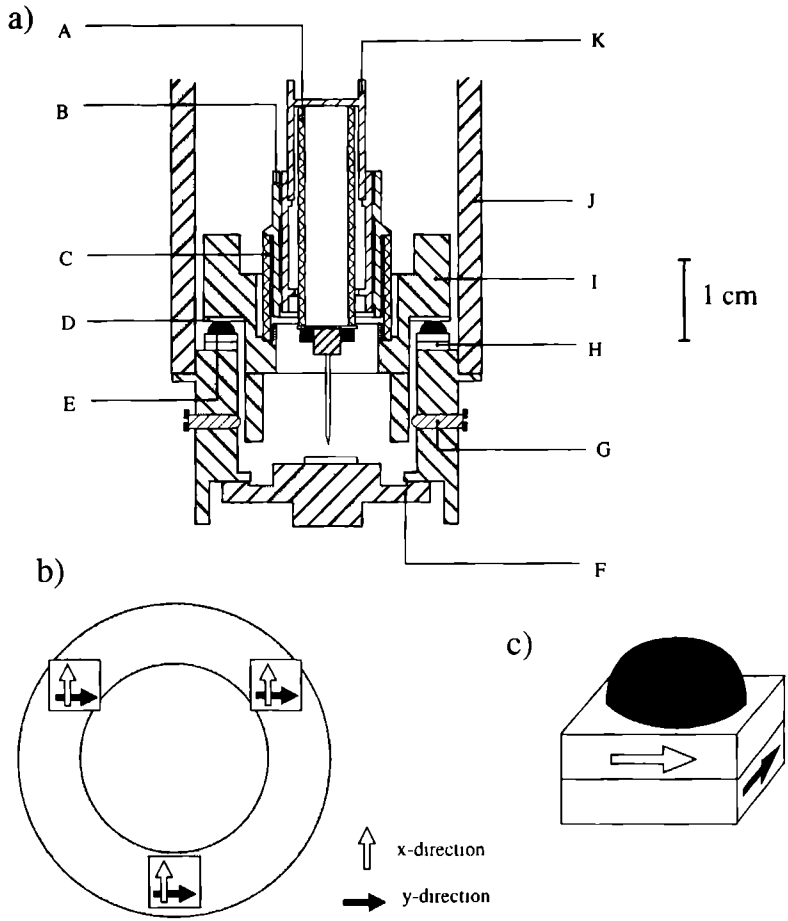

Figure 2.14: *The ^{3}He-STM. The halftone parts are made of copper: (A) scan tube, (B) holder for plunger, shown more in detail in Figure 2.7, (C) outer piezo tube, (D) stainless-steel disk covered with titanium carbo nitride, (E) zirconium oxide balls supporting the scan head at three points, (F) sample holder (copper), (G) adjustment screws, (H) shear piezo plates, (I) body of scan head (copper), (I) suspension of the STM (copper). The suspension also serves as a thermal shield to prevent parts of the STM that are not sufficiently cooled, to increase the effective temperature of the sample. The arrangements of the shear piezo's is shown in b) and c). The scan head can be moved either in x or y direction by inertia forces. The coarse is z-approach is identical to that of the ^{4}He-STM.*

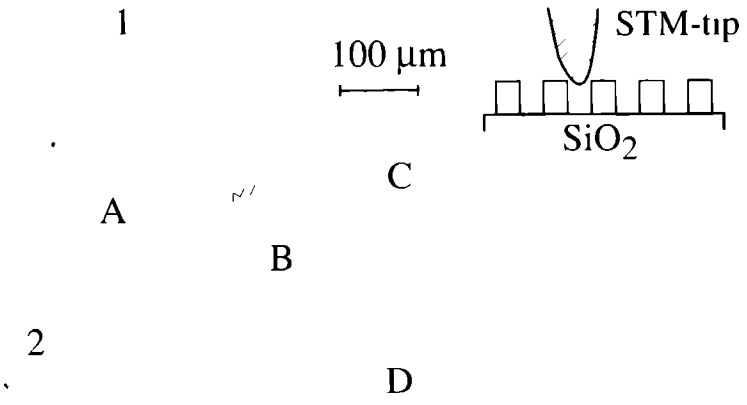

Figure 2 15 *Josephson-junction array (A) A bias current through the array from contact 1 to 2 will generate voltage differences between the superconducting islands of the array The islands at one of the edges of the array (in between the arrows) are attached to Pt lines (B) These lines can be contacted by the STM in between the slabs C and D (detail, other details of the sample are shown in Chapter 6) The lines are separated from eachother by the insulating SiO_2-substrate With a blunt tip however the surface can still be imaged*

six shear piezo's, three for each direction, on top of part (I) Since the mass of the scanhead is large compared to that of the sliders of the sample holder in the ^{4}He-STM, amplitudes and frequencies of the waveform applied to the piezo's have to be adjusted The scanhead is cooled by a bundle of copper wires The z-coarse approach is the same as used in the ^{4}He-STM In order to increase the scansize a longer scantube [29] has been mounted

Since the ^{3}He-STM is largely made out of copper, has more mass and is larger than the ^{4}He-STM it is more sensitive to vibrations Our main objective with this STM is to use it as a displacable contact, with the possibility to search the location of interest However, also with this STM we have been able to obtain atomic resolution

A sample which has been investigated with the ^{3}He-STM is shown in Figure 2 15 The center diamond consists of an array of Al-Al_2O_3-Al Josephson junctions If a current is injected in the array from contact 1 to 2 vortices will

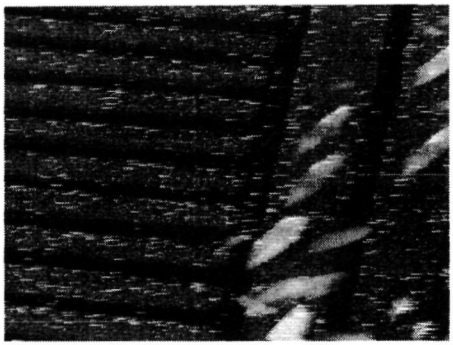

Figure 2.16: *STM image obtained on the sample shown in Figure 2.15. The image is taken in the area where the lines of the large square slabs are interrupted by the lines which are connected to the array. Because of the larger scan area, the image presented here was obtained at room temperature*

flow perpendicularly to the bias current. These moving vortices induce voltage differences between the islands of the array. By monitoring the voltages at the end of the array information about the vortex dynamics in the array can be deduced.

With STM it is possible to measure voltages as a function of position, however it is not possible to perform these measurements directly on the Al islands of the array, since this material gives an insulating surface. For this reason Pt lines were connected to the array, each one in contact with a single superconducting island, and thus showing the same voltages as the end of the array. The lines are high with steep walls and therefore the STM tip will not be able to reach the insulating area's in between. To be able to position the tip above these lines, two slabs of lines of a different direction were patterned on both sides. These lines serve as markers to find the lines of interest.

First, at room temperature, the tip and the structure are aligned relative to each other with an optical microscope and the x-y coarse approach range is limited by adjustment screws. Then, after the tip is retracted several millimeters, the STM is mounted on the ^{3}He-insert and cooled down to 350 mK. At low temperatures one slab is at a positive voltage and the other at a negative voltage. So, after coarse z-approach we can determine by the sign of the detected tunnel current towards which direction we have to move the scanhead. Finally by using this information and the information that is obtained from topographic measurements we reach the lines that are in contact with the vortex array (Figure 2.16).

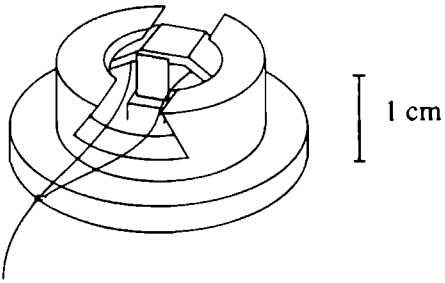

Figure 2 17 *Sample holder with cleaver The copper wire is rolled up around a spindle*

More details about this experiment can be found in Chapter 6

2.6 Surface conditions and preparation

One of the major problems in scanning tunneling microscopy is the preparation of the surface Native oxides at the surface can be thick enough to form an insulating layer, making it impossible to establish a non-contact tunnel current But also thinner oxides will significantly reduce the usefulness of the STM, since usually they show a large density of electron traps Tunneling spectroscopy on such surfaces will mainly yield information about the traps in the oxide, instead of about the material underneath Surface preparation can only be omitted when inert materials are used, such as noble metals or some layered materials

An obvious way to avoid surface oxides to play a role is to do the experiment under UHV conditions However, various other solutions have proven to be successful On semiconductors, for example, a stable surface can be obtained by passivating the surface dangling bonds [30] For STM experiments at low temperature an attractive method is to cleave the sample in situ Since at 4 2 K the vacuum can is cooled down more than 85 Kelvin below the boiling point of oxygen, the vapor pressure of oxygen is extremely low (10^{-15} Torr) Under these conditions surfaces which normally oxidize very quickly, can be studied for several days without serious contamination For this reason, the x-y sample holder in one of the STMs has been replaced by an in situ cleaver, shown in Figure 2 17 The cleaver consists of a small sledge which can be pulled over the sample holder The cleaver can be controlled from outside the cryostat by turning a small spindle in the vacuum can (the axis is a long rod, which extends to outside the insert) A thin copper wire rolled up around the spindle forces the sledge to cleave the

sample In measurements extending over three days and more on III-V compound semiconductors we have not observed any oxygen contamination at the sample surface

2.7 STM control electronics

The distance between tip and sample is regulated by a feedback system [31], which is schematically represented in Figure 2 18 At a constant tip-sample bias voltage the tunnel current is kept at a preset reference value by continuously adjusting the tip height The STM control electronics compares the measured tunnel current with the reference current and changes the voltage on the z-piezo accordingly During scanning in the constant current mode the tip-height is varying continuously, and it is the speed of the feedback system that determines the allowed scan speed A constant current image is obtained by monitoring the voltage applied to the z-piezo as function of the x and y position of the tip

As in any feedback system phase shifts at higher frequencies make it necessary to limit the gain of the various component in the feedback loop and therefore compromises have to be made concerning the speed of the control system

The electronic part of the feedback system is usually incorporated in a so-called control unit The control unit allows for example to modify the feedback parameters, to set the desired scan area, or to change the tunnel bias voltage Parameters are set by hand (adjusting potentiometers) or by computer (using a GPIB port) Control units are widely commercially available In the work presented in this thesis an Omicron control unit [32] has been used

2.8 Measurement modes

In addition to the previously discussed constant current mode, various other ways exist to operate an STM

To image arbitrary surfaces the constant current mode is the one mostly used In this mode the feedback system is continuously active and therefore the risk of a tip crash is minimized At very flat surfaces the constant *height* mode can be preferred In this mode the feedback is off, or very slow, and surface is imaged by mapping the tunnel current as a function of position In the constant height mode the scan speed is not limited by the feedback system, however the danger of a tip crash is apparent

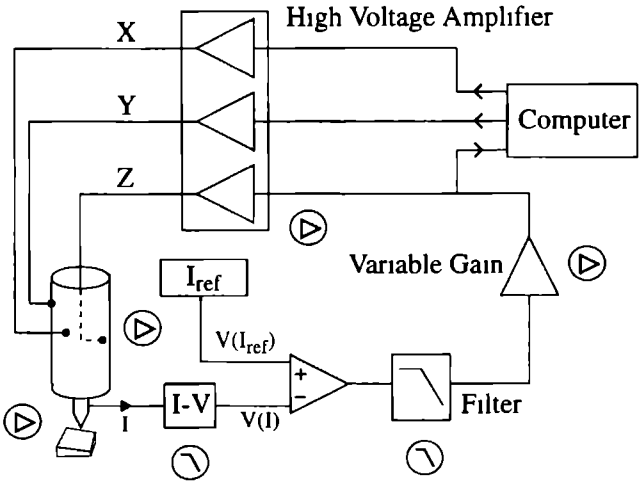

Figure 2 18 *Schematic of the STM electronic circuit At several locations in the feedback circuit the signal is amplified or filtered The small circles indicate the location where either filtering (low pass symbol) or amplification (triangle) takes place A voltage applied to the z piezo results in a change in tip height, which gives a different tunnel current The gain of this part is strongly non-linear, since the tunnel current depends exponentially on the tip sample distance Therefore the system may oscillate at higher reference currents*

Also when spectroscopy curves are obtained with the STM, the feedback system has to be switched off In the spectroscopy mode the tunnel current is measured as a function of the applied bias voltage, at constant tip-sample distance The tip-height is set with the feedback system active by the chosen values for the tunnel voltage (V_{set}) and the reference current (I_{ref}) After the feedback has been switched off, the bias voltage is sweeped over a preset range in a time of the order of seconds Subsequently, the feedback system is activated again

In a similar mode one can obtain the tunnel current as a function of the tip-sample distance Here, with the feedback off, the tip-height is varied gradually over a certain interval With this type of measurement information about the height and the shape of the tunnel barrier can be acquired Since the STM feedback compares the tunnel current with a reference current it is clear why in this mode and in the spectroscopy mode the feedback should be interrupted

With the Omicron control unit it is possible to perform these measurements spatially resolved At every point first the tip-sample distance is regulated, and

then, with the feedback off, either the bias voltage or the tip-sample distance is swept

Another way to obtain information about the distance or bias voltage dependences of the tunnel current is to modulate these parameters with a small ditter signal The frequency should be too high for the present feedback settings, but should also be low enough to be able to measure the effect on the tunnel current clearly With a lock-in the derivative of the dependences can be obtained from the in-phase signal

As a last measurement mode we will discuss the contact mode By placing the STM-tip gently on top of the surface, contacts can be made on distinct places of the sample The procedure is usually to first image the area of interest, and then after the feedback has been switched off, to bring the tip in contact with the sample by adjusting the voltage on the z-piezo by hand In the contact mode currents are much larger and therefore a less sensitive IV-convertor can be used

2.9 Energy resolution in tunneling spectroscopy

One of the important applications of STMs is the use in tunneling spectroscopy Tunneling spectroscopy allows to measure the density of states (DOS) as a function of energy by varying the voltage over a tunnel barrier (see Chapter 1) While in topography measurements the spatial resolution is important, in spectroscopic measurements the energy resolution determines what details can be resolved

At moderate temperatures the energy resolution is in the first place limited by the Fermi-Dirac distribution of the conduction electrons on both sides of the tunnel barrier Filled states above the Fermi energy and empty states below the Fermi energy give a thermal spread in the spectroscopy measurements of $\sim 3k_BT$ At room temperature the energy resolution is therefore limited to $\sim$80 meV, at 4 K the resolution is improved to $\sim$1 meV

As the temperature is reduced the electronic setup can start to limit the energy resolution In tunneling spectroscopy an energy resolution of 0 1 meV requires a voltage noise over the tunnel junction less than 0 1 mV, taken over the full band of frequencies relevant for the physical phenomenon under investigation The critical part in spectroscopic measurements is the IV-convertor, which converts the tunnel current through the vacuum barrier in an output voltage At the same time however the voltage between tip and sample should be well defined The usual IV-convertor circuit is shown in Figure 2 19 Since the gain of the operational amplifier (op-amp) is very high, the tip is in first order

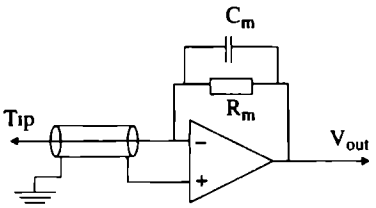

Figure 2 19 *IV-convertor circuit The output buffer circuit is omitted for clarity The cylinder represents the coaxial cable*

kept at zero potential The output gives $V_{out} = -I_{tun}R_M$ In discussing the non-ideal properties of this circuit it is important to distinguish between noise at IV-converter output and noise at input of the op-amp At the output the reduced accuracy can be improved by averaging over a larger data set Noise at the input of the op-amp however results in a less well defined tip voltage, and affects the measurements irreversibly If the IV-convertor allows voltage noise to reach the STM tip, the voltage across the tunnel barrier is less well defined, and the spectroscopy resolution will decrease Deviations from the ideal behavior are due to a number of reasons First, in scanning tunneling microscopy a large measurement resistance R_M (because tunnel currents are very small) and a large bandwidth B are required Typical values like $R_M = 100$ MΩ and $B = 3$ kHz give a Nyquist noise $V_{rms} = \sqrt{4k_BBRT} = 0\,07$ mV for a resistor at room temperature Secondly, at higher frequencies the gain of the operational amplifier is decreasing, and above a frequency specific for the opamp, is smaller than one At these frequencies the circuit in Figure 19 is no longer adequate Broad band high frequency voltage fluctuations due to external disturbances can enter the circuit and reduce the energy resolution of the spectroscopy measurements

Usually the IV-convertor circuit is situated at room temperature and the coaxial cable between the STM-tip and the input of the IV-convertor has a length exceeding that of the STM insert, typically between one and two meters Due to the very large measurement resistor small currents induced in the cable by external disturbances will already give large variations in the output of the IV-convertor High frequencies however will also generate voltage variations at the tip Disturbances can be due to electromagnetic interference or mechanical vibrations of the coaxial cable

A method to determine the energy resolution of the setup is to perform spectroscopy measurements on a superconductor with a well defined gap Δ at a well defined temperature The obvious candidate is $NbSe_2$ ($\Delta = 1\,1$ meV), because

of its excellent surface quality The measured dI/dV can be fitted to the BCS density of states [33], including the voltage noise at the tip as one of the fit-parameters Hess demonstrated that $NbSe_2$ should show a BCS density of states [34] Several authors [35, 36] however report curves that do not demonstrate a clear BCS density of states In their measurements the DOS does not vanish below the superconducting gap The deviations are attributed to high current densities in the superconductor close to the tip or to pair breaking at its surface We found that with every improvement in the electronic setup the dI/dV curves on $NbSe_2$ resembled more the expected BCS-shape Therefore, we conclude that voltage noise is a very likely candidate to explain the non-zero sub-gap conductance In our setup we minimized the sensitivity for mechanical vibrations by fixing the coaxial cable thoroughly We could reduce the voltage noise V_{noise} to 0 7 mV by grounding the shield of the tip coaxial cable near the STM, instead of at the top of the insert The biggest improvement was achieved by improving the shielding for rf-radiation and by filtering these frequencies out of the leads with pi-filters With these changes V_{noise} reduced to 0 35 mV This value however still implies that at 1 5 K the voltage noise limits the spectroscopy resolution

2.10 Acknowledgements

We thank J G H Hermsen and J W Gerritsen for interesting discussions and valuable advice and the Nijmegen workshop for skilfully fabricating the ^{4}He-STMs A Huis (Delft) machined most parts of the ^{3}He-STM and was always prepared to make modifications W J H Vollenberg participated in the construction of a ^{3}He-setup in Nijmegen, in which an STM was placed inside the ^{3}He-can This setup is not described in this chapter, but the experience acquired with it was of great value later on We thank A van Oudenaarden for his work on the Delft ^{3}He-system and for making the necessary modifications on the wiring of the insert G A de Goey contributed many ideas in enhancing the energy resolution in the spectroscopy measurements

2.11 Appendix A

In designing an STM with a high resonance frequency a more quantitative knowledge of how different variables affect the resonance frequency might be helpful As mentioned earlier the construction has to be rigid, lightweight and compact So, both the geometry of the design and material properties are of importance

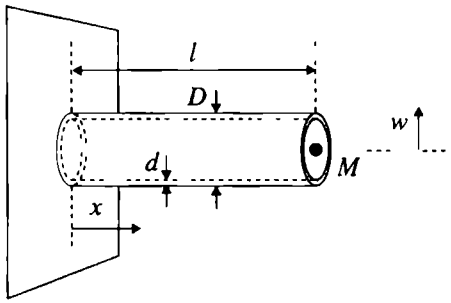

Figure 2 20 *One side clamped beam, circular symmetric*

To understand how these variables influence the resonance frequency, we calculate the frequency of the lowest bending mode of a tube-shaped beam which is clamped on one side (Figure 2 20) The beam has a length l, a diameter D, a wall thickness d and the relevant material properties are the elastic modulus E, and a density ρ At the free end the tube is loaded with a mass M This geometry is a useful one, since, as discussed in this chapter, the STM model consist of two levers each with one free end Also, the construction of the STM is often circular symmetric to avoid thermal drift The masses at the end of the bar here correspond to tip or sample holder

The equation [37, 38] for the bending of a beam w as a function of position x is

$$EI\frac{d^2w}{dx^2} = -M_b(x), \tag{2 1}$$

where I is the moment of inertia of the cross section and M_b is the bending moment Using

$$\frac{dM(x)}{dx} = Q(x), \tag{2 2}$$

where $Q(x)$ is the restoring cross-force in the beam, we find

$$EI\frac{d^3w}{dx^3} = -Q(x) \tag{2 3}$$

When the bending of the bar is not in equilibrium the bending will generate an acceleration For a section length Δx, the force is equal to

$$\Delta x\rho_L\frac{d^2w(x,t)}{dt^2} = Q(x+\Delta x) - Q(x) \tag{2 4}$$

With (3) we obtain

$$\rho_L \frac{\partial^2 w}{\partial t^2}(x,t) + EI \frac{\partial^4 w}{\partial x^4}(x,t) = 0, \tag{2 5}$$

which is the equation of motion of the bar The boundary conditions of the system in Figure 2 20 are

$$\begin{aligned} w(0,t) &= 0 \\ \frac{\partial w}{\partial x}(0,t) &= 0 \\ \frac{\partial^2 w}{\partial x^2}(l,t) &= 0 \\ M\frac{\partial^2 w}{\partial t^2}(l,t) &= EI\frac{\partial^3 w}{\partial x^3}(l,t) \end{aligned} \tag{2 6}$$

The solution of (2 5) has the form $w(x,t) = \varphi(x)\cos pt$, with which we obtain for the equation of motion

$$EI\frac{d^4\varphi}{dx^4} - \rho_L p^2 \varphi(x) = 0 \tag{2 7}$$

The rewritten boundary conditions are

$$\begin{aligned} \varphi(0) &= 0 \\ \varphi'(0) &= 0 \\ \varphi''(l) &= 0 \\ EI\frac{d^3\varphi}{dx^3}(l) &= -Mp^2\varphi(l) \end{aligned} \tag{2 8}$$

The general solution of (2 7) is of the form

$$\varphi = A\cos kx + B\sin kx + C\cosh kx + D\sinh kx, \tag{2 9}$$

where k is defined by,

$$k^4 = \frac{\rho_L}{EI}p^2 \tag{2 10}$$

The nontrivial solution of (7) en (8) with the lowest k-value gives the first resonance frequency of the cantilever beam, with

$$f_{res} = \frac{k^2\sqrt{EI}}{2\pi\sqrt{\rho_L}} \tag{2 11}$$

The resonance frequency can be calculated numerically for a given set of parameters l, D, d, E, ρ, and M By varying the parameters we can investigate their influence on the resonance frequency and deduce some general guidelines to maximize the resonance frequency

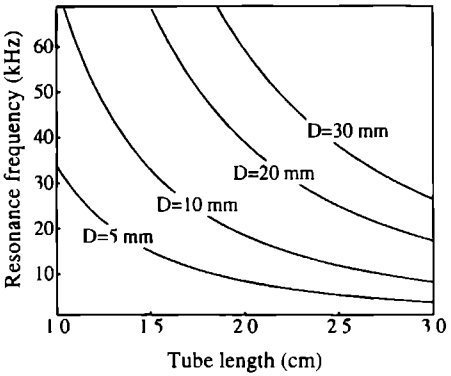

Figure 2 21 *Unloaded tube The resonance frequency as a function of the tube length for different tube diameters Material properties* $E = 12\times10^{10}$ *Pa,* $\rho = 7\,0\times10^{3}$ *kg/m*^{3} *The wall thickness is 1 mm*

First we look at the length dependence of f_{res} Figure 2 21 shows calculations on an unloaded tube, clamped on one side As the length l is increased, the resonance frequency decreases as $1/l^2$ From the dependence on the diameter D, it follows that for a given length the resonance frequency can be optimized by increasing the diameter This holds as long as $D < l$, since at larger diameters other vibration modes become important So, high resonance frequencies are achieved by small lengths and cubic shapes

A mass at the free end of a cantilever will reduce its resonance frequency The

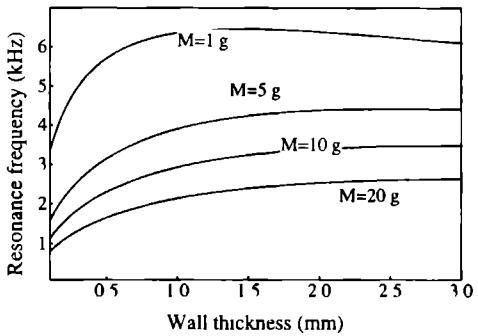

Figure 2 22 *The effect of the wall thickness on the resonance frequency of a loaded tube for different masses Material properties* $E = 12\times10^{10}$ *Pa,* $\rho = 7\,0\times10^{3}$ *kg/m*^{3} *The tube diameter is 1 cm*

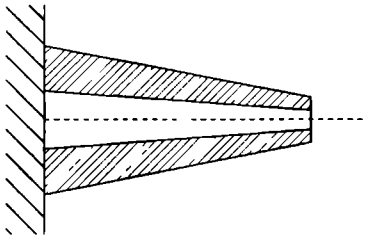

Figure 2 23 *A conical shaped beam The larger diameter at the clamped side increases the stiffness At the free end the mass per unit length is small*

situation is similar to the well known case of a mass M suspended by a spring, where the resonance frequency is given by $\sqrt{k/M}$ (k is the spring constant) The spring constant of the beam k_{beam} at length l is approximately given by $\pi d D^3/8$ With a given mass M the resonance frequency has to be optimized by increasing the stiffness of the beam In our model of Figure 2 20 a possible method is to increase the wall thickness However this will also result in a larger mass of the beam itself, which again reduces the resonance frequency Calculations on the effect of the wall thickness on the resonance frequency of the beam are shown in Figure 2 22 From these calculations we can conclude that increasing the wall thickness is only effective up to a certain limit To increase the resonance frequency substantially it is more effective to choose a larger tube diameter In fact one has to distinguish between mass that acts as a load and mass that increases the stiffness The best beam shape therefore is a conical one (Figure 2 23), which has a small mass at the end, and a high stiffness at the base This shape can also be recognized in our STM design of Figure 2 6

References

[1] G Binnig, H Rohrer, Ch Gerber, and E Weibel, Appl Phys Lett **40**, 178 (1982)

[2] G Binnig, H Rohrer, Ch Gerber, and E Weibel, Phys Rev Lett **49**, 57 (1982)

[3] Some comprehensive information about piezoelectric elements can be found in C J Chen, *Introduction to scanning tunneling microscopy*, (Oxford University Press, New York and Oxford, 1993)

[4] G Binnig and D P E Smith, Rev Sci Instrum **57**, 1688 (1986)

[5] G Binnig and H Rohrer, Helv Phys Acta **55**, 726 (1982)

[6] J E Demuth, R J Hamers, R M Tromp, and M E Welland, J Vac Sci Technol A **4**, 1320 (1986)

[7] J G H Hermsen, H van Kempen, B J Nelissen, L L Soethout, G F A van de Walle, P J W Weijs, and P Wyder, Surf Sci **181**, 183 (1987)

[8] D W Pohl, Rev Sci Instrum **58**, 54 (1987)

[9] L E C van der Leemput, Ph D Thesis, University of Nijmegen, The Netherlands

[10] M Okano, K Kajimura, S Wakiyama, F Sakai, W Mizutani, and M Ono, J Vac Sci Technol A **5**, 3313 (1987)

[11] D W Pohl, IBM J Res Develop **30**, 417 (1986)

[12] *ASM metals reference book, second edition* (American Society for Metals, Metals Park, OH, 1983)

[13] *Thermophysical properties of matter, The TPRC data series* (IFI/Plenum, New York, 1970), Vol 1

[14] Vernitron limited Bulletin, 1976

[15] Vernitron data sheet, unpublished

[16] P J M van Bentum, L E C van de Leemput, and P A A Teunissen, J Microsc **152**, 11 (1988)

[17] A P Fein, J R Kirtley, and R M Feenstra, Rev Sci Instrum **58**, 1806 (1987)

[18] P Davidsson, H Olin, M Persson, and S Pehrson, unpublished

[19] The ^{4}He-STM has been described previously in J W G Wildoer, A J A van Roij, H van Kempen, and C J P M Harmans, Rev Sci Instrum **65**, 2849 (1994)

[20] Piezo-electric tube PZT 5A with diameter 6 4 mm, length 12 7 mm and wall thickness 0 5 mm

[21] Ch Renner, Ph Niedermann, A D Kent, and Ø Fischer, Rev Sci Instrum **65**, 965 (1990)

[22] J W Lyding, S Skala, J S Hubacek, R Brockenbrough, and G Gammie, Rev Sci Instrum **59**, 1897 (1988)

[23] This device originated from the design of another low temperature STM developed in the Nijmegen group J G A Dubois, J W Gerritsen, J G H Hermsen, and H van Kempen, Rev Sci Instrum **66**, 4146 (1995)

[24] Stycast is a product of Emerson and Cuming, Inc We have used Stycast 2850 FT

[25] The ceramic layer consists of titanium carbo nitride, deposited by Gimex technische keramiek b v , The Netherlands

[26] We use the Model 75 from Wavetek San Diego, Inc

[27] Ph Niedermann, R Emch, and P Descouts, Rev Sci Instrum **59**, 368 (1988)

[28] For the x and y coarse positioners this direction dependence can be attributed to the leafspring clamping the sliders together This leafspring also gives a force in the plane of the sample The direction dependence for the z coarse positioner can be attributed to gravity

[29] Piezoelectric tube PZT 5A with diameter 6 4 mm, length 25 4 mm and wall thickness 0 7 mm With this scantube the scanrange is 2 μm at liquid helium temperatures

[30] See for example R M Silver, J A Dagata, and W Tsjeng, J Appl Phys **76**, 5122 (1994)

[31] P Horowitz and W Hill, *The art of electronics*, (Cambridge University Press, Cambridge, 1980)

[32] Omicron STM control unit, with STMPRG version 3 11

[33] M Tinkham, *Introduction to superconductivity*, (Robert E Krieger publishing company, Inc , Malabar, 1975)

[34] H F Hess, R B Robinson, R C Dynes, J M Valles, Jr and J V Waszcak, Phys Rev Lett **62**, 214 (1989)

[35] Ch Renner, A D Kent, Ph Niedermann, Ø Fischer, and F Lévy, Phys Rev Lett **67**, 1650 (1991)

[36] S H Tessmer, D J van Harlingen, and J W Lyding, Phys Rev Lett **70**, 3135 (1993)

[37] A G Webster, *Partial differential equations in mathematical physics*, (Dover publications, Inc , 1927)

[38] E Mönch, *Einführungslesung Technische Mechanik*, (R Oldenbourg Verlag GmbH, München, 1986)

Chapter 3

Scanning tunneling microscopy on the InAs(110) surface: Landau levels, tip induced accumulation, and Fermi-level pinning by a single step edge

Abstract: We describe scanning tunneling spectroscopy measurements on InAs(110) surfaces at 4 2 K Clean, in situ cleaved flat surfaces show resonances that are strongly tip-dependent, and in magnetic field oscillations in the density of states due to Landau quantization are observed The data show that the work function of the STM-tip critically influences the spectra Monoatomic steps at the surface give a local increase in the number of surface states, which leads to pinning of the Fermi-level at the step edge As a consequence the local electron density is increased significantly in the vicinity of the steps Separate bound states in the step area are observed, indicating the formation of a 1D quantum wire InAs surfaces covered with a thin oxide layer show Fermi-level pinning at ~150 mV above the bulk conduction band edge

---

Parts of this chapter have been presented at the 148 WE-Heraeus-Seminar "STM-Related Spectroscopies of Semiconductor Interfaces" *Scanning tunneling microscopy observation of Landau levels at the (110) InAs surface*, by J W G Wildoer, A J A van Roij, C J P M Harmans, and H van Kempen, Bad Honnef (Germany), 1 September 1995

3.1 Introduction

Scanning tunneling microscopy is a powerful technique to investigate the electronic properties of semiconductor surfaces By imaging the surface at different bias voltages, the energies and positions of the surface states can be determined In this way it has been possible for example to confirm the π-bonded chain structure of the Si(111)2×1 surface [1], and to selectively image either the Ga atoms or the As atoms of the GaAs(110) surface [2] These kinds of measurements provide information about the dangling bond state density on the atomic scale

Recently, several experiments have demonstrated that it is also possible to use the STM to investigate the spatial behavior of the conductance and valence bands in the vicinity of distortions in the electrostatic potential The edges of these bands determine the transport properties of a a semiconductor, and therefore the possibility to investigate the energy bands spatially resolved can be of great value In semiconductors, the Fermi wavelength, and also screening length, exceed the atomic scale As a consequence dopants in the subsurface region of the surface can influence the carrier density at the surface Johnson *et al* [3] and Zheng *et al* [4] showed that these local variations in the band-bending appear as hillock-like features in STM images of the GaAs(110) surface, superimposed on the atomic sublattice On semiconductor GaAs/AlGaAs heterostructures Feenstra *et al* [5], and also Wu *et al* [6] were able to image the energies of resonant states in a quantum well by scanning tunneling spectroscopy In their experiments the measurements were performed on clean cross-sections of the heterostructure after it was cleaved under UHV conditions The combination of topography and spatially resolved spectroscopy on the quantum well enables to quantify the influence of local variations in the thickness of the layers

In this chapter we present a low temperature STM study of the InAs(110) surface We do not focus on the dangling bond state densities, but will concentrate on the behavior of the conduction electrons at the InAs(110) surface The surfaces of InAs are interesting for a number of reasons Already in the 1960s transport measurements demonstrated the presence of surface two dimensional electron gasses (2DEGs) at InAs surfaces Such a 2DEG would be directly accessible with an STM-tip Furthermore, InAs is a low band-gap semiconductor, E_g = 350 mV, and has a very low effective electron mass at the conduction band edge, m_{eff}= 0 023 m_e Landau level splitting may therefore already be observable at relatively low magnetic fields, also with the moderate energy resolution that can be obtained at liquid-^{4}He temperatures

The combination of a high quality surface 2DEG and the possibility to investigate Landau levels spatially resolved would open new experimental prospects Transport properties in 2DEGs subjected to Landau quantization are highly anomalous The most famous example of this is the quantum Hall effect, discovered by von Klitzing, Dorda and Pepper in 1980 [7] During the last decade it has become clear that under the quantum Hall conditions all current is carried at the boundaries of the 2DEG by so-called edge channels Edge channels are formed at the intersections of the Landau levels with the Fermi energy In general, these intersections are located at the edges of the 2DEG since there the Landau levels are bent towards higher energies due to the confining potential The possibility to investigate Landau levels spatially resolved could yield relevant detailed information about sizes and shapes of the edge channels

In the experiments described here we have used a low temperature STM equipped with an *in situ* cleaver [8], mounted in a cryostat, inside a 10 T magnet At liquid He temperatures the vapor pressure of oxygen is extremely low ($< 10^{-15}$ Torr) Surfaces of III-V compound semiconductors, which normally oxidize very quickly, will stay clean for many days under these conditions Besides the very low oxygen pressure, performing the experiments at liquid He temperatures also has the advantages of an enhanced spectral resolution ($k_B T \approx 0\,4$ meV at 4 K) and the absence of thermal drift of the scan head with respect to the sample As most III-V semiconductors InAs has a zinc-blende structure and cleaves along the (110) plane With the experimental setup we are able to investigate the InAs(110) surface under various conditions Cleaving the sample at low temperatures results either in atomically flat or in stepped surfaces Also the sample can be cleaved at room temperature, either in ambient, giving a thick oxide, or in the vacuum can at low oxygen pressures, resulting in a thinner oxide

The data we present in this chapter demonstrate that it is possible to resolve Landau levels by scanning tunneling microscopy To our knowledge these measurements are the first observations of Landau levels with a scanning probe technique We discuss the influence of the STM-tip on the observed spectra Furthermore we present measurements which show that the band-bending at the surface is sensitive to the presence of steps and oxides at the surface On clean, in situ cleaved surfaces we do not find evidence for an intrinsic surface 2DEG

The electronic properties of InAs surfaces have been studied by various other techniques In 1963 Mead and Spitzer [9] found by analyzing the diode characteristics of metal-semiconductor interfaces that the Fermi-energy at the surface of InAs was pinned above the conduction band edge The resulting surface charge

layer can be quantized in the direction perpendicular to the surface, and depending on the doping concentration in the InAs a 2DEG can be formed directly at the InAs surface. The existence of the 2DEG was for the first time indicated in transport measurements by Kawaji and Gatos [10]. Tsui investigated the n-type InAs accumulation layer by planar tunneling spectroscopy, and was able to directly determine the energies of the Landau levels, both in the surface 2DEG and in the bulk conduction band [11, 12]. The planar method used by Tsui is quite similar to tunneling spectroscopy with an STM In the planar geometry usually an oxide is used as an insulator between the two electrodes, whereas in an STM geometry the vacuum barrier separates the electrodes Also, tunneling spectroscopy with an STM allows to investigate the surface spatially resolved The experiments mentioned above [9, 10, 11, 12] have provided mainly information about the macroscopic properties.

3.2 Observation of Landau levels

The InAs used in our experiments is lightly n-doped, n = 2 5 10^{16} cm^{-3} yielding a Fermi energy of 10 meV. This doping concentration ensures a finite bulk conductivity at low temperatures, irrespective of the presence of a surface 2DEG. All the measurements presented in this chapter are performed with Pt(90%)Ir(10%) tips, cut in ambient with scissors. The bias voltages are applied to the sample relative to the tip This implies that at positive voltages the Fermi level of the tip is lined up in the conduction band of the InAs An energy diagram is shown in Figure 3 1. The dI/dV vs V curves (abbreviated by dI/dV) are obtained by numerically differentiating the recorded $I - V$ curves Before discussing the measurements in magnetic field we show first the general zero field features

3.2.1 B = 0

In our first experiments on InAs, surfaces were investigated that were cleaved in air, a few minutes before cooling down the STM These surfaces were hard to image, because a substantial oxide layer had formed in the short time they were exposed to air The poor reproducibility of the topographic images indicated that the tip was touching the surface continuously, because the oxide on the surface was too thick to allow tunneling without contact. Spectroscopy curves obtained on this surface were rather irreproducible, and although the main semiconductor features, like the gap and valence and conduction band, could still be resolved,

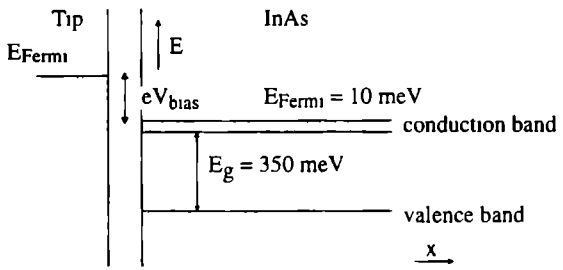

Figure 3.1. *Energy diagram of the tip-vacuum-InAs system. Bias voltages are applied to the sample relative to the tip. At positive voltages electrons tunnel from the tip into the InAs conduction band. The InAs is degenerate, wit a Fermi energy of 10 meV, and a band gap of 350 mV.*

the prospects to obtain more detailed information were limited.

On surfaces that were cleaved in situ at low temperatures atomic resolution was easily achieved. As shown in Figure 3.2, depending on the polarity of the bias voltage either the In or As atoms are imaged. The images are similar to those obtained by Feenstra *et al.* on GaAs [2]. STM images generally depend on the polarity of the bias voltage, since at negative tip voltages electrons tunnel into the unoccupied states of the sample, whereas at positive tip voltages electrons from the occupied states carry the tunnel current. Apart from the energy dependent density of states on both atoms, also a geometric effect influences the images of

Figure 3.2 *Topographic images of the in situ cleaved InAs (110) surfaces, obtained at a) V_{sample} = -500 mV (As lattice), and b) V_{sample} = 500 mV (In lattice). The scan area of both images is 32 Å^2.*

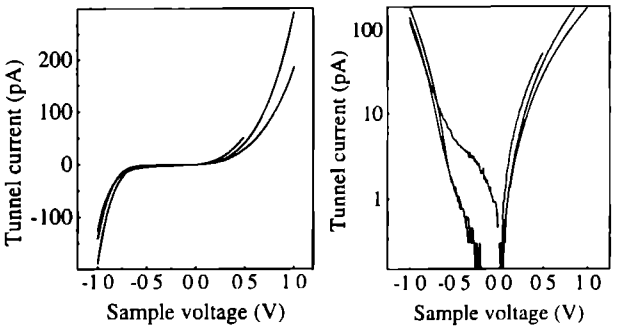

Figure 3 3 *$I - V$ spectra of the InAs gap obtained with different tips The logarithmic plot shows the behavior of the tunnel current at voltages inside the gap*

Figure 3 2, since the surface As atoms are tilted in the vertical direction From a detailed analysis of their data Feenstra *et al* were able to give an estimate for this buckling angle at the GaAs(110) surface The surface buckling is also present at the InAs surfaces (which were cleaved at low temperatures) and at low bias voltages ($|V| \lesssim 300$ mV) both polarities only show the As atoms

Figure 3 3 shows spectroscopy curves obtained on clean InAs (110) surfaces with different tips The tunneling spectra give a band gap of 0 50 $\pm$ 0 10 V, larger than the expected value of 0 35 V The deviation is attributed to tip induced band-bending In spectroscopy measurements on semiconductors the varying electric field between tip and sample will influence the surface electrostatic potential, and as a consequence gaps in general appear larger [16, 17]

In the majority of the experiments we observed sharp features in the dI/dV near the onset of the conduction band (Figure 3 4) These features are not due to defects or contaminants at the surface, since by topography it is assured that spectra are taken on flat and clean terraces, tens of nanometers away from any irregularity present at the surface The occurrence and the energies of these sharp resonant-like features is tip-dependent With a particular tip, $I - V$ curves are identical over the whole surface (with the exception of areas with steps and defects) The origin of the resonances will be discussed in section 3 3

3.2.2 B $\neq$ 0

Figure 3 5 shows $I - V$ and dI/dV curves obtained with magnetic fields of 3 T and 4 T, applied perpendicular to the surface Besides the peaks below the

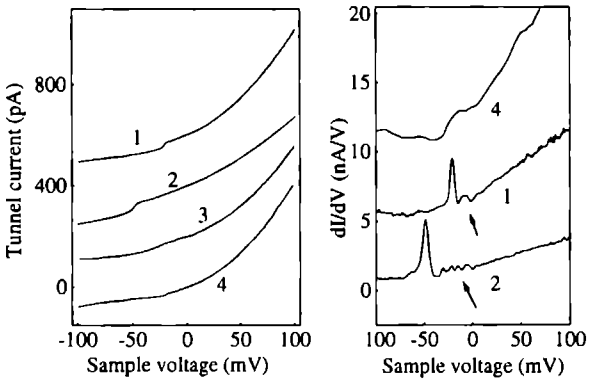

Figure 3 4 *$I-V$ spectra near the onset of the conduction band The resonances in the dI/dV are reproducible and independent of position (also the small ones indicated by the arrows) In some cases no resonances are observed The curves are offset for clarity*

conduction band edge, which were already present at zero field, oscillations in the dI/dV at higher voltages are present The period of the oscillations scales with the applied magnetic field From Figure 3 5 we estimate the periods to be ~12 mV at 3 T and ~16 mV at 4 T These values are of the same order as the expected Landau level splittings ($\hbar B/m_{eff}$) of 15 mV and 20 mV (with m_{eff}= 0 023 m_e) We therefore conclude that the oscillations in the dI/dV are due to Landau quantization in the plane of the the sample surface An important

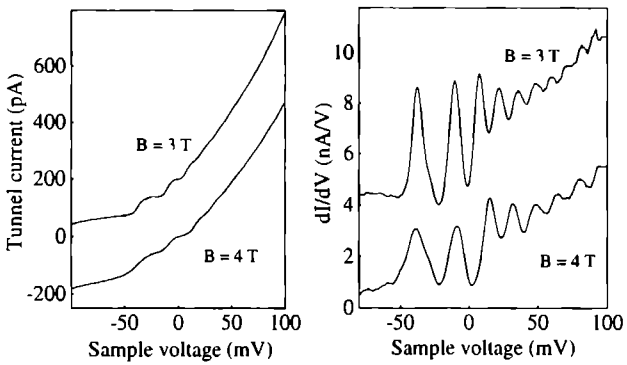

Figure 3 5 *$I-V$ and dI/dV at $B = 3$ T and $B = 4$ T Oscillations at positive sample voltages scale with magnetic field The curves are offset for clarity*

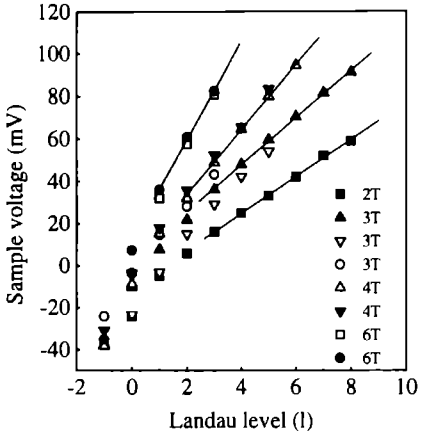

Figure 3 6· *The maxima in the dI/dV as a function of the Landau level number l. Measurements at the same magnetic field, but with different tips, are indicated by different symbols.*

question which has to be addressed, is whether the oscillations originate from bulk electrons or from an eventual surface 2DEG

Landau levels in the bulk conduction band are related to the three dimensional electron gas In Figure 3 6 the voltages at which the oscillation maxima occur are shown as a function of the Landau level number l for different magnetic fields From this figure we can clearly distinguish two regimes· one where the Landau level separation is nearly constant, and an other where the separation is not constant and where the voltages corresponding with the maxima of the oscillations are tip-dependent.

In the bulk conduction band the Landau level separation is constant and scales with magnetic field. From the oscillation period (solid line fits) we obtain an effective electron mass of 0 028 $\pm$ 0.03 m_e This value is larger than the one known for the conduction band minimum (0.023 m_e) In our measurements the oscillation period is however obtained between 40 and 100 meV above the conduction band edge, where the effective electron mass is expected to be slightly higher due to the nonparabolicity of the band edge [18] A similar increase of m_{eff} has been observed by Tsui [11] through planar InAs-oxide-Pb junctions

At the lower voltages the positions of the maxima of different measurements do not coincide As can be seen in Figure 3 6, a different tip results in a shift of the low bias voltage maxima to higher or lower energies.

The peaks in the dI/dV below the bulk conduction band edge do not show

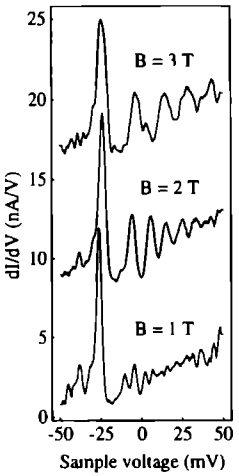

Figure 3 7 *Landau levels at low magnetic fields The peak at -25 mV does not split into seperate levels when the magnetic field is increased, and also it does not shift to higher energies The curves are offset for clarity*

a dependence on the applied magnetic field Figure 3 7 shows spectra obtained at low magnetic fields The first peak at -25 mV does not shift and also does not give rise to separate Landau levels (the Landau levels observed are all in the conduction band) Therefore we conclude from Figure 3 7 that the peaks at negative sample voltage should not be attributed to a surface 2DEG, and we will discuss their origin in the next section

The absence of a surface 2DEG at the clean InAs(110) surface does not come as a full surprise On atomically flat InAs(110) surfaces all surface atoms carry one dangling bond The In dangling bonds have an energy in the conduction band (1 3 eV above the conduction band minimum), and the As states an energy in the valence band (-1 2 eV below the valence band maximum) [13] Since the band gap is free of intrinsic surface states, no band-bending at the surface is expected Appelbaum and Baraff [14] proposed a different mechanism for degenerate semiconductors that result in a surface 2DEG Their model predicts that at the surface of a degenerate semiconductor with a long Fermi-wavelength extra conduction electrons are required at the surface to screen the abrupt end of the crystal In our experiments we did not find evidence for such a self-induced deficiency two-dimensional electron gas

3.3 Tip influences

In Figure 3 6 the properties of the tip affect the bias voltage position of the peaks There are several tip-dependent parameters that can influence the spectra Every tip is characterized by a unique transfer Hamiltonian matrix [15], which is determined by the outer-most atoms of the tip The transfer Hamiltonian matrix defines which states have the largest probability for tunneling between tip and sample Secondly, the work function difference between tip and sample, together with the applied bias voltage, determines the magnitude of the local electric field in the tip region, and therefore the local density of states The spatial profile of the electric field depends on a third tip-dependent parameter, namely the geometric shape of the tip

Since the Landau levels at higher energies appear to be less sensitive to tip changes than those at lower electron densities (Figure 3 6), the peak position voltage shifts have to be attributed to differences in the local electric field This suggests that every PtIr tip has a different work function W_{tip} Tip changes resulting in a shift of Landau level positions were occasionally also observed during the experiments

Usually metal surfaces have larger work functions than semiconductor surfaces At zero bias this results in a tendency to deplete the semiconductor surface Gobeli and Allen have determined the work function of the InAs(110) surface W_{InAs} to be 4 9 eV [19], whereas for PtIr we can estimate a value of 5 5 eV [20] Work functions are however sensitive to surface conditions and the surface structure [21, 22] This sensitivity can account for the different energies of the Landau levels with different tips

The sharp peaks in Figure 3 4 and in the negative bias voltage range in Figures 3 6 and 3 7 are situated at energies below the bulk conduction band edge We therefore conclude that in these measurements an accumulation layer is formed instead of the anticipated depletion layer Since we did not find any evidence for a magnetic field dependence of peaks at negative bias voltages, the accumulation layer is only present in the vicinity of the tip, and in fact forms a small accumulation dot The electrons in the dot locally screen the electric field originating from the tip Depending on the work function difference between tip and sample, and the spatial profile of the electric field, one or more electrons will be present When the Fermi energy of the tip is decreased, the localized states of the dot will become available for tunneling (Figure 3 8) With every new state the tunnel current increases stepwise, giving a peak in the dI/dV From this explanation it

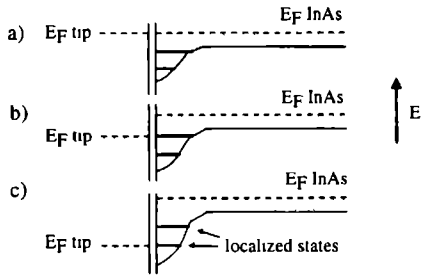

Figure 3.8: *Tip induced localized states contribute to the tunnel current when the Fermi-level of the tip is decreased. In b) and c) the Fermi-level equals the energy of one of the localized states The energies of the bound states vary with the applied bias voltage*

follows that, in many of our experiments, $W_{tip} < W_{InAs}$ (if however no peak-like features are present at negative sample voltages, $W_{tip} > W_{InAs}$) An intriguing question is why these single states have such a large influence on the total tunnel current

Since with a particular tip $I - V$ curves are identical over the flat terraces of the InAs surface, the work function of the tip appears to be decisive for the work function difference between tip and sample. In our setup tips can not be prepared in situ, and are cut in ambient with scissors Before cutting the tip, scissors and PtIr wire are cleaned extensively with isopropyl alcohol (IPA). Furthermore, the PtIr is cut in such a way that the tip is composed of material inside the wire. Realistically however, contamination of the tip surface due to exposure to air can not be avoided. To provide the heat exchange at low temperatures, the vacuum can is filled with 760 Torr of He gas at room temperature. Although He is an inert gas its presence at the tip and sample surfaces is likely to influence both work functions [23] The tip handling procedures and the amount of He exchange gas have been comparable in all the experiments, and it is most likely that variations in the geometry of the outer-most atoms of the tip are responsible for the work function differences. An argument that supports this assumption is that occasional tip changes (as can be observed in topographic images) also result in different spectra

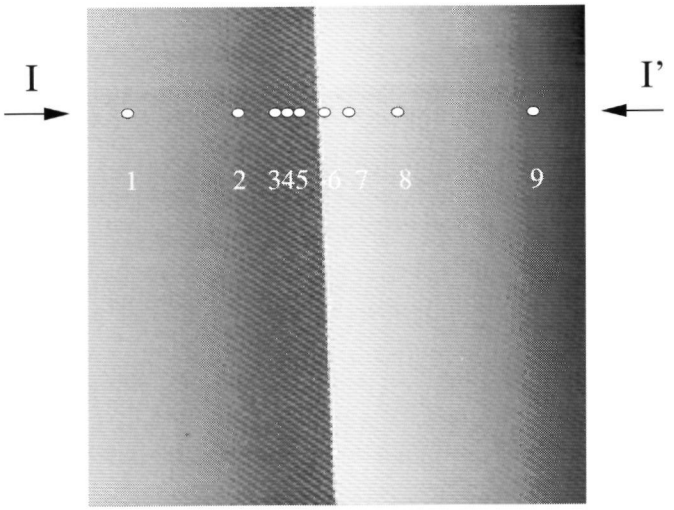

Figure 3.9: *Mono-atomic step. The scanrange is 460 Å². At a distance of 300 Å to the right of the step a second step was found. The arrows I and I' indicate a line along which spectroscopy curves are taken. The white dots are positions corresponding to the spectroscopy curves shown in Figures 3.10 and 3.11.*

3.4 Step edge Fermi-level pinning

To obtain a surface 2DEG the Fermi level has to be pinned in the conduction band. In the preceeding sections we have concluded that the clean and flat InAs(110) surface does not lead to such pinning. In the remaining part of this chapter we discuss that lead to Fermi-level pinning, i.e. in the vicinity of steps, and in the presence of a thin oxide at the surface. A desirable consequence of Fermi-level pinning is that the influence of the electric field of the tip is reduced [17, 24].

Figure 3.9 shows a mono-atomic step in the $[1\bar{1}2]$ direction at the InAs(110) surface. The step is almost straight, with only a small number of irregularities. Several $I-V$ curves taken along the line I-I' are plotted in Figure 3.10. In between the measurements the tip-sample distance was regulated at a sample voltage of +50 mV, in order to avoid variations in the electron density influencing the tip height. At negative sample voltages the tunnel current is larger in the vicinity of the step, indicating an increase in the number of states available for tunneling.

The edge of the conduction band in the vicinity of the step can be observed

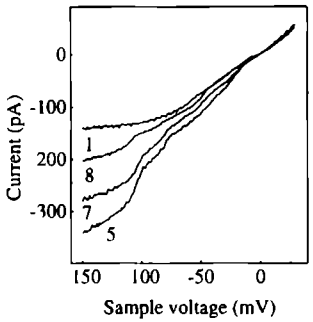

Figure 3 10 *I-V curves taken along the line I-I' of Figure 3 9 The numbers correspond with the positions indicated in Figure 3 9*

directly from the dI/dV curves shown in Figure 3 11 The differentiated $I - V$ curves show a peak appearing at -100 mV at a distance of approximately 75 Å from the step Approaching the step, the peak amplitude increases, while its position on the voltage axis remains unchanged At smaller negative sample voltages similar peaks are present Also in these measurements the peaks have to be attributed to bound states We attribute these bound states to the formation of a local charged trench resulting from the Fermi-level pinning at the step edge

Figure 3 12 schematically represents this trench The lateral dimensions of the trench will be of the order of the Fermi wavelength (which can be calculatated to be around 8 nm) In this trench, states are quantized in the direction perpendicular to the step direction The variations in the peak amplitudes as a function of position in Figure 3 11 are a consequence of the spatial variations of the wave function amplitude At the edge of the trench this amplitude is low, resulting in a smaller probability for the electrons to tunnel from the bound state into the tip Unfortunately we have not been able to also observe bound states with a minimum at the step edge, corresponding to higher wave numbers

The arrangement of the atoms at the surface and the subsurface layer of InAs(110) is shown Figure 3 13a From Figure 3 9 we can determine the angle between the direction of the step and the lattice direction **b** to be 55 ± 2^o The zincblende lattice has no inversion symmetry, and therefore the angle does not define the step completely The two possibilities are represented in Figures 3 13b and 3 13c [25] From images obtained on the same surface at positive bias voltages we can determine the positions of the In atoms with respect to the As atoms The additional information shows that the step of Figure 3 9 corresponds

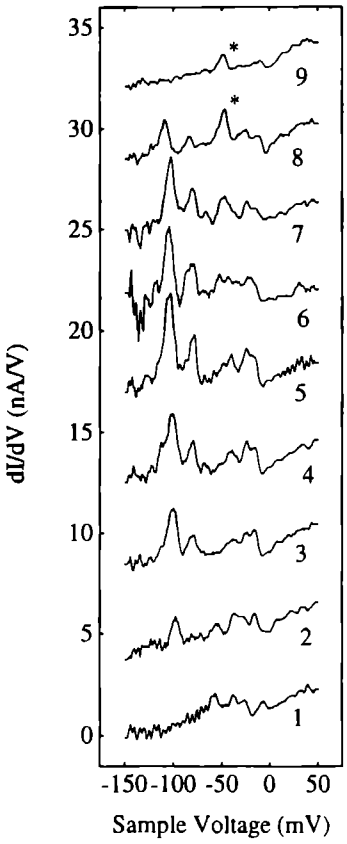

Figure 3 11 *Differentiated I-V curves along the line I-I' of Figure 3 9 We attribute the peaks indicated with an asterisk to a second step just outside the scan area The numbers correspond with the positions indicated in Figure 3 9 The curves are offset for clarity*

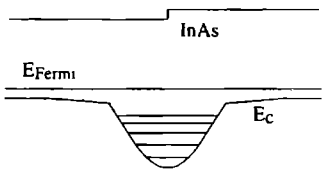

Figure 3 12 *Schematic representation of the accumulation region generated by the Fermi-level pinning at step The lowest levels in the trench are separated, whereas the higher levels form a continuous band*

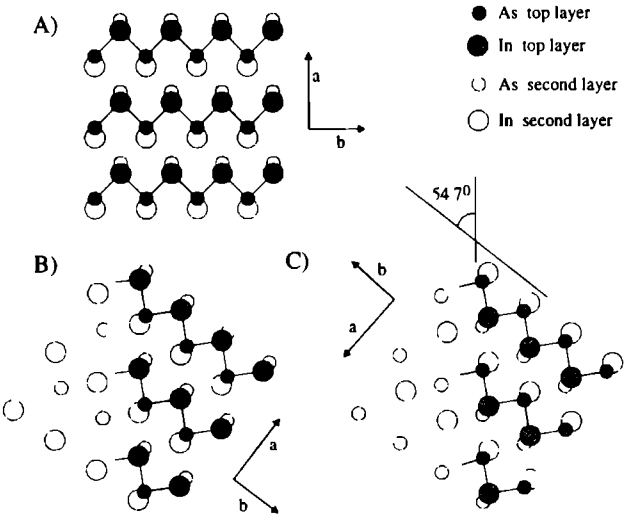

Figure 3 13 *(a) Atomic arrangement at the InAs(110) surface (b) Step with extra In dangling bonds (c) Step with extra As dangling bonds*

to the situation in Figure 3 13b (apart from the irregularities in the real step)

The step edge introduces additional dangling bonds In the case discussed here these belong to the In atoms The large amount of dangling bonds at the step edge will very likely lead to a rearrangement of the atoms near the step edge, which will determine the energies of the surface states A calculation of the reconstruction, including screening of the conduction electrons, would allow a quantitative comparison with our data The accumulation of electrons can be understood from basic principles On atomically flat InAs(110) surfaces all surface atoms provide one dangling bond Therefore, at the step of Figure 3 9 the number of In dangling bonds exceeds the As dangling bonds roughly by a factor two Charge neutrality however requires an equal amount of dangling bonds below and above the Fermi energy [26], and therefore the Fermi level is pinned by the In dangling bonds Our data indicate that also with two equivalent dangling bonds per atom the energies of the In surface states are in the conduction band This has also been suggested by Van Laar *et al*, based upon spectroscopy measurements with several macroscopic techniques [27]

The number of extra conduction electrons n_{step} in the vicinity of the step can be estimated to be half the number of extra In dangling bonds in the ideal case $n_{step} = 6\ 8\ 10^8\ \mathrm{m}^{-1}$ The bound states in the small trench of Figure 3 12 in fact

represent one dimensional subbands The number of states in a 1D free electron gas (per unit length) n_{1D} is given by

$$n_{1D} = \frac{2}{\pi}\sqrt{\frac{2m_{eff}\epsilon_F}{\hbar^2}}, \tag{3 1}$$

where ϵ_F is the Fermi energy with respect to the bottom of the 1D subband So, the first subband at ~100 meV below the Fermi energy contains 1 6 10^8 m^{-1} electrons From these numbers we can conclude that, in agreement with the experimental data, more than one subband is required to allocate the extra electrons

A step with an identical orientation as the one of Figure 3 9 showed similar results Here the first peak was however situated at a sample voltage of ~-90 mV Since the bound states do not change in energy when the tip is moved perpendicular to the step direction, the tip induced band bending has to be of minor importance in the vicinity of step edges There are however several other factors that can cause differences Most important are deviations from the exact atomic arrangement of Figure 3 13b Furthermore, straight steps like the one in Figure 3 9 are rare, and their length is limited The finite length of the straight section and also the vicinity of other steps will influence the local electron density (caption Figure 3 11) Steps with different indices either showed no bound states, or only at small bias voltages

In summary, surface states provided by steps are able to pin the Fermi level in the conduction band Spectroscopy measurements show additional structure is present in the density of states near the step, indicating the existence of one dimensional channels The steps can form an interesting theoretical and experimental model system since the number of surface states can be known, and the tip influences are less important, since the Fermi level is pinned

3.5 Thin oxides

In the experiments by Kawaji and Gatos [10] and Tsui [11, 12] the InAs surfaces were covered with oxides Although thick native oxides appeared to be incompatible with scanning tunneling microscopy, thinner oxides should allow a non-contact tunnel current A thin oxide was formed on the InAs(110) surface by cleaving the sample in the vacuum can of the STM insert at room temperature In this environment the cold trap action of the walls of the insert is absent and the oxygen pressure is higher than in the previously discussed experiments

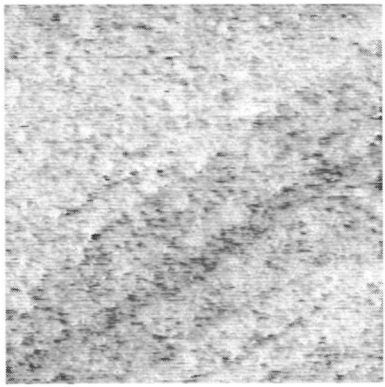

Figure 3.14: *InAs(110) surface covered with a thin oxide. The scanrange is 460 Å^2. Steps can still be observed.*

Within a few minutes after cleaving the sample, the STM is cooled down to 4.2 K, preventing further oxidation of the cleaved surface.

The obtained surface allows to record reproducible images, which prove a non-contact tunnel current is established. The images are different from those on surfaces that were cleaved at low temperatures, and do not show atomic resolution. Figure 3.14 shows an image in which still features of steps are present, indicating the oxide is thin.

Several spectroscopy curves obtained on this surface are plotted in Figure 3.15 The curves do show an onset of the conduction band below the Fermi-energy at $\sim$-150 mV, but are rather position dependent.

The inhomogeneity of the $I - V$ curves over the surface can has two possible origins. A "dirty" oxide will result in a broad distribution of surface state energies. As a consequence the band structure varies as a function of position. Opposing this explanation is the rather constant energy for the Fermi-level pinning in Figure 3.15. Another effect of the surface states is that they influence the tunnel current between tip and sample. Since tunneling spectroscopy with an STM lacks the spatial averaging of planar junctions, the sensitivity for surface states can not be neglected. Most probable is that both effects contribute to the spatial dependence of the $I - V$ curves.

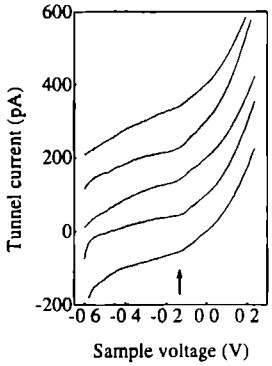

Figure 3 15 *Spectroscopy curves obtained at various positions of the oxidized InAs (110) surface At the voltage indicated by the arrow all curves show a kink in the tunnel current Also the onset of the valence band is visible The curves are offset for clarity*

3.6 Conclusions

We have investigated the InAs(110) surface under various surface conditions by low temperature scanning tunneling microscopy Clean surfaces show no indications of Fermi-level pinning, and are sensitive to the electric field of the STM tip At energies in the bulk conduction band Landau levels can be observed The Landau levels allow to investigate the electric field dependence of the state density at the semiconductor surface The data show that with tips that were prepared in ambient, significant variations in the measured spectra can take place The tip work function also did occasionally show changes during the experiment, which indicates that the work function parameter is very sensitive Steps and oxides have demonstrated Fermi-level pinning in the conduction band Spectra obtained in the vicinity of straight steps indicate the existence of a quasi one dimensional electron gas at the surface

A surface 2DEG suitable for investigation with an STM requires very homogeneous Fermi-level pinning Apparently oxidation under the conditions described section 3 5 does not fulfil this requirement The step edge data of section 3 6 show that increasing the number of dangling bonds in the conduction band can provide the necessary Fermi-level pinning

3.7 Acknowledgements

This work was supported by the Dutch Foundation for Fundamental Research of Matter FOM, which is in turn financially supported by the Dutch Organization for Scientific Research NWO. We gratefully acknowledge M C M M van der Wielen and R. Jansen for useful discussions and A J A van Roij for technical assistance.

References

[1] R M Feenstra, W A Thompson, and A P Fein, Phys Rev Lett. **56**, 608 (1986)

[2] R M Feenstra, J.A. Stroscio, J. Tersoff, and A P Fein, Phys Rev Lett **58**, 1192 (1987).

[3] M.B. Johnson, O Albrektsen, R M Feenstra, and H.W.M Salemink, Appl Phys. Lett **63**, 2923 (1993).

[4] J.F. Zheng, X. Liu, N. Newman, E.R. Weber, D F. Ogletree, and M Salmeron, Phys. Rev. Lett. **72**, 1490 (1994).

[5] R.M. Feenstra, D.A Collins, D.Z.-Y. Ting, M.W Wang, and T.C. McGill, Phys Rev Lett. **72**, 2749 (1994).

[6] W. Wu, S.L. Skala, J.R. Tucker, J W. Lyding, A Seabaugh, E A. Beam III, and D. Jovanovic, J Vac Sci. Technol. A **13**, 602 (1995).

[7] K. v Klitzing, G Dorda and M.Pepper, Phys Rev. Lett. **45**, 494 (1980)

[8] The setup is described in Chapter 2.

[9] C A Mead and W G Spitzer, Phys. Rev Lett. **10**, 471 (1963)

[10] S Kawaji and H.C. Gatos, Surface Science **7**, 215 (1967).

[11] D C Tsui, Phys. Rev B **4**, 4438 (1971).

[12] D C Tsui, Phys Rev. B **8**, 2657 (1973).

[13] J van Laar, A Huijser, and T L. van Rooy, J. Vac Sci Technol **14**, 894 (1977).

[14] J A Appelbaum, and G.A. Baraff, Phys. Rev Lett. **26**, 1432 (1971)

[15] C.J Chen, *Introduction to scanning tunneling microscopy*, (Oxford University Press, New York and Oxford, 1993).

[16] R M Feenstra and J A. Stroscio, J Vac. Sci Technol. B **5**, 923 (1987)

[17] R M Silver, J A Dagata, and W Tsjeng, J Appl Phys **76**, 5122 (1994)

[18] H Reisinger, H Schaber, and R E Doezema, Phys Rev B **24**, 5960 (1981)

[19] G W Gobeli and F G Allen, Phys Rev **137**, A245 (1965)

[20] D R Lide, *CRC Handbook of Chemistry and Physics* (CRC Press, Boca Raton, 1991), 72^e edition

[21] For example *Solid state surface science*, edited by M Green, (Marcel Dekker, New York, 1969)

[22] Many of the older experimental results on work functions are worthless because of poor vacuum techniques See for example G Herrmann and S Wagener, *The oxide coated cathode*, (Chapman and Hall, London, 1951), Vol 2, p 78

[23] In a recent article He has also been found to influence the tunnel current between two metal electrodes R G Keijsers, J Voets, O I Shklyarevskii, and H van Kempen, Phys Rev Lett **76**, 1138 (1996) About the influence of He on work functions, see for example J Patigny, Y Barbaux, and J - P A Beaufils, in *Adsorption-desorption phenomena*, ed F Ricca (Academic Press, London and New York), 49 (1972), and references therein

[24] A Vaterlaus, R M Feenstra, P D Kirchner, J M Woodall, and G D Pettit, J Vac Sci Technol B **11**, 1502 (1993)

[25] A possible explanation for the existance of straight steps is that the lattice is partly ionic, in which case straight steps have the lowest energy

[26] W Monch, *Semiconductor Surfaces and Interfaces* (Springer-Verlag, Berlin, Heidelberg, 1993)

[27] The techniques used by Van Laar *et al* [J van Laar, A Huijser, and T L van Rooy, J Vac Sci Technol **14**, 894 (1977)] are photoemission, low-energy-loss spectroscopy, and contact potential difference (CPD) measurements

Chapter 4

Semiconductor band-switching by charging a small grain with a single electron

Abstract: We observe a very abrupt change in the electron density in STM-measurements on an InAs(110) surface in the vicinity of a small conductive grain The observed features are a consequence of charge quantization on the grain, which acts as a single electron gate electrode The band-bending at the surface changes stepwise when an extra electron is added to the grain, resulting in in a sharp closed curve around the grain in topographic images Also features due to the screening of the residual charge of the grain are discussed

This chapter is an extended version of the paper *Semiconductor band-switching by charging a small grain with a single electron*, by J W G Wildoer, A J A van Roij, C J P M Harmans, and H van Kempen, Phys Rev B **53**, 10695 (1996)

Charges located close to a semiconductor interface will change its local electronic properties significantly. These charges can for example be present at charge traps in oxides near the interface, and will cause spatial variations in the energies of the valence and conduction bands of the semiconductor. Similar effects will occur in a system consisting of small charged grains on a semiconductor surface. On such a surface a scanning tunneling microscope gives the opportunity to study spatially resolved effects in the band-bending, associated with one individual charged grain. If the charge on such a grain can be controlled, effects in the band-bending induced by one single extra electron should be observable in the vicinity of the grain.

Scanning tunneling microscopes can reveal spatial variations in the local density of states with unprecedented lateral resolution. At low temperatures very small deviations are already observable, which has in recent years yielded for example images of the distribution of quasi particles in a vortex core [1] and of standing waves of surface electrons [2]. In these experiments Fermi-energies are large and the influence of the tip on the local density of states at the surface is negligible At surfaces however where the density of states around the Fermi-energy is sensitive for electrical fields, the presence of the STM-tip will have a local influence This is the case with semiconductors, but also in some sense with systems where charging energies play a role The influence complicates the interpretation of spectroscopic data, but on the other hand can be used intentionally to vary the electrostatic potential of a surface very locally [3]

In this chapter we present STM-measurements showing abrupt changes in the band-bending, caused by charging a small grain on an InAs(110) surface Charges are induced on the grain by the electrostatic action of the tip, which is simultaneously used to probe the changes in the electron density at the semiconductor surface. This double use of the tip is possible since the electric field of the tip extends over a far larger area than the area where the tunneling takes place We observe a very abrupt change in the conduction electron density on the InAs (110) surface when the tip is in the vicinity of a small conductive grain The change in the density of states is very clearly visible as a sharp circle-like closed curve in topographic images (Figure 4 1a), which also show the atomic lattice of the InAs (110) surface. We explain the observed features as a consequence of charge quantization on the small grain

Charge quantization experiments performed with an STM are usually done in a double junction geometry [4, 5, 6, 7] The tip then acts as one of the leads to a small metallic grain, which is situated on a thin insulating layer on top of a

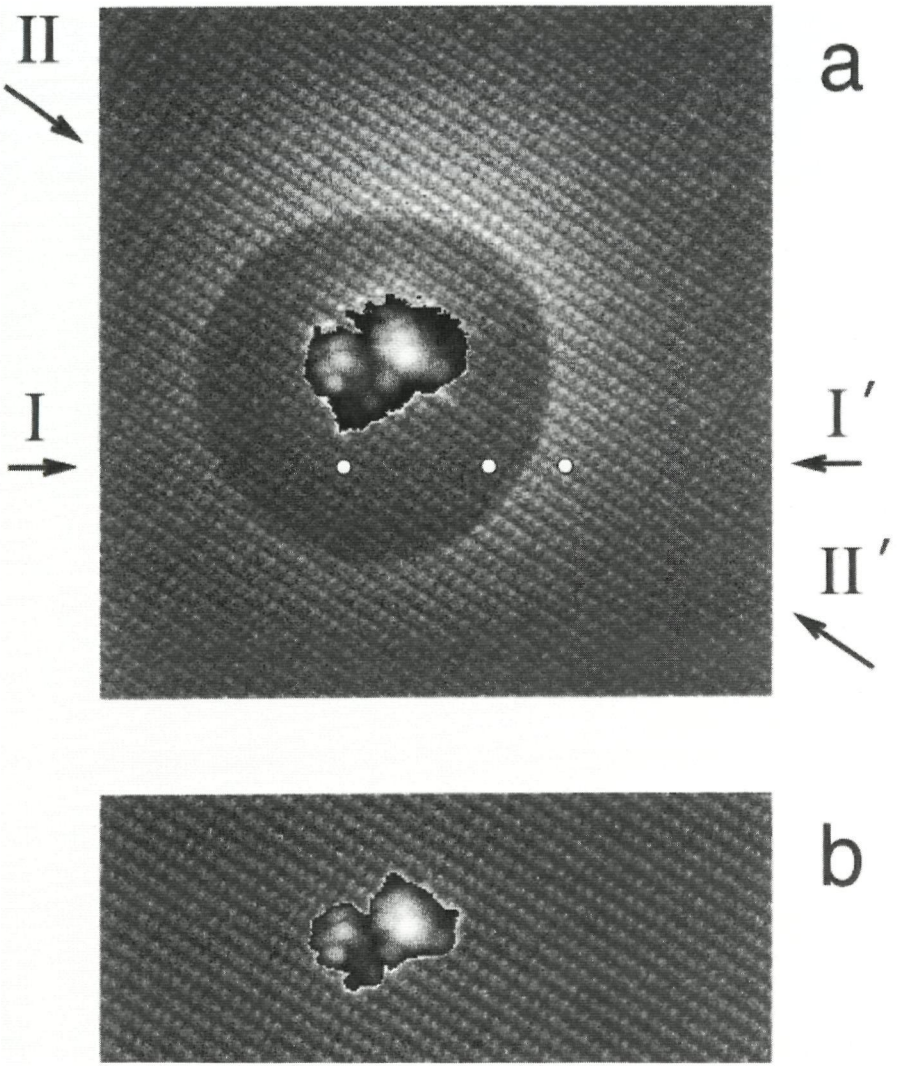

Figure 4.1: *Constant-current STM images at sample voltages of (a) -400 mV and (b) 400 mV. The scan range is 230 Å^2, (b) is only partially depicted. The tunnel current is 150 pA. The arrows I and I' indicate a line along which spectroscopy curves are taken. The three white dots are positions corresponding to the spectroscopy curves shown in Figure 4.2a. The scales can be deduced from Figure 4.4, in which a cross section along the line II-II' is shown. The details in the structure of the grain show that it is conductive. The data are unfiltered.*

conducting substrate (this is the other lead). If the capacitance of the grain to its environment is sufficiently small the charging energy dominates the electron transport. The advantage of using an STM to form these geometries is that the tunnel resistance and the capacitance of one of the junctions can be varied by changing the position of the tip. In practice however the capacitance can only be varied by a small amount, since the tunnel current falls off exponentially when the tip-grain distance is increased.

In the experiment described here, charges are detected *indirectly* and therefore also the tip-to-grain capacitance can be varied substantially We will show that the circle observed in Figure 4.1a is a line of constant tip-to-grain capacitance, and in this way images the electric field of the STM-tip.

The InAs used in this experiment is lightly n-doped, n = 2.5 10^{16} cm^{-3} with a Fermi energy of 10 meV. The (110) surface was obtained by in-situ cleaving the crystal at low temperature with a small sledge mounted on the sample holder of the STM. The STM was enclosed by a vacuum can which was filled with helium gas to provide sufficient heat exchange with the helium bath Due to the cold-trap action of the walls of the insert surfaces stay clean for several days in our set-up. The STM used in this experiment is similar to one described elsewhere [8], but modified for cleaving at low temperatures. The STM-tips were made by cutting Pt(90%)-Ir(10%) wires. The temperature during the measurements was 4.2 K.

If cleaving was successful large atomically flat terraces were observed, separated by mono-atomic steps. Similar to images of GaAs [9] either In or As atoms are shown, depending on the bias voltage.

The small grain present in Figures 4 1a and 4 1a was found on a large atomically flat terrace after the feedback system was oscillating for a short time directly after the tip approach. During oscillation tip-sample distances vary with relatively large amplitudes, and at some instances the tip can be very close to the sample surface. This can have caused a losely connected part of the tip to deposit onto the sample, since electrostatic forces increase considerably at small distances [10]. We make however no assumptions on the exact nature of the grain, but conclude from our measurements that it is conductive. After half an hour of measuring the grain disappeared, and was presumably picked up by the tip. After this, the flat surface showed no defects, and the other features present in Figure 4.1a had disappeared This shows that the observed phenomena are caused solely by the grain and not by defects at the sample surface.

The sharp circle shown by the topographic images, can be excluded to origi-

nate from a real change in height, since it is only present when the sample voltage is negative Positive sample voltages only show a regular lattice (Figure 4 1b) Also, at the circle in Figure 4 1a [11] the underlying lattice is still clearly visible and shows no distortion A very remarkable feature of the circle is its extreme sharpness The change in z deflection takes place on a length scale shorter than the lattice constant Furthermore it is worth noting that the circle is not located symmetrically around the small grain

In addition to topographic images $I - V$ curves have been taken along the line I-I' indicated in Figure 4 1a $I - V$ curves are obtained by interrupting the feedback system and subsequently sweeping the tunnel voltage over a preset range in about 0 5 s The tip height is set with the feedback-system active by choosing a tunnel voltage (V_{set}) and a reference current (I_{ref}) Figure 4 2a shows three I-V curves taken at $x = 85$ Å (I), $x = 135$ Å (II) and $x = 160$ Å (III) In these measurements the tip-height was regulated with a sample voltage $V_{set} = +400$ mV (the tip voltage was kept at zero) and a reference current $I_{ref} = 150$ pA V_{set} was chosen at this value to avoid the variations in the local electron density to influence the tip height With the sample voltage of +400 mV the Fermi-level of the tip is well above the conduction band-edge of the InAs, so therefore all $I - V$ curves are taken at the same tip-sample distance

Since the InAs used is a (degenerate) semiconductor, the shape of the curves is asymmetric At positive voltages electrons tunnel from the tip into the conduction band and the available number of states for tunneling is much larger than at negative sample voltages Note that in the gap (negative voltage) the differential conductance is not zero, which indicates tip induced band-bending

A more remarkable feature is the sharp jump present in curves I and II at negative sample voltages At the voltage of the jump the differential resistance is negative Although the effect in the $I - V$ curves is small, it is present in all curves taken within the region of the circle The bias voltage where the jump takes place varies with position as shown in Figure 4 2b The voltage increases when the edge of the circle is approached and roughly equals -400 mV at the edge Since this is the tunnel voltage which was used in Figure 4 1a we conclude that the dark area in Figure 4 1a is defined by the value of the bias voltage and maps the occurrence of a jump in the $I - V$ curves between zero and the bias voltage From Figure 4 2b we thus conclude that a smaller bias voltage results in a smaller circle

The jump in the $I - V$ curves cannot be explained by straightforward tip-induced band-bending, because of its negative differential resistance and also

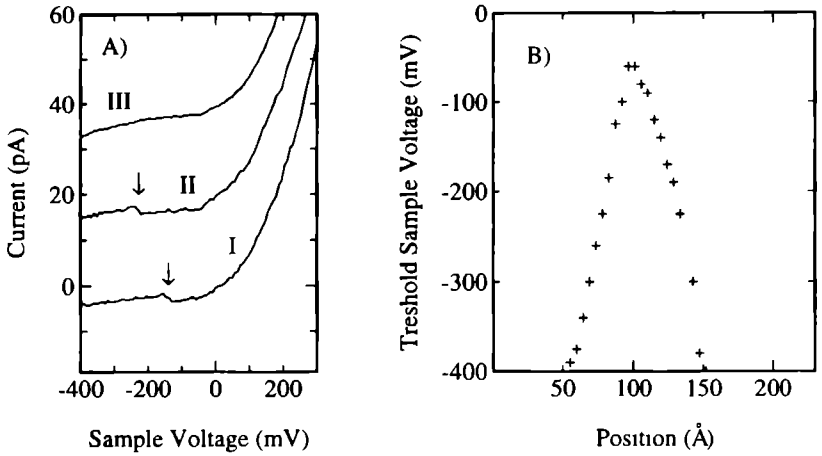

Figure 4 2 *(a) Spectroscopy curves taken along the line I-I' of Figure 4 1a at x = 85 Å (I), x = 135 Å (II) and x = 160 Å (III) (x is taken relative to the left side of Figure 4 1a) Curves II and III have an offset for clarity (b) Threshold Sample Voltage as a function of position along the line I-I' (x is taken relative to the left side of Figure 4 1a)*

not by interference effects of the conduction electrons, given the abruptness of the transition in the topographic images (the Fermi wavelength of the InAs can be calculated to be around 8 nm) The shape of the $I - V$ curves indicates a *switching* of the conduction band between two levels This switching is induced by the bias voltage between tip and sample and results in a stepwise decrease of the conduction electron density

We explain the observed features by single electron charging of the grain induced by the electric field of the tip The charge on the grain leads to band-bending at the semiconductor surface Because of the quantized nature of the electron charge only discrete levels are possible The model we use is shown in 4 3 The bias voltage required to charge the grain can be given simply by [7]

$$V_T = -\frac{e}{2C_T}\left(1 - \frac{2Q_0}{e}\right) + \frac{\Delta W}{e}, \tag{4 1}$$

where Q_0 is the offset charge of the grain and C_T represents the tip-to-grain capacitance The work function difference between the tip and the InAs surface is accounted for by the term ΔW To allow charging, the tunnel resistance from grain to substrate, R_G, has to be larger than h/e^2 Note that the grain to substrate capacitance, C_G, has no influence in this model The data of Figure 4 2b

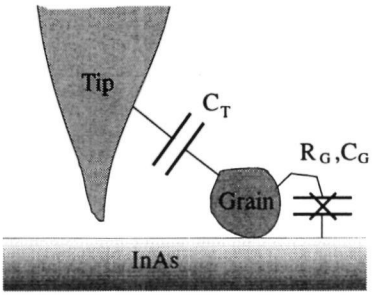

Figure 4.3: *Representation of the model. The tip induces an extra electron on the grain when the bias voltage exceeds a value determined by the tip-to-grain capacitance* C_T.

are in agreement with the model, since by increasing the tip-grain distance the capacitance C_T is decreased. It is difficult to estimate Q_0 from these data since the work function difference ΔW is unknown, largely because it depends critically on the shape of the tip.

At the sharp circle of Figure 4.1a a tip-sample voltage of 400 mV was required to charge the grain, and consequently the circle is a line of constant tip-grain capacitance C_T. The deviations from the symmetric shape of the circle are a consequence of the shape of the tip. In fact, from this measurement it is possible to extract quantitative information about the shape of the tip. Larger grains will result in smaller charging energies and in that case more circles of equal capacitance should be observable, each one corresponding to a successive integer number of electrons on the grain.

Apart from the dark area described earlier, also a slowly fading brighter circle is present in Figure 4.1a, which is located symmetrically around the grain. In the brighter circle the conduction electron density is enhanced compared to far away from the grain. Outside the circle the grain is not charged by the tip, but still influences the band-bending in the surrounding area via its residual positive charge.

The cross section along the line II-II' indicated in Figure 4.1a is shown in Figure 4.4. On both sides of the grain the sudden increase in tip-height is followed by a gradual decrease. In fact the grain closely approximates a screened point charge, for which the potential $\phi(r)$ is given by [12]:

$$\phi(r) = \frac{Q}{r - r_0} e^{-(r-r_0)/l_s}, \tag{4.2}$$

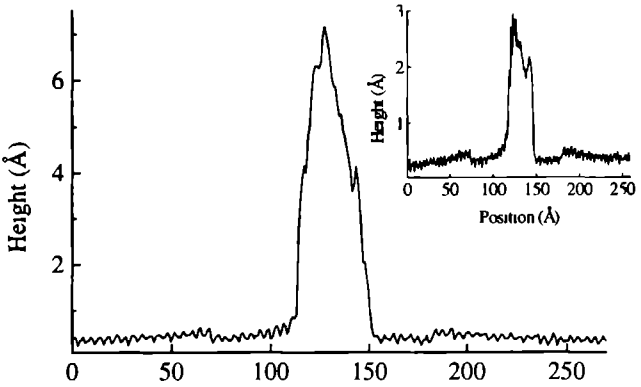

Figure 4 4 *(a) Cross section along the line II-II' in Figure 1(a) The depicted cross section is taken through the highest point of the grain, showing its maximum height is circa 7 Å Further both the atomic lattice and the height change at the edges of the circle are clearly visible Inset Other cross section The band-switching event can be observed more clearly*

where l_s is the screening length and Q the point charge at r_0 The (positive) residual charge results in an increase in the number of states density below the Fermi energy In the charged situation, the grain induced band-bending appears to be rather small, since the tip-height is almost equal to far away from the grain The band-bending at the surface both in the charged and the uncharged situation are illustrated schematically in Figure 4 5 The band-bending is not only determined by the work function difference, as with large interfaces, but also by the charging conditions The work function difference between grain and InAs determines Q_0 in (1), whereas the charging energy and the external electrical field determine the energies of the charged states in the grain, and through these also the actual band-bending Since the fading brighter circle (the uncharged situation) is caused by the residual charge A, the influence of the tip on its shape will be of minor importance Therefore, in contrast to the charging circle, the screening circle has a symmetric shape The screening length l_s can be calculated to be 4.3 nm [12]

Essential for the quantization of charge on the grain is that the wavefunctions of the grain the InAs surface are sufficiently separated ($R_G > h/e^2$) We do not have a simple explanation for the presence of a barrier in our case, where we have to consider an interface of atomic dimensions However at any interface polarisation charges should compensate for a difference in work function, and also

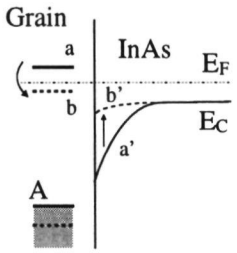

Figure 4.5: *Band-bending in the charged (dashed line) and the uncharged situation. Switching of the conduction band from a' to b' will occur when the charged state is moved below the Fermi energy. A is the highest occupied level of the grain in the absence of the tip and determines the residual charge of the grain.*

at the grain-InAs surface these should be present. Possibly these polarization charges are responsable for the potential barrier between the grain and the InAs surface. Also the offset charge Q_0 of the grain should should be due to this polarization, since no other charges are present that could induce an offset.

To image features like the ones described here properly, both tip and grain shape should be such that no double tip effects occur. Also, changes in the electron density are only present within a small area around the grain, determined by the screening length. We observed abrupt transitions also around other grains (Figure 4.6), however the effects were less clear than in the case we discussed. Attempts to deposit metallic grains in a more controlled way by field evaporating from a gold tip at low temperature were unsuccessful. However, various other techniques for depositing small metallic particles at low temperatures exist and in a more dedicated setup systems like the one described here should be relatively easy to obtain.

In the experiment the STM is both used to charge the grain and to probe

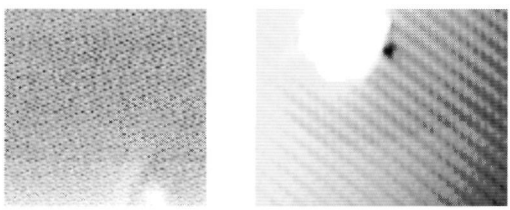

Figure 4.6: *Other grains with similar transitions in the band-bending, (left)* V_{Sample} *= -200 mV, (right)* V_{Sample} *= -400 mV.*

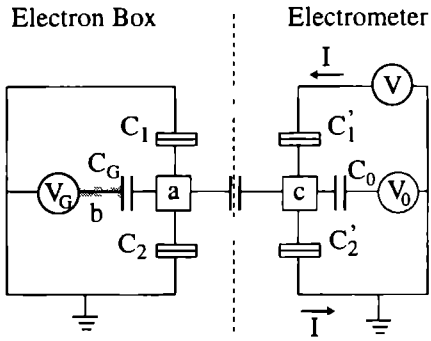

Figure 4 7 *Single electron box configuration, (a) electron box, (b) gate electrode, (c) centre island of the electrometer circuit*

the electron density The system has similarities with the single electron box configuration (SEB) realised by Lafarge *et al* [13] In their circuit, which is schematically represented in Figure 4 7, the charge on a small island, the electron box (a) is varied by applying a voltage on a gate electrode (b) The charge on the electron box contributes to the induced charge Q_n on the center island of the double junction (c), and will in this way modify the current (I) through the double junction Since the charge on the electron box is quantized, also the charge Q_n will vary non-continuous, resulting in a sawtooth-like dependence of the current on the applied gate voltage V_G Each sawtooth in the $I - V_G$ curve corresponds to one extra electron on the grain The circuit of Figure 4 7 consists of two parts, one charges the electron box, the other measures its charges In the experiment described in this chapter, the capacitive coupling of the tip to the grain charges the grain, whereas via the measured tunnel current the charge on the grain can be determined

In conclusion, we have been able to observe effects in the electron density in a semiconductor associated with the quantized charge of a small grain on its surface In the vicinity of the grain the conduction band switches between two levels, depending on the charge of the grain In the experiment the STM is both used to charge the grain and to probe the electron density In the topographic measurements the tip-to-grain capacitance and the screening area are imaged The system presented offers the possibility to study charging effects both in a direct and an indirect way, simply by varying the position of the tip More experimental data can yield quantitative information about Q_0 in these systems

and the role of the work function in the charging process

This work was supported by the Dutch Foundation for Fundamental Research of Matter FOM, which in turn is financially supported by the Dutch Organization for Scientific Research NWO. We are grateful to C. Schönenberger for the InAs material.

References

[1] H.F. Hess, R.B. Robinson, and J V. Waszcak, Phys Rev Lett. **64**, 2711 (1990).

[2] M.F Crommie, C.P. Lutz and D M. Eigler, Nature **363**, 524 (1993).

[3] M C M.M. van der Wielen, A.J.A. van Roij, and H. van Kempen, Phys. Rev Lett. **76**, 1075 (1996).

[4] P J.M van Bentum, R.T.M. Smokers, and H van Kempen, Phys. Rev. Lett. **60**, 2543 (1988).

[5] R Wilkins, E Ben-Jacob, and R C. Jaklevic, Phys. Rev Lett **63**, 801 (1989)

[6] J G A Dubois, E.N.G.Verheijen, J.W Gerritsen, and H. van Kempen, Phys Rev B **48**, 11260 (1993)

[7] C T Black, M.T. Tuominen, and M. Tinkham, Phys. Rev B **50**, 7888 (1994)

[8] J.W.G Wildöer, A.J.A. van Roij, H. van Kempen, and C.J P.M. Harmans, Rev Sci Instrum **65**, 2849 (1994).

[9] R.M Feenstra, J A Stroscio, J Tersoff, and A P. Fein, Phys. Rev Lett **58**, 1192 (1987).

[10] Oscillating the feedback the feedback system is often done deliberately to obtain stable tips.

[11] Shape and size of the circle reproduced exactly in images taken over half an hour.

[12] See for example, C Kittel, *Introduction to Solid State Physics* (John Wiley and Sons, Inc., 1971)

[13] P Lafarge, H Pothier, E R Williams, D Esteve, C. Urbina, and M H Devoret, Z Phys B **85**, 327 (1991)

Chapter 5

Proximity induced mosaic vortices observed by scanning tunneling microscopy

Abstract: The induced superconducting properties of a thin granular Au film evaporated on top of a Nb layer are investigated by means of low temperature scanning tunneling microscopy and spectroscopy Density of states measurements at different points of the Au surface show identical BCS-like curves, despite the irregular topography of the surface An applied magnetic field causes the appearance of proximity induced vortices, which have an irregular mosaic structure The results are explained by the formation of induced bound states in the grains

The work presented in this chapter was done in cooperation with G A de Goeij, S E Shafranjuk, H van Kempen and C J P M Harmans

In recent years low temperature scanning tunneling microscopy and spectroscopy (STM) has been successfully applied to investigate the inhomogeneous properties of superconductors [1] Particularly, the capability of an STM to measure the local electronic properties on a scale much smaller than the superconducting coherence length ξ_S has proven to be very powerful in investigating the core of a vortex, which can appear in an external magnetic field [2, 3]

Another intriguing phenomenon related to non-homogeneous superconductivity, where the STM can be valuable is the proximity effect [4], which determines the electronic properties in the vicinity of an interface between a normal metal (N) (with a zero or negative BCS coupling constant λ_{ph}) and a superconductor (S) The theoretical description of the proximity effect is still a matter of debate One disputed point is whether or not the energy gap penetrates from S to N (where $\lambda_{ph} \leq 0$)

A direct way of investigating the density of states in the N-side of an N/S junction is by performing tunnel spectroscopy on this side This technique has been applied in planar thin film N/I/N/S junctions [5, 6], which showed BCS-like dI/dV-curves on the N-side of the N/S-sandwich However, a strong disadvantage of this technique is that the data obtained with these macroscopic sized junctions provide information only about the position-averaged electron spectrum Low temperature scanning tunneling spectroscopy enables to record the density of states on the N-side of the N/S interface with high spatial resolution In combination with topographic measurements this can provide information about the spatial dependence of the proximity effect and the influence of the structure of the N-film on the local spectra

A particularly interesting geometry is obtained when a superconductor is covered with a granular N-film, with a thickness comparable to the grain size In this case the N-film is in the clean limit in the direction perpendicular to the film, whereas in the parallel direction substantial scattering can take place Here we will present data obtained on such a system, consisting of a 20 nm thick Au film evaporated on a 100 nm thick Nb layer The effect of the grain boundaries is most dramatic in magnetic fields, where they cause a mosaic-like spatial dependence of the density of states Spectroscopy curves in the vicinity of an induced vortex show different behavior than one would expect for the case of an ordinary vortex The results can be explained satisfactory by a semi-classical bound state model

The Nb/Au bilayer was evaporated on an oxidized Si substrate in a electron gun evaporator with a base pressure of 1×10^{-7} Torr The 20 nm Au film was deposited on the 100 nm Nb layer without breaking the vacuum and within

Figure 5.1: *STM topographic image of the Nb/Au bilayer obtained at 1.5 K. The scanrange is 150 × 150 nm^2.*

a few minutes after the Nb was evaporated. During evaporation the substrate was mounted on a copper plate kept at 290 K. At room temperature both the formation of alloys and the occurence of significant mixing can be excluded with these metals. The critical temperature of the Nb/Au bilayer film was determined to be 7.0 ± 0.1 K and the residual resistance ratio (RRR) 1.85.

Our STM-measurements [7] are performed in a pumped ^{4}He bath at 1.5 K. Figure 5.1 shows a topographic image of the Nb/Au bilayer. The Au-film has a granular structure with grain sizes varying between 25 nm and 35 nm (in the plane of the film). The stable tunnel current and the perfect reproducability of the images on this surface assures that indeed the inert Au-toplayer is imaged. An uncovered 100 nm Nb film evaporated under the same conditions was imaged by an atomic force microscope and showed small grains with a 10 to 15 nm size. These values give an upper limit for the mean free elastic length. Hence, we estimate the superconducting coherence length in the Nb, ξ_{Nb}, to be smaller than 35 nm [9]

Tunnel spectroscopy curves taken on different Au grains, but also at different positions on an individual grain show nearly identical BCS-like curves. The curves (Figure 5.2) have a gap edge peak height which is larger than would result from a BCS tunneling density of states at 1.5 K, as was also observed in planar junctions [5] Also the dI/dV returns faster to its normal value outside the gap than in the BCS-case The curves do not show charging effects, from which we conclude that the transparencies from each grain to its environment are high.

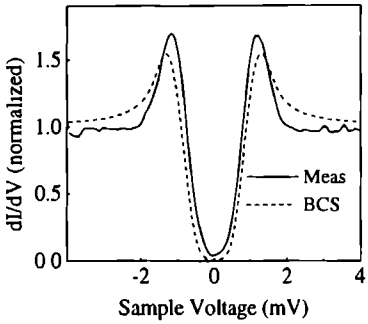

Figure 5 2: *Measured spectroscopy curve at 1.5 K (solid line) and calculated BCS-curve (including voltage modulation due to noise V_{noise} = 0 3 mV) for 1 5 K (dashed line).*

In a magnetic field, applied perpendicular to the Nb/Au bilayer, I-V curves taken at different positions on a single grain still are very similar However, once we compare spectroscopy curves taken on adjacent grains, very clear changes can be seen, as shown in Figure 5.3 In particular the subgap density of states varies strongly from grain to grain, while the width of the gap is approximately constant on the different grains.

In order to map the spatial dependence of the density of states over a larger area, we measured the tunnel current as a function of bias voltage at constant tip-sample distances over an area of 300 × 300 nm^2 At every position first the tip-sample distance was regulated by the STM feedback system at a preset tunnel current and bias voltage. Subsequently, with the feedback system off, the tunnel current was measured at a fixed number of different bias voltages inside and outside the superconducting gap Spatial variations in differential conductance at a certain voltage results in spatial variations in the measured tunnel current. To prevent variations in the density of states from influencing the tip sample distance the bias voltage during feedback was chosen outside the superconducting gap at 5.8 mV, the reference current was 150 pA.

Figure 5.4 shows current images obtained in this way at a sample voltage of -0.7 mV, measured in different magnetic fields. In the dark areas the depth of the gap is reduced. The formation of a vortex lattice is clearly visible (the vortex densities are in agreement with the applied magnetic fields). At zero field (Figure 5.4f) we observe no structure in the current image, except for a small feature on the right hand side of the picture. At 1.1 ± 0 1 T the overlap of the

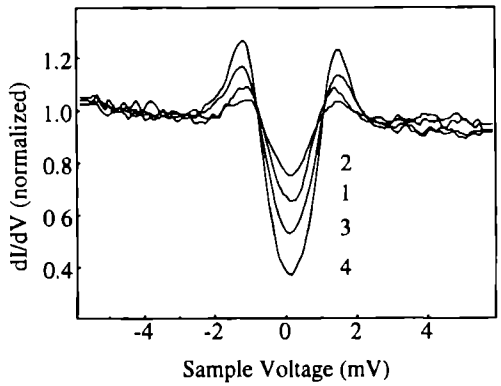

Figure 5 3 *Tunnel spectroscopy curves taken on adjacent grains at a magnetic field B = 0 15 T. Position and size of the grains can be deduced from corresponding numbers in Figure 5 4c The magnetic field is applied perpendicular to the Nb/Au bilayer.*

vortices is such that no features in the current images are present anymore More remarkable is the shape of the vortices. The measured tunnel current, reflecting the density of states, changes mostly at the grain boundaries. This is in agreement with the spatial dependence of the spectroscopy curves discussed earlier. The spatial dependence causes the vortices to have a mosaic-like structure In Figure 5 4 the mosaic-planes in the current images can be mapped on the individual grains in Figure 5 4a. A cross section of the topographic image is shown in Figure 5.5. From the cross-section we can conclude that a significant fraction of each grain is imaged and not only its highest point [8].

We first discuss the results within the mean field approach as used in the Bogoliubov-de Gennes equations [9]. In this description of the proximity effect the induced gap in the normal metal is assumed to be zero since $\lambda_{ph} \leq 0$, and the proximity effect is only due to the phase coherence between the electrons and holes in the normal metal and Cooper pairs in the superconductor According to the model, tunnel spectra taken on the N side of an N/S interface can however still show a BCS-like shape since bound states that are present in the N-film [10, 11] can also give BCS-like singularities in the spectra To give the BCS-shape, the energy of the lowest bound state has to coincide approximately with the gap energy of the superconductor. The bound states originate from multiple Andreev [12] reflection at the N/S interface and normal reflection at the N-vacuum interface of the combined electron-hole wavefunctions. In a simplified

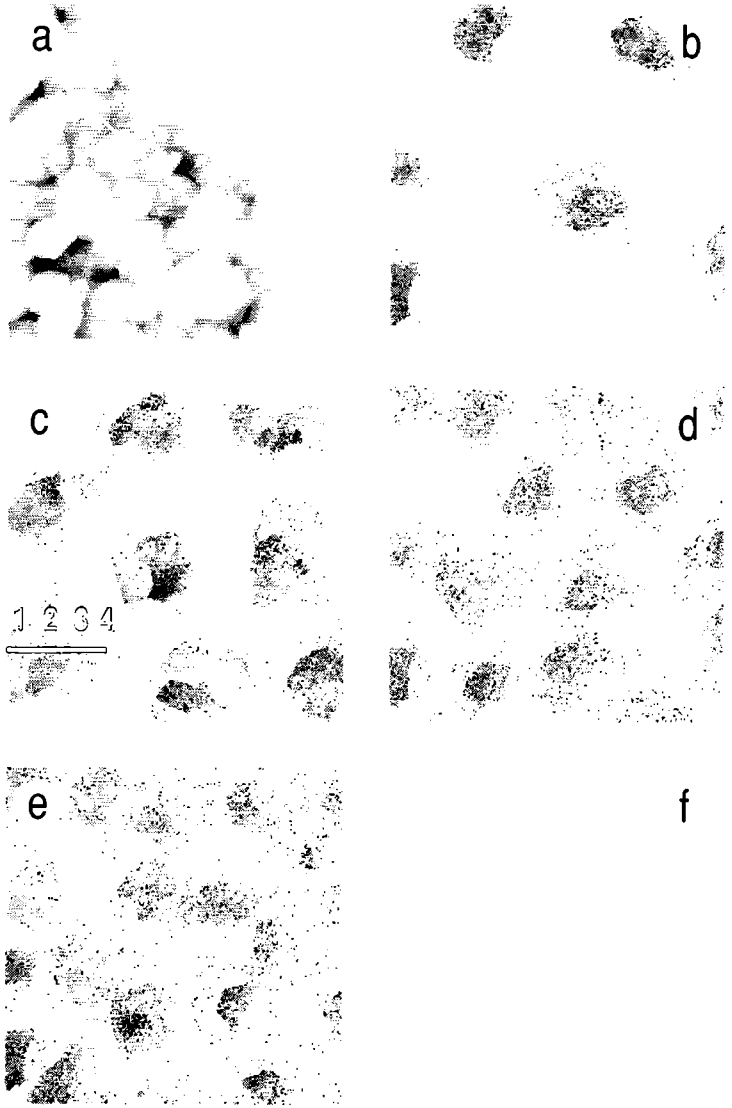

Figure 5.4: *Topographic image (a) and current images, obtained at a bias voltage of -0.7 mV, in magnetic fields perpendicular to the Nb/Au bilayer: (b) 0.08 T, (c) 0.15 T, (d) 0.25 T, (e) 0.33 T and (f) zero field. Note that the feature in f is related to a spot where two grains are on top of each other. The line in c intersects four grains. These grains correspond with the curves in Figure 5.3. A cross section of the topographic image, indicated in (a), is given in Figure 5.5.*

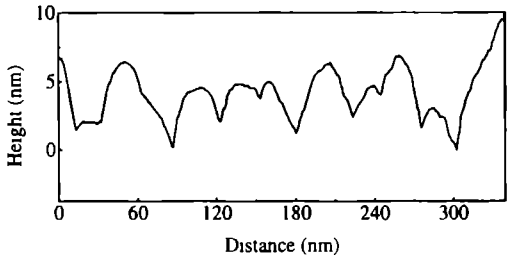

Figure 5 5 *Cross section of the topographic image Figure 4a Heigth differences are of the order of 5 nm The cross section demonstrates that the tip is quite sharp*

model the trajectories can be represented as in Figure 5 6a The difference in acquired phase by the electrons and the holes over the trajectory, together with the phase shifts at the N/S interface have to satisfy the Sommerfeld condition for a bound state The phase shift at the interface is energy dependent and is zero at the gap energy of the superconductor

In order to estimate the dependence of the energy of the lowest bound state level on the thickness of the N-film, we use a semi-classical approach in which the total density of states results from a sum of all possible trajectories We neglect the proximity effect in the superconductor We note that the trajectories in the N/S bilayer are nearly equivalent to those in the S/N/S geometry, for which Kulik [13] found a simple relation for the energies of the bound states The energy levels for the N/S bilayer are the same as for the S/N/S system, once we take the thickness of N in S/N/S twice the thickness as in N/S, and add the boundary

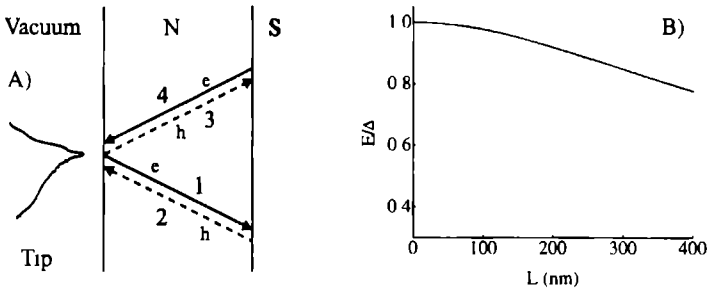

Figure 5 6 *(a) Bound state trajectory in an S/N junction (b) Calculated thickness dependence of the energy of the lowest bound state level, with* $v_F = 1\ 39 \times 10^6$ *m/s and* $\Delta = 1\ 0$ *mV*

condition that at the center of the S/N/S the wavefunction should be zero [4] Therefore the energies of the bound states E_n (relative to the Fermi-energy) in the normal film of the N/S bilayer are given by

$$\cos^{-1}\left(\frac{E_n}{\Delta}\right) + \frac{2E_nL}{\hbar v_F} = 2\pi n \quad n = 0, \pm 1, \pm 2, \quad , \tag{5 1}$$

where Δ is the gap of the superconductor, L is the thickness of the normal film and v_F the Fermi-velocity of the normal metal For short L only a solution for $n = 0$ is possible, E_0 In the regime where $L \ll \pi\hbar v_F/2\Delta$ the energy E_0 is only weakly dependent on the thickness of N or the length of the trajectory, which explains the absence of significant thickness dependence in our spectra at different positions on the Au-film Figure 5 6b shows that for trajectories which correspond to an N-thickness of less than 100 nm the deviation of E_0 from Δ is less than 3 % The total density of states at a given position results from a summation over all possible trajectories (So, all possible angles in Figure 5 6b)

In magnetic field the situation changes considerably As vortices appear in the superconductor, the value of the superconducting gap varies over the interface In the spectroscopy curves of Figure 5 3 however, we do not find smaller gap values, but instead only changes in the DOS-amplitudes The measurements suggest that in the vicinity of a vortex a fraction of the bound states resulting from the zero-field gap persists, while others are transformed into normal extended states, which can exist due to the presence of the vortex Close to a vortex the superconducting gap is strongly inhomogeneous over the interface In general trajectories like in Figure 5 6a then encounter the N/S interface at two different gap values In thin N-layers Andreev reflection at different gap values will not allow the formation of a bound state (the Sommerfeld condition can not be satisfied, Figure 5 7) Since the probability of two reflections at the N/S interface to occur at the same reduced gap value within the vortex region is small, no peak-like structure due to smaller gap values are observed On grains in the vicinity of the vortex and even on top of the center of the vortex still a small contribution of zero-field gap bound states is present This contribution can originate from trajectories which have both reflections outside the vortex area, but also from trajectories which penetrate the superconductor inside the vortex and reflect at the vortex boundary

On individual grains the spectra appear to be approximately constant and the density of states changes mainly at the grain boundaries Within the present model the only possible conclusion is that a significant fraction of states is localized within the grain This is due to limited transparency of the grain boundaries

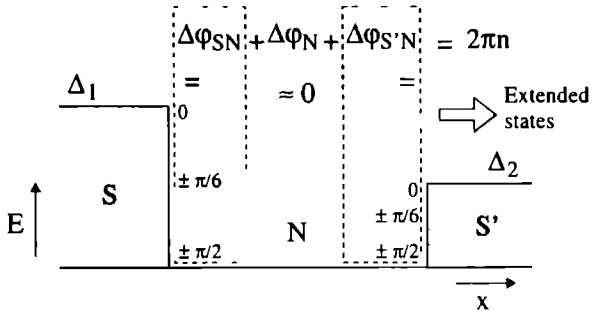

Figure 5 7 *SNS' geometry The equation is the condition for a bound state If the N-layer is very thin the difference in acquired phase by the electrons and the holes is neglectable, and the Andreev refections at the SN and the S'N interfaces have to give a phase shift equal to a multiple of 2π The phase shifts as a function of energy at the interfaces are given by* $\cos^{-1}(E/\Delta)$ *Some values are shown in the grey boxes For short L only the* $n = 0$ *is possible, however if* Δ_1 *and* Δ_2 *differ substantially the Sommerfeld condition can not be satisfied*

The non-unity transparencies are unlikely to be due to tunnel barriers between the grains, since Au does not oxidize A difficult aspect in the model is the absence of geometric effects on the density of states on different positions on the grain, as one would expect the bound state trajectories to be sensitive for this In Figure 5 4 only a few grains show a gradient in the density of states over the grain

The previous discussions have been based on a semi-classical bound state model, which predicts no induced gap in the normal metal However the zero-field spectroscopic data can also be explained very well by assuming that there is an induced gap $\Delta_N \neq 0$ in the thin Au-film Based on the zero-field data only it is in fact impossible to distinguish between both mechanisms, since deviations from the BCS-shape like in Figure 5 2 can be explained by introducing an energy dependent gapfunction $\Delta_N(E)$ in the normal metal The spatially resolved spectra in magnetic field however gives additional information, from which it may be possible to discriminate

A model that predicts an induced gap $\Delta_N \neq 0$ in the normal metal is the tunnel Hamiltonian proximity model [14], introduced by McMillan The gap is due to the tunneling interaction between states in the normal metal and states in the superconductor The assumptions in the model are only valid if the tunneling matrix elements are small At the Nb/Au bilayer interface this is very unlikely

to be the case, given the evaporation conditions mentioned earlier However if one still does apply the model, spectroscopy curves like the ones we observed can be obtained For this, tunneling times (which determine the interaction) have to be chosen very short, violating the assumptions of the model

To describe the situation in magnetic field within this approach one can model the Nb/Au bilayer as a superconducting substrate covered by a monolayer of coupled normal grains The induced energy gap functions vary from grain to grain A grain on top of a vortex does not experience a gap from the region of the superconductor it contacts and will only receive contributions from its neighboring grains This model would explain the mosaic-like spatial dependence of the density of states However also here it is required that the grains are only weakly coupled, which is rather unrealistic Also, qualitative agreement with the curves in Figure 5 3 is difficult to obtain For only a very limited range of fit parameters the energy of the peak-like structure in the DOS remains at the zero-field gap energy for grains in the vicinity of the vortex, as is the case in Figure 5 3 (and also in other measurements) In the actual sample the variations in grain sizes, transparencies and contact areas will give a broad distribution of these parameters We conclude that a description of our results in terms of the tunnel Hamiltonian proximity model is not very likely

In conclusion, by using spatially resolved spectroscopy, we have been able to study the proximity effect in a granular normal system on a microscopic scale In magnetic field the position dependence of the density of states is governed by the grain boundaries, which gives mosaic shaped vortices The spectroscopy curves in the vicinity of a vortex do not show a reduction of the superconducting gap, but only changes in the DOS-amplitudes The observed phenomena can be explained by a semi-classical bound-state model which assumes no induced gap in the normal metal A description in terms of the tunnel Hamiltonian proximity model should result in variations in the superconducting gap between the grains, which we do not observe

This work was supported by the Dutch Foundation for Fundamental Research of Matter FOM, which in turn is financially supported by the Dutch Organisation for Scientific Research NWO The authors like to thank L C Mur and H S J van der Zant for discussions and practical assistance S E S likes to thank the University of Nijmegen, the Research Institute for Materials (RIM) and NWO for visitor grants

References

[1] A L de Lozanne, S A Elrod, C F Quate, Phys Rev Lett **54**, 2433 (1985)

[2] H F Hess, R B Robinson, R C Dynes, J M Valles, Jr and J V Waszcak, Phys Rev Lett **62**, 214 (1989)

[3] Ch Renner, A D Kent, Ph Niedermann, Ø Fischer, F Lévy, Phys Rev Lett **67**, 1650 (1991)

[4] see for example E L Wolf, *Principles of electron tunneling spectroscopy* (Clarendon press, New York, 1985)

[5] C J Adkins, B W Kington, Phylos Mag **13**, 971 (1966)

[6] S M Freake, Phylos Mag **24**, 319 (1971)

[7] J W G Wildoer, A J A van Roij, H van Kempen, and C J P M Harmans, Rev Sci Instrum **65**, 2849 (1994)

[8] The particular shape of the tip determines the fraction of the grain that is imaged With a tip radius several times larger than the grain sizes, the tip only tunnels to the highest points of the grains, and in fact instead of the grain the tip is imaged In this case tunneling spectroscopy as a function of position only reveals the density of states at the top of the grain From Figure 5 5 we can however conclude that the tip is quite sharp A sharp tip assures that a significant fraction of the grain can be reached Similar results as in Figures 5 3 and 5 4 were obtained with other sharp tips

[9] P G de Gennes, in Superconductivity of Metals and Alloys (Benjamin, New York, 1966)

[10] P G de Gennes, D Saint-James, Phys Lett **4**, 151 (1963)

[11] G Kieselmann, Phys Rev B **35**, 6762 (1987)

[12] A F Andreev, Zh Eksp Teor Fiz **46**, 1823 (1964) [Sov Phys JETP **19**, 1228 (1964)]

[13] I O Kulik, Zh Eksp Teor Fiz **57**, 1745 (1969) [Sov Phys JETP **30**, 944 (1970)]

[14] W L McMillan, Phys Rev , **175**, 537 (1968)

Chapter 6

The scanning tunneling microscope-tip as a positionable contact: probing a Josephson-junction array at subKelvin temperatures

Abstract: We describe an experiment in which we have used a scanning tunneling microscope to contact a lithographically fabricated structure at 350 mK The STM enables to probe the structure, a Josephson-junction array, at various positions The experiment demonstrates that it is possible to combine the use of a scanning tunneling microscope with transport measurements on lithographically fabricated structures at temperatures below 1 K We focus on course positioning the tip above the structure of interest, the influence of the STM on the electronic noise, and the effective temperature of the sample during the measurements In first order the flux flow through the array is uniformly distributed

This project has been performed together with A van Oudenaarden, who is currently doing his Ph D research on Josephson junction arrays A v O also fabricated the sample described in this chapter

6.1 Introduction

Electron transport measurements through lithographically fabricated submicron structures have proven to be a successful method to reveal mesoscopic phenomena in small solid state systems Lithographically fabricated structures are mechanically stable, can be cooled down easily, and allow repeatable experiments Bondpads patterned on the sample substrate provide contact to the structure for a limited number of leads As the characteristic energy scales of these systems are small, the measurements have to be performed at low temperatures For example, in order to resolve the 0D states in a semiconductor quantum dot [1, 2], or to achieve a clear Coulomb-blockade in Single Electron Tunneling (SET) devices [3, 4, 5], temperatures well below 1 K are required (i e well below the common ^{4}He-temperature range)

In general, transport measurements yield information about the non-local properties of a mesoscopic structure In some experiments additional spatially resolved information can be required In these cases one can increase the number of leads connected to the structure However if the required spatial resolution is high, or the number of leads becomes very large, this solution will be impractical In such cases a more versatile and flexible solution is to use a low temperature STM and to operate it as a displaceable voltage probe or current injector

In this chapter we present an explorative experiment in which we have used a low temperature STM to contact a Josephson-junction array High quality arrays are fabricated with Al for the superconducting islands and Al_2O_3 [6] for the tunnel barriers Aluminum has a superconducting transition temperature T_c of 1 2 K and experiments on these arrays are preferably performed at temperatures below 1 K In the experiment we have recorded the spatial distribution of the vortices flow in a simple Josephson-junction array In this chapter we however primarily focus on the technical aspects of the experiment, which has been performed in a ^{3}He-setup, with a lowest temperature of 350 mK One of the obvious difficulties of the experiment is to position the tip above the structures of interest Since in general the scan range of the STM is much smaller than the dimensions of the structure, the tip has to be positioned by some coarse motion mechanism The strategy of the coarse positioning also has to take into account that insulating parts of the surface have to be avoided The STM is described in Chapter 2 (section 2 5) Useful measurements require stable point contacts, small electronic noise, and a stable temperature The measurements on the Josephson-junction array demonstrate that these conditions can be met and that pursuing results

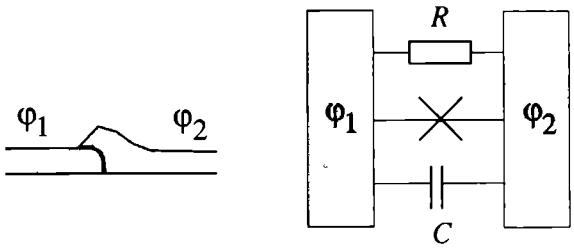

Figure 6.1: *A Josephson junction and its representation in the RCSJ model. The phases of the order parameter are φ_1 and φ_2.*

with this method on this and various other systems can be worthwhile. We start with a brief introduction about Josephson-junction arrays.

6.2 Josephson-junction arrays

Josephson-junction arrays consist of weakly coupled superconducting island arranged in a regular lattice. The islands are separated by thin tunnel barriers. The overlap area of the tunnel junctions defines the capacitance C and the normal state resistance R in the resistively and capacitively shunted Josephson junction (RCSJ) model (Figure 6.1). At zero temperature and in the absence of an external magnetic field all islands have the same superconducting phase. As a magnetic field is applied, the presence of vortices will lower the total energy. Vortices carry a magnetic flux equal to the flux quantum $h/2e$ and give rise to phase differences between the superconducting islands. All closed contours around a single vortex have an integrated phase difference of 2π.

A bias current driven through the array exerts Lorentz forces on the vortices in the direction perpendicular to the current flow. Moving vortices imply a time rate of change of the phase differences, and will generate voltages between the islands of the array. The voltage difference is governed by the Josephson relation

$$V = \frac{\Phi_0}{2\pi}\frac{d\phi}{dt}, \tag{6.1}$$

where ϕ is the phase difference between the islands, and Φ_0 the flux quantum $h/2e$.

If the bias current is increased through an array, like shown in Figure 6.2, and simultaneously the voltage over the contacts 1 and 2 is measured, three regimes can be distinguished. At low bias currents no voltages are build up over the array. Vortices are pinned to their initial positions and a perfect supercurrent

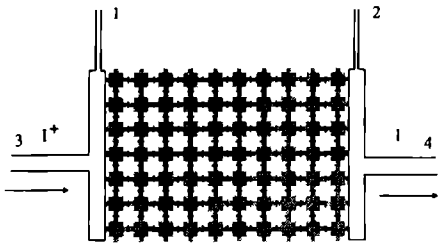

Figure 6 2 *Rectagular Josephson junction array with four leads (the black lines between the islands are tunnel barriers) The voltage between the probes 1 and 2 is monitored as a function of the applied bias current (from 3 to 4)*

is observed Increasing the bias current depins the vortices, and a small voltage will be present over the contacts 1 and 2 For N independent vortices crossing the array, the Josephson relation gives a voltage difference

$$V = \frac{\Phi_0}{2\pi}\frac{2\pi uN}{Wp}, \tag{6 2}$$

where u is the average velocity of the vortices, p the lattice constant of the array, and W the number of islands in the direction parallel to the bias current When the bias current is increased further row switching occurs This transition to the dissipative state occurs at the same current for all the junctions in a particular row (a row consists of all the island in the direction perpendicular to the applied bias current), however can vary slightly from one row to another With each switching row the voltage over the probes increases with $2\Delta/e$, where Δ is the superconducting gap

In magnetic fields vortices are present in the ground state of the array The vortex density is usually expressed by the frustration parameter f, which is defined as the average magnetic flux through a unit cell of the array divided by the flux quantum Φ_0 The flux flow through a Josephson-junction array strongly depends on the frustration parameter [6]

The dynamic properties of vortices in Josephson-junction arrays have received considerable attention in recent years Vortices are supposed to behave like particles with a mass Van der Zant *et al* [7] demonstrated that vortices can move ballistically, while later experiments by others [8, 9] also suggest quantum mechanical properties of the vortices Spatially resolved measurements on the dynamics of vortices can yield relevant new information about the nature of vortices in Josephson-junction arrays

6.3 Sample design and experimental setup

To enable the investigation of a Josephson-junction array with an STM several modifications have to be made to the usual sample layout A major constraint of scanning tunneling microscopy is that it requires conductive surfaces It is therefore not possible to perform the measurements directly on the Al islands of the array, since native oxides on the aluminum will give an insulating surface In the sample used in this experiment we connected Pt lines to the outer islands of the array The layout of the sample is shown in Figure 6 3 The Pt lines are 30 nm high, 500 nm wide, and are separated 350 nm from each other On both sides of the lines connected to the array, large square slabs with lines of a perpendicular direction are present The lines are evaporated directly on the insulating SiO_2 substrate A blunt tip will not be able to reach the insulating substrate, and therefore it is possible to image these lines with an STM (a sharp tip will become blunt after an encounter with the SiO_2)

The array consists of 32×32 cells with a lattice constant of 7 μm The normal state junction resistance R is $\sim$1 kΩ, and the capacitance 50 fF

The sample is mounted on a copper sample holder, which is in direct contact with the cold finger The PtIr tip is glued into a copper tip holder as shown in Figure 6 4 The protruding part of the tip is kept as short as possible (typically < 1 mm) in order to provide optimal heat exchange Six leads are attached to the sample, four to the array itself (see Figure 6 3)and two to the square slabs The four contacts to the array enable to perform the regular four-point measurements The contact established with the STM-tip will be the fifth contact, and voltages measured with the tip have to be taken relative to one of the two other voltage probe contacts

First, at room temperature, tip and sample are aligned by adjustment screws The alignment should ensure that at low temperatures the tip can only encounter the sample on one of the square slabs After the STM has been mounted to the ^{3}He-insert and cooled down to 350 mK, the tip is moved towards the sample with the coarse z-approach The bias voltages on the two slabs have opposite signs So, the position of the STM-tip relative to the lines connected to the array can be determined from the sign of the tunnel current With the coarse x or coarse y positioners we can move the tip in the direction of the array-lines with large steps (during coarse positioning the tip is retracted) When the polarity of the tunnel current has changed, the tip (and therefore the scan head) is moved in the opposite direction with smaller intervals After the tip has been positioned above

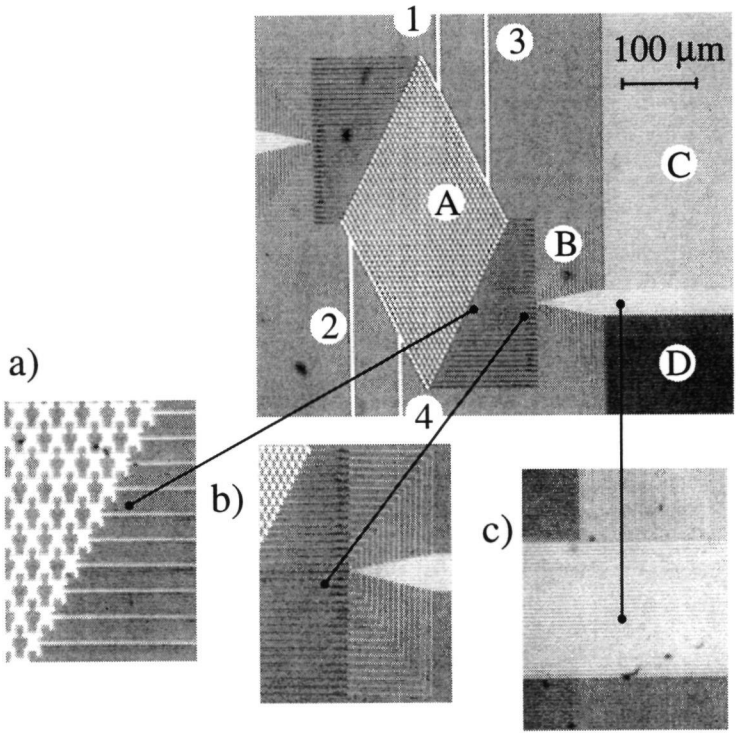

Figure 6.3: *Sample layout. The center diamond (A) is the Josephson junction array. 1, 2, 3, and 4 are the leads for the four-point measurements. The Pt lines connected to the array are brought together (B), and are will be contacted by the STM in between the large square slabs C and D. the slabs consist of lines of perpendicular direction. Details are enlarged in a), b) and c).*

the first line, the feedback is switched off, and the tip scan tube is elongated by adjusting a potentiometer by hand.

Once contact is established, the IV-convertor is switched off, and the tip is connected to a voltmeter. After the measurements on a particular line are completed, the tip is retracted and moved to the next line and the sequence is repeated. Note that in this experiment the STM tip is used to measure voltages, and therefore the resistance of the point contact will have no influence.

Several measures have been taken to reduce the electronic noise. Most the wires to the STM and to the sample are filtered by pi-filters. The wires witch

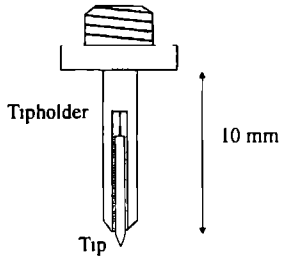

Figure 6 4 *Copper tip holder The PtIr tip is glued into a copper wire in order to provide optimal heat exchange The diameter of the wire is 1 5 mm*

could not be filtered in this way, as for example the wires for the coarse approach of the STM, were fixed to the ground potential of the setup during the measurements

6.4 Results

In Figure 6 5 four point measurements are plotted with the STM-tip as one of the probes, on consecutive lines On each next line, the voltage above the critical current, between the STM-tip and one of the fixed contacts increases by $2\Delta/e$ (with respect to the other contact the voltage decreases) The measurements demonstrate that it is possible to contact adjacent lines Also, the voltage differences in the normal state allows to determine which line is contacted by the STM-tip

From the value of the superconducting gap that we can obtain from the data of Figure 6 5, we can estimate an upper limit for the sample temperature For the gap we find 0 18 meV, which assures $T < 500$ mK Figure 6 6 shows a single I-V curve In the horizontal part of the curves, steps in the current at equal voltage intervals should be observable These steps, which should be due to the switch of individual rows to the dissipative state (row-switching) are only rarely observed The steps in the current are however very small for relatively large arrays, and apparantly the noise level in the setup is not low enough to observe these small steps The presence of the STM gives a small increase in the noise level in voltage measurements In regular measurements $V_{rms} \sim 0\ 2\mu V$, while with the STM, $V_{rms} \sim 0\ 8\mu V$ We attribute this increase to a minor experimental detail, namely that the coaxial cable contacting the STM-tip has a different path through the

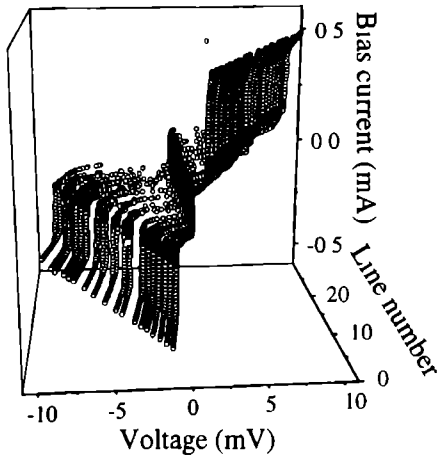

Figure 6 5 *Four-point measurements on consecutive lines Above the critical current (~ 0 1 mA) the voltage between the STM tip and one of the regular contacts of the array increases with 0 36 mV with each line Figure 3 6 shows a single I-V curve*

insert than the other wires (which are twisted) This can give rise to addition magnetic interference

In the flux flow regime voltages are due to the motion of vortices perpendicularly to the applied bias current We recorded the voltages on the consecutive lines for a bias current of 10 μA at two different fields In Figure 6 7 the upper curve corresponds to the a field of $4\,9\times10^{-6}$ T and the lower curve to a field of

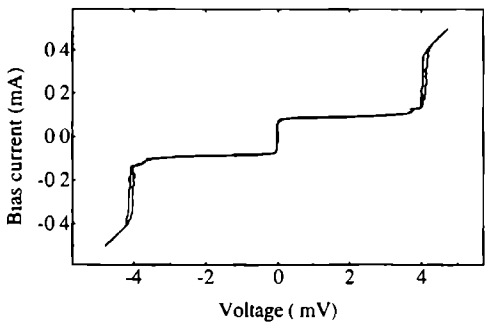

Figure 6 6 *I-V curve for line number 12 All curves are slightly hysteretic No additional steps in the horizontal part of the curve due to row-switching are observed*

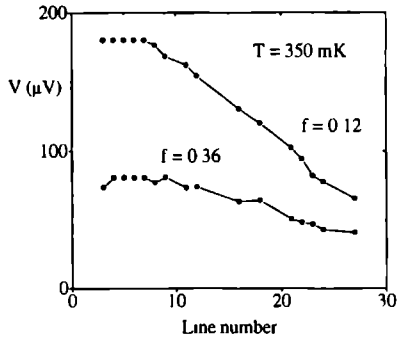

Figure 6 7 *Voltages measured on consecutive lines in the flux flow regime* I_{bias} *= 10* μA *The frustrations are f = 0 12 and f = 0 36*

14 7×10^{-6} T At these fields the frustration parameters are respectively 0 12 and 0 36 In first order the voltages depend linearly on the the line number, suggesting a uniform flow of vortices through the array A more detailed analysis of the data in Figure 6 7 is at present premature, and requires a careful investigation of possible measurement errors

6.5 Conclusions

By the experiment described in this chapter we have demonstrated the possibility to use an STM-tip as a displaceable contact in transport measurements on lithographically fabricated structures at temperatures <1 K We have not observed any increase in the effective temperature of the sample due to the presence of the STM The influence on the electronic noise is limited The searching strategy is fast and reliable In future experiments other strategies to circumvent the insulating parts have to be developed For example, in the case of a Josephson-junction array, evaporating a high pillar of a noble metal (Au or Pt) on every island may enable to probe the islands of the array directly (Figure 6 8)

References

[1] A T Johnson, L P Kouwenhoven, W de Jong, N C van der Vaart, and C J P M Harmans, Phys Rev Lett **69**, 1592 (1992)

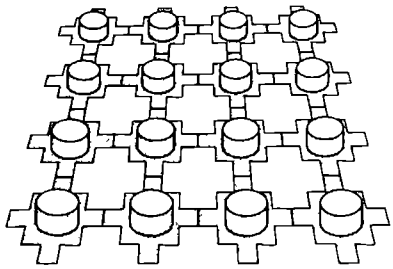

Figure 6.8: *A pillar of a noble metal on each island enables to contact the islands seperately.*

[2] E.B. Foxman, P.L. McEuen, U. Meirav, N.S. Wingreen, Y. Meir, P.A. Belk, N.R. Belk, M.A. Kastner, and S.J. Wind.

[3] T.A. Fulton, and G.J. Dolan, Phys. Rev. Lett **59**, 109 (1987).

[4] L.J. Geerligs, V.F. Anderegg, P.A.M. Holweg, J.E. Mooij, H. Pothier, D. Esteve, C. Urbina, and M.H. Devoret, Phys. Rev. Lett. **64**, 2691 (1990).

[5] P. Lafarge, H. Pothier, E.R. Williams, D. Esteve, C. Urbina, and M.H. Devoret, Z. Phys. B. **85**, 327 (1991).

[6] H.S.J. van der Zant, Ph.D. thesis (1991), Technische Universiteit Delft, The Netherlands.

[7] H.S.J. van der Zant, F.C. Fritschy, T.P. Orlando, and J.E. Mooij, Europhys. Lett. **18**, 343 (1992).

[8] W.J. Elion, J.J. Wachters, L.L. Sohn, and J.E. Mooij, Phys. Rev. Lett. **71**, 2311 (1993).

[9] A. van Oudenaarden and J.E. Mooij, to be published.

Samenyatting

Dit proefschrift beschrijft de resultaten van een project waarin lage temperaturen scanning tunneling microscopy is toegepast om elektronische eigenschappen te onderzoeken op de zogenaamde mesoscopische scaal In het regime tussen clusters van enkele tientallen atomen, en kunstmatige structuren met karakteristieke afmetingen van de orde van een micrometer, kunnen de elektronische eigenschappen van geleiders noch beschouwd worden als totaal macroscopisch, noch als totaal microscopisch Om deze reden wordt de natuurkunde in dit regime gewoonlijk aangeduid als mesoscopisch

De scanning tunneling microscoop (STM) is een instrument dat bekend staat vanwege zijn hoge plaatsopgeloste resolutie Het maakt gebruikt van een metalen punt die op een zeer kleine afstand boven een oppervlak wordt gehouden, dicht genoeg om een tunnelstroom te realiseren Door de naald te bewegen over het oppervlak kan een topografische afbeelding van het oppervlak verkregen worden

In de experimenten beschreven in dit proefschrift wordt de STM-naald niet alleen gebruikt om oppervlakken af te beelden, maar in de eerste plaats als een verplaatsbaar en variëerbaar tunnelkontakt Omdat om de STM-naald zeer nauwkeurig gepositioneerd kan worden, is het mogelijk zeer kleine strukturen plaatsopgelost af te tasten Dit kan bijvoorbeeld door middel van tunnelspektroscopie, waarbij de bias-spanning over STM-punt en sample gevarieerd wordt Onder bepaalde randvoorwaarden biedt scanning tunneling spektroscopie de mogelijkheid de toestandsdichtheid als funktie van de energie van een oppervlak plaatsopgelost af te beelden

Kunstmatig gefabriceerde submicronstrukturen hebben bewezen zeer waardevol te zijn in het bestuderen van mesoscopische verschijnselen Transportmetingen bij zeer lage temperaturen (typisch <1 K) door deze strukturen kunnen gedetailleerde informatie opleveren over de mechanismen van het elektronentransport Ook in dit type experimenten kan de STM mogelijk een nuttig instrument zijn In de gebruikelijke transportmeting liggen het aantal kontakten en hun positie vast In een experiment met een STM kan de STM-punt dienen als een verplaatsbaar (tunnel)kontakt

Een van de doelstellingen van dit project was om een STM te integreren in transportmetingen bij milliKelvin temperaturen Hiervoor was het noodzakelijk een STM te ontwikkelen, geschikt voor deze temperaturen, en met de mogelijkheden om in drie dimensies over grotere afstanden de tip t o v het sample te verplaatsen

In hoofdstuk 2 zijn de twee lage temperaturen STMs die we hebben ontwikkeld beschreven Beginnende met een aantal ontwerpcriteria betreffende de mechanische stabiliteit van STMs, beschrijven we eerst de STM voor vloeibaar helium temperaturen (1-4 K), de ^{4}He-STM De ^{4}He-STM is zeer kompakt en heeft grofverplaatsingsmogelijkheden in drie dimensies De STM-punt en het sample worden gekoeld door helium

gas Bij temperaturen beneden 1 K kan helium gas niet langer gebruikt worden en zal een andere methode toegepast moeten worden De STM voor temperaturen laager dan 1 K, de ^{3}He-STM, is voor een groot deel gemaakt van koper De ^{3}He-STM is gebaseerd op dezelfde principes als de ^{4}He-STM, maar is geschikt voor experimenten bij temperaturen lager dan 1K

De hoofdstukken 3, 4 en 5 beschrijven experimenten die zijn uitgevoerd met de ^{4}He-STM In hoofdstuk 3 presenteren we spektroscopiemetingen aan InAs(110) oppervlakken Aan het InAs oppervlaak kan zich een oppervlakte tweedimensionaal elektronen gas bevinden Echter, de pieken waargenomen in de spektra op schone InAs(110) oppervlakken zijn sterk tip-afhankelijk en moeten worden toegeschreven aan werkfunktieverschillen In magneetveld zijn oscillaties in toestandsdichtheid waargenomen als gevolg van Landau-kwantisatie Spektra in de nabijheid van stappen laten de aanwezigheid van gebonden toestanden zien, hetgeen een aanwijzing is voor de vorming van 1D kwantumdraden aan de staprand

Hoofdstuk 4 behandelt het effekt van kleine geladen korrels op de lokale bandbuiging aan het halfgeleideroppervlak De halfgeleider is InAs Ladingen in de nabijheid van halfgeleideroppervlakken kunnen lokale depletie- of accumulatiegebieden veroorzaken We hebben meerdere gevallen waargenomen, waar in de nabijheid van een korrel STM-metingen een abrupte verandering in de elektronen dichtheid laten zien In een geval was het mogelijk een uitgebreidere dataset te verkrijgen De data laten zien dat de waargnomen effekten een gevolg zijn van ladingskwantisatie op de korrel De bandbuiging verandert stapsgewijs als een extra elektron wordt aangebracht op de korrel

De geinduceerde supergeleidende spektra van een dunne goudfilm op een niobiumlaag worden bediscussieerd in hoofdstuk 5 Toestandsdichtheidmetingen op verschillende punten vaan het goudoppervlak geven identieke BCS-achtige curves, ondanks het onregelmatige oppervlak In magneetveld nemen we deindduceerde vortices waar, met een mozaiek-achtige struktuur The spektroscopiemetingen in de nabijheid van een vortex laten geen afname van de supergeleidende gap zien, maar alleen veranderingen in de amplitudes van de toestandsdichtheid De waargenomen verschijnselen kunnen verklaard worden met een semi-klassiek gebonden-toestanden model Het laatste hoofdstuk van dit proefschrift demonstreert de mogelijkheid een STM te integreren in transport experimenten aan kunstmatig gefabriceerde strukturen bij temperaturen lager dan 1 Kelvin De struktuur, een Joephson-junctie array is vrij eenvoudig en dient in de eerste plaats om onze methode te testen We laten zien dat we de tip kunnen positionering op de lijnen die van belang zijn, en dat de invloed op de temperatuur van het sample gering is Verdere experimenten op geavanceerdere strukturen zullen moeten uitwijzen of essentiele plaatsopgeloste informatie verkregen kan worden op deze manier

Summary

This thesis presents the results of a project in which low temperature scanning tunneling microscopy has been applied to investigate electronic properties at the so-called mesoscopic scale In the regime ranging from clusters of several tens of atoms to artificial structures with characteristic sizes of the order of one micrometer, the electronic properties of conductors can neither be considered as completely macroscopic nor as completely microscopic Therefore the physics in this regime is usually referred to as mesoscopic

The scanning tunneling microscope is a well known instrument for its ability to image surfaces with very high spatial resolution It uses a sharp metal tip that is kept at a very small distance above the surface, close enough to establish a non-contact tunnel current By moving the tip across the surface a topographic image of the surface can be obtained

In the experiments described in this thesis the STM-tip is not only used to image the surfaces, but in the first place as a displaceable and variable tunneling contact The possibility to position the STM-tip very accurately, enables to probe small structures spatially resolved One of the most powerful ways to operate the STM is in tunneling spectroscopy Under certain conditions, scanning tunneling spectroscopy allows to probe the density of states as a function of energy spatially resolved

Artificially fabricated submicron structures have proven to be very valuable in investigating mesoscopic phenomena Transport measurements at very low temperatures (typically < 1K) through these structures can yield detailed information about electron transport mechanisms Also in these kind of experiments an STM can possibly be a useful instrument In the usual transport measurement the number of of contacts and their positions are fixed In an experiment with an STM, the STM-tip can serve as a versatile and displaceable (tunnel) contact In this way additional spatially resolved information can be obtained

One of the objectives of this project was to incorpororate an STM in transport measurements at milliKelvin temperatures For this it was necessary to develop an STM that could be operated at these temperatures, and that offered coarse positioning facilities in three dimensions

In chapter2 the two low-temperature STMs we have developed are pesented Starting with a number of design criteria concerning the mechanical stability of scanning tunneling microscopes, we first descibe the STM for liquid-helium temperatures, the ^{4}He-STM ^{4}He-STM is very compact and has coarse approach facilities in three dimensions Tip and sample are cooled by helium exchange gas At temperatures below 1 K exchange gas can no longer be used, and a diffeerent method of cooling tip and

sample and the other parts of the STM should be applied The STM for subKelvin temperatures, ^{3}He-STM, is largely made of copper The ^{3}He-STM is based on the same principles as the ^{4}He-STM, however it does enable experiments below 1 K

Chapters 3, 4 and 5 describe experiments that have been performed with the ^{4}He-STM In chapter 3 we present spectroscopy measurements on Indium Arsenide (110) surfaces InAs surfaces have been reported to carry a surface two dimensional electron gas (2DEG), due to pinning of the Fermi-level at the surface In our experiments on clean in situ cleaved surface we do not find evidence for the presence of a 2DEG Peaks observed in the spectra are strongly tip-dependent, and have to be attributed to work function differences In magnetic field oscillations in the density of states due to Landau quantization are observed Spectra in the vicinity of steps show the presence of bound atates, indicating the formation of a 1D quantum wire at the step edge

Chapter 4 focuses on the effect of small charged grains on the loacl band-bending at a semiconductor surface The semiconductor is InAs Charges in the vicinty of semiconductor surfaces can give rise to local depletion or accumulation regions We have observed several cases in which in the vicinity of small grains STM-measurements show abrupt changes in the band-bending In one case a more extended set of data was acquired The data demonstrate that the observed features are a consequence of charge quantization on the grain The band-bending changes stepwise when an extra electron is added to the grain, resulting in a sharp closed curve around the grain in topographic images

The induced superconducting spectra of a thin Au film on top of a Nb layer are discussed in chapter 5 Density of states (DOS) maesurements at different points of the Au surface show identical BCS-like curves, despite the irregular topography of the surface In magnetic field we observe proximity induced vortices, which have an irregular mosaic structure The spectroscopy curves in the vicinity of a vortex do not show a reduction of the superconducting gap, but only changes in the DOS-amplitudes The observed phenomena can be explained by a semi-classical bound-state model which assumes no induced gap in the normal metal

In the last chapter of the thesis we demonstrate the possibility to incorporate an STM in transport experiments on artificially fabricated structure at temperatures below 1 Kelvin The structure, a Josephson-junction array, is kept rather simple and serves primarily to test the usefulness of our approach We show that we can position the tip above the lines of interest, and that the influence on the temperature of the sample is limited Further experiments on more advanced structures should prove that essential spatially resolved information can be extracted with this technique

Curriculum vitae

Jeroen Wildoer
geboren op 10 maart 1967 te Andijk

1979 - 1985	V W O at Keizer Karel College, Amstelveen
1985 - 1991	Applied Physics at the Delft University of Technology Universiteit, graduate research at the Delft Institute of MicroElectronics and Submicrontechnology (DIMES)
1991 - 1993	First part of Ph D research, at the University of Nijmegen in the group Experimental Solid State Physics 2 of Prof Dr H van Kempen
1994 - 1996	Second part of Ph D research, at the Delft University of Technology in the group Quantum Transport of Prof Dr ir J E Mooij